# DETECTION OF VIRAL PARTICLES BY USING PROBE-GATED SILICA NANOPARTICLES

by
Meltem Ercan

Submitted to Graduate School of Natural and Applied Sciences
in Partial Fulfillment of the Requirements
for the Degree of Doctor of Philosophy in
Biotechnology

Yeditepe University
2022

DETECTION OF VIRAL PARTICLES BY USING PROBE-GATED SILICA NANOPARTICLES

APPROVED BY:

Assoc. Prof. Dr. Bilge Güvenç Tuna ……
(Thesis Supervisor)
(Yeditepe University)

Prof. Dr. Veli Cengiz Özalp
(Co-Supervisor)
(Atılım University)

Prof. Dr. Soner Doğan ……
(Yeditepe University)

Assist. Prof. Dr. Hale Arık Taşyıkan ……
(Yeditepe University)

Assoc. Prof. Dr. Pınar Buket Thomas ……
(Maltepe University)

Assist. Prof. Dr. Murat Kavruk ……
(Arel University)

DATE OF APPROVAL: ..../..../20..

*Dedicated to my lovely children…*

I hereby declare that this thesis is my own work and that all information in this thesis has been obtained and presented in accordance with academic rules and ethical conduct. I have fully cited and referenced all material and results as required by these rules and conduct, and this thesis study does not contain any plagiarism. If any material used in the thesis requires copyright, the necessary permissions have been obtained. No material from this thesis has been used for the award of another degree.

I accept all kinds of legal liability that may arise in case contrary to these situations.

Name, Last name Meltem Ercan

Signature ……..

# ACKNOWLEDGEMENTS

First of all, I want to thank my Ph.D. supervisor, Assoc. Prof. Dr. Bilge Güvenç Tuna, for all the help, patience, and encouragement she gave me during my Ph.D. Without her push, I would not have been able to finish this thesis. Prof. Dr. Veli Cengiz Özalp, my co-supervisor, helped me get my Ph.D. by giving me his time, advice, and great knowledge.

Also, I'm very thankful to Prof. Dr. Soner Doğan for all the help, encouragement, and time he gave me.

Asst. Prof. Dr. Pınar Buket Thomas, Asst. Prof. Dr. Hale Arık Taşyıkan, and Asst. Prof. Dr. Murat Kavruk were on my dissertation committee. I'd like to thank them for their help, support, guidance, and time.

I'd like to thank Prof. Dr. Zeynep Karakaş, Prof. Dr. Banu Mansuroğlu, and Asst. Prof. Dr. Ayşegül Kuşkucu, who were on my qualifying exam committee, for their help and valuable contributions.

Also, I'd like to thank Dr. Serap Demir Tekol, Dr. Ali Doğan Dursun, and Dr. Caner Çelik for working together on this study and article and for their help and valuable contributions.

I'd like to thank my friends Dilara Buse Durdabak and Furkan Yaşaryıldız for helping me with my thesis and being there for me. I'm very happy to work with them. I'd also like to thank everyone in the lab for their understanding and help: Arda Keleş, Atakan Ayden, Ayşenur Doğan, Ceren Çolak, Elif Öztemiz, and Elif Yılmaz.

Lastly, I'm grateful to my parents, Figen Kazak and Necmi Kazak, for all the love, faith, and support they've given me my whole life. I also want to thank my dear husband, Sercan Ercan, who is also my best friend. I wouldn't have been able to finish my Ph.D. without his constant help, understanding, patience, and never-ending love. Most of all, I want to thank my son and my daughter for making me feel the best. I'm also very proud to give my thesis to Salih Egemen and Saliha Melek, my two children.

# ABSTRACT


## DETECTION OF VIRAL PARTICLES BY USING PROBE-GATED SILICA NANOPARTICLES

Early diagnosis of viral infections at point-of-care location is considered as a critical tool in the infection control. Reverse transcription-polymerase chain reaction (RT-PCR) has been a commonly employed detection methodology for virus detection, which is utmost importance for human health. But RT-PCR is a long process that has many steps. Large-scale monitoring projects are also hard because they need complicated equipment and people with a lot of experience. Therefore, the aim of this thesis study is to develop a rapid detection method working directly with samples taken from the nose and throat of SARS-CoV-2 patients. The novel method developed in this thesis based on fluorescein releasing from mesoporous MCM-41 type of silica nanoparticles (MSNPs) during hybridization between a conjugated complementary single strand oligonucleotide and SARS-CoV-2 RNA samples.

For this purpose, firstly, mesoporous MSNPs were characterized by TEM to determine microstructure, BET to determine pore size and surface area and DLS to detect particle size. Then, MSNPs were loaded by fluorescein and capped by specific gene sequences probes immobilized on the surface of the nanoparticles. Three target (NSP12, NSP9 and Egene) regions selected from SARS-CoV-2 genome and tested with synthetic oligonucleotides. The test prototype was optimized in different pH and temperature conditions. Last, the human swap samples were used for verification.

As a result, NSP12 gene-based detection of the SARS-CoV-2 was used to garner the best detection yield compared to NSP9 gene and E gene oligonucleotide MSNPs conjugates. The optimum target detection time was determined as 15 minutes. The basic pH damaged the structure of probe-gated MSNPs. The limit of detection with experiments using patient samples was 1.4, Relative Fluorescence Units with 84% accuracy.

As a conclusion, in this thesis, a generic method based on nucleic acid-gated silica nanoparticles to detect SARS-CoV-2 in 15 minutes directly from patient swap samples was developed. This nanoparticle-based method could be improved for SARS-CoV-2 variants or any kind of different virus genome, including RNA viruses as it is faster, promising for sensitive detection, easy to operate, and less expensive than current methods.

# ÖZET


## PROB-GİRİŞLİ SİLİKA NANOPARTİKÜLLER KULLANARAK VİRAL PARÇACIKLARIN TESPİTİ

Bakım noktasında viral enfeksiyonların erken teşhisi, bulaşıcı hastalıkların kontrolünde kritik bir araç olarak kabul edilir. Ters transkripsiyon-polimeraz zincir reaksiyonu (RT-PCR), insan sağlığı için son derece önemli olan virüs tespiti için yaygın olarak kullanılan bir tespit metodolojisidir. Ancak RT-PCR birçok aşaması olan uzun bir prosedürdür. Gerekli vasıflı personel ve karmaşık enstrümantasyon, büyük ölçekli izleme çabalarında da zorluklar ortaya çıkarmaktadır. Bu nedenle bu tez çalışmasının amacı, doğrudan SARS-CoV-2 hastalarının burun ve boğazından alınan örneklerle çalışan hızlı bir tespit yöntemi geliştirmektir. Bu tezde geliştirilen yeni yöntem, konjuge tamamlayıcı tek zincirli bir oligonükleotid ile SARS-CoV-2 RNA numuneleri arasındaki hibridizasyon sırasında mezogözenekli MCM-41 tipi silika nanopartiküllerden (MSNP'ler) salınan floresana dayanmaktadır. Bu amaçla ilk olarak mezogözenekli MSNP'ler mikro yapıyı belirlemek için TEM, gözenek boyutunu ve yüzey alanını belirlemek için BET ve parçacık boyutunu belirlemek için DLS ile karakterize edilmiştir. Daha sonra MSNP'ler, floresein ile yüklendi ve nanoparçacıkların yüzeyinde hareketsiz hale getirilmiş spesifik gen dizileri probları ile kapatıldı. SARS-CoV-2 genomundan üç hedef bölge (NSP12, NSP9 ve Egene) seçildi ve sentetik oligonükleotitlerle test edildi. Test prototipi farklı pH ve sıcaklık koşullarında optimize edilmiştir. Son olarak, doğrulama için insan sürüntü örnekleri kullanıldı. Sonuç olarak, NSP9 geni ve E geni oligonükleotit MSNP'ler konjugatlarına kıyasla en iyi saptama verimini elde etmek için SARS-CoV-2'nin NSP12 gen tabanlı tespiti kullanıldı. Optimum hedef tespit süresi 15 dakika olarak belirlenmiştir. Bazik pH, prob kapılı MSNP'lerin yapısına zarar verdi. Hasta numuneleri kullanılarak yapılan deneylerde saptama sınırı, %84 doğrulukla 1,4 nispi floresan ünitesi (RFU)'dur. Sonuç olarak, bu tezde, doğrudan hasta sürüntü örneklerinden SARS-CoV-2'yi 15 dakikada tespit etmek için nükleik asit kapılı silika nanopartiküllere dayalı jenerik bir yöntem geliştirilmiştir. Bu nanoparçacık tabanlı yöntem, SARS-CoV-2 varyantları veya RNA virüsleri de dahil olmak üzere her türlü farklı virüs genomu için geliştirilebilir, çünkü daha hızlıdır, hassas tespit için umut vericidir, kullanımı kolaydır ve mevcut yöntemlerden daha ucuzdur.

# TABLE OF CONTENTS

# LIST OF FIGURES

# LIST OF TABLES

# LIST OF SYMBOLS/ABBREVIATIONS

| | |
|---|---|
| APTES | (3-Aminopropyl) triethoxysilane |
| BET | Braunauer, Emmett and Teller |
| CoV | Coronavirus |
| Covid-19 | Coronavirus disease 2019 |
| DLS | Dynamic light scattering |
| DNA | Deoxyribonucleic acid |
| ELS | Electrophoretic light scattering |
| FAM | Fluorescein amidites |
| FL | Fluorescein |
| FTIR | Fourier transform infrared spectroscopy |
| LOD | Limit of detection |
| MCM-41 | Mobile crystalline material-41 |
| MERS | Middle east respiratory syndrome |
| MSNP | Mesoporous MCM-41 type silica nanoparticle |
| NP | Nanoparticle |
| PBS | Phosphate buffered saline |
| RFU | Relative fluorescence units |
| RNA | Ribonucleic acid |
| SARS | Severe acute respiratory syndrome |
| TEM | Transmission electron microscopy |

# 1. INTRODUCTION

The main component of infection control is the early detection of virus-related illnesses. Traditional virus detection solutions typically call for highly trained individuals and sophisticated equipment. In addition, these tests may require expensive consumables and could be time and energy consuming. Therefore, quick diagnosis techniques are needed for virus identification. The recent Covid-19 pandemic also brought this requirement to light. In the current Ph.D. thesis, a sensitive and direct approach for the identification of viruses in samples was developed using both synthetic sequence of the Severe Acute Respiratory Syndrome Coronavirus 2 (SARS-CoV-2) and the swab samples from human subjects.

Viruses have always been one of the most dangerous things for people's health. For example, between 1889 and 1894, the Myxovirus influenzae that caused the Russian flu killed about a million people, most of whom were over 50 years old [1]. Then, an outbreak of the H1N1 virus, also called the "Spanish flu," killed at least 50 million people around the world between 1918 and 1919. The unique thing about this pandemic was that it killed a lot of healthy people, even those in their 20s to 40s [2]. After that, an Asian flu outbreak caused by the H2N2 virus killed between 1 and 1,5 million people between 1957 and 1958 [3]. Viruses have also spread among people in recent times. In 2009, H1N1, which is also called "swine flu," was first seen in the United States. It then spread to the rest of the world. Also, the Centers for Disease Control and Prevention (CDC) said that between 151.700 and 575.400 people died around the world during the year. It was thought that, around the world, 80% of deaths happened to people younger than 65 [4].

In this context, coronavirus takes important part of modern human history since whole world is devastated because of it. There were no flight in the sky, people are locked at home for months, even doctors or nurses could not hug their children.

Coronaviruses are a type of virus in the order Nidovirales. Over the past 20 years, they have been the cause of a lot of sickness in the eastern part of the world. For example, SARS-CoV, which stands for Severe Acute Respiratory Syndrome Coronavirus, was the cause of the first known coronavirus outbreak in 2002. The first time this was said to have happened was in China's Guangdong Province, in the city of Foshan [5]. Then, in 2012, the Middle East Respiratory Syndrome-Coronavirus (MERS-CoV) became known. After that, an outbreak

of SARS-CoV-2, which is also known as Covid-19, was reported for the first time in the Wuhan area of the Republic of China in December 2019. The World Health Organization (WHO) gave the virus the name Covid-19 (Corona-Virus Disease-2019) on February 11, 2020, because it was first found in 2019 [6]. In particular, WHO was told in December 2019 that people in Wuhan City, Hubei Province, China, were getting pneumonia for no known reason. Because of this, the illness was seen for the first time in December 2019 during an outbreak of pneumonitis in Wuhan, China [7].

After the Chinese government and WHO agreed that there was a public health problem, which turned out to be one of the worst times in human history, The scientific research found a link between the group of people with pneumonia that was found through epidemiology and the Huanan South China seafood market in the Wuhan region of China. As soon as the symptoms of the disease showed up, chest X-rays (PA) and computed tomography (CT) scans were done. It was found that coughing, a fever, chest pain, and acute respiratory distress syndrome were all caused by pneumonia (ARDS). After looking into these respiratory infections, scientists found a type of Beta-Coronavirus that shared between 75 and 80% of its genetic sequence with SARS-CoV found in the Middle East in 2002 [8,9]. On January 7, 2020, WHO gave the 2019-nCoV acute respiratory disease name to a new coronavirus (CoV) whose agent had never been found in humans before [9]. The International Committee on Virus Taxonomy (ICTV) named and registered this virus as SARS-CoV-2. This made it easy for people all over the world to recognize because it was very similar genetically to SARS-CoV, which first appeared in 2002. The illness caused by this new virus was given the name "Coronavirus Illness-2019" or "Covid 19" by the WHO on February 11, 2020 [9–12].

Genomic research showed that SARS-CoV-2 was 88–90% similar to two coronaviruses that come from bats and are similar to SARS-CoV (bat-SL-CoVZC45 and bat-SL-CoVZXC21). The SARS-CoV-2 virus, which is the cause of the current outbreak, is similar to the SARS-CoV virus, which caused an outbreak in 2002. SARS-CoV-2 and SARS-CoV share about 79% of their genes, while SARS-CoV and MERS-CoV share about 50% of their genes [9,13,14]. Scientists did a lot of research on Coronaviruses and found that a highly contagious and dangerous virus was spread widely from one person to another. However, the origin of the intermediate host and how the virus got to humans is still unknown [13,15].

Due to its ability to transfer from person to person, the disease has spread quickly. Due to the alarming situation's continuous rapid progression, WHO on March 12, 2020, declared a global pandemic [16].

## 1.1. VIRUS

In the simplest definition, it is possible to define viruses as obligate intracellular parasites. The word virus, which means poison in Latin, was first used by the French scientist Louis Pasteur. The other Latin meaning of virus is the essence derived from the cell. They cannot reproduce by dividing, they must use the host cell and use enzymes. Mature viruses capable of infecting living cells are called virions. Viruses were first seen with the electron microscope in 1931 by Ernst Friedrich Ruska together with Max Knoll. Viruses are among the microorganisms that can infect, just like bacteria, fungi, mycoplasma, rickettsia, and chlamydia [17-19].

The most important features of viruses are that they contain only one DNA or RNA as genetic material. Viruses differ from others in terms of their structure, biological properties, and reproduction methods they follow. Viruses are organisms that have a unique reproduction method, do not have the necessary organelles for energy production and structural synthesis, carry a single type of nucleic acid, and are basically composed of nucleic acid and the protein sheaths surrounding it. The sizes of viruses are expressed in units of nm. Viruses are generally between 17-300 nm in size. The smallest known virus particle among animal viruses belongs to circoviruses and is 17 nm in diameter. The largest virus particle is seen in poxviruses with dimensions of 200-300 nm [20-22].

### 1.1.1. Structure of Viruses

For a light microscope to view viruses, they are extremely small. They are nucleoproteins that can only be propagated in living cells and have the power to harm the body. All viruses, from single-celled creatures to big plants and animals, are parasitic inside the cell and cause sickness in a wide range of living things. There are viruses that can infect humans as well as animals and cause diseases like rabies, chicken pox, and flu. Some of them cause disease by infecting plants, fungi, bacteria, and mycoplasmas. Each virus is composed of nucleic acid

and a protein capsid that surrounds it. Viruses are different from other microorganisms. They contain a single nucleic acid, DNA or RNA. No virus has both DNA and RNA. Viruses cannot divide and do not form replication structures inside the cell [23].

In the basic structure of the virus, there is a nucleic acid and a protein shell named capsid, around it, protecting it from external factors. This basic structure is defined as the nucleocapsid. The genetic material in the center of the nucleocapsid is composed of DNA or RNA structure. The structure that makes up the capsid is capsomeres, which are substructure units. Capsomeres are structures of viruses that can be seen in the electron microscope. In some virus families, there is an envelope of lipoprotein structure surrounding the nucleocapsid [24].

In the classification of viruses, their general taxonomic structures are listed; virales, viridae, virinae, virus for Species, Order, Family, Subfamily, Genus, and Species, respectively. The second principle in classification is to take the nucleic acid genome as the criterion. All viruses are classified by considering their 4 characteristics [25].

- Nucleic acid (DNA or RNA) in the virion
- The symmetry of the capsid
- Enveloped or non-enveloped
- Dimensions of virion and capsid

The international authority on the classification and naming of viruses is the International Virus Taxonomy Committee (ICTV), which was established in 1971 [26,27].

The single-celled microorganisms studied in microbiology can be listed as bacteria, fungi, rickettsia, mycoplasma, and chlamydia [27]. As in every cell structure, microorganisms contain nucleic acids in DNA and RNA structure, and they have metabolic systems that work in a certain order so that they can synthesize the necessary energy and macromolecules in the cell (Table 1.1.).

Table 1.1. Viruses and other microorganisms [28]

| Feature | Bacteria | Rickettsia | Mycoplasma | Chlamydia | Virus |
|---|---|---|---|---|---|
| >300nm diameter | + | + | + | + | Most are less than 300 nm |
| Reproduction in the inanimate environment | + | - | + | - | - |
| Reproduction by division | + | + | + | + | - |
| DNA and RNA | + | + | + | + | DNA or RNA |
| Infectious nucleic acid | - | - | - | - | + |
| Ribosome | + | + | + | + | - |
| Metabolism | + | + | + | + | - |
| Seen with a light microscope | + | + | + | + | (only smallpox viruses can be seen) |
| Ability to pass filters | - | - | - | - | + |

### 1.1.2. Morphological Structures of Viruses

The morphological structure of viruses is defined as virus symmetry. The morphological structures of viruses are collected in three groups icosahedral (cubic), helical, and complex structure symmetry. In addition to these, there are different morphologies seen in viruses such as bacteriophages that infect bacteria and other microorganisms (Table 1.2.). Except for the viruses of the Poxviridae family, which can be seen with light microscopes, detailed information and images regarding the morphological characters of other viruses could be obtained after the discovery of the electron microscope and its use in the field of virology [28].

Table 1.2. Morphological features of some DNA and RNA viruses [28]

| **DNA Viruses** | | | | | |
|---|---|---|---|---|---|
| **Family** | **Diameter (nm)** | **Envelope** | **Symmetry** | **Capsomer** | **Sensitivity to Ether** |
| Adenoviridae | 70-90 | | Icosahedral | 252 | Insensitive |
| Hepadnaviridae | 42 | + | Icosahedral | ? | Sensitive |
| Herpesviridae | 150 | + | Icosahedral | 162 | Sensitive |
| İridoviridae | 125-300 | + | Icosahedral | 1892 | Sensitive |
| Papovaviridae | 45-55 | | Icosahedral | 72 | Insensitive |
| Parvoviridae | 18-26 | | Icosahedral | 32 | Insensitive |
| Poxviridae | 230x400 | + | Complex | ? | Sensitive and some species insensitive |
| **RNA Viruses** | | | | | |
| **Family** | **Diameter (nm)** | **Envelope** | **Symmetry** | **Capsomer** | **Sensitivity to Ether** |
| Arenaviridae | 110-130 | + | Helical | ? | Sensitive |
| Birnaviridae | 60 | - | Icosahedral | 92 | Insensitive |
| Bunyaviridae | 90-120 | + | Helical | ? | Sensitive |
| Calicivirade | 35-40 | - | Icosahedral | 32 | Insensitive |
| Coronaviridae | 75-160 | + | Helical | ? | Sensitive |
| Filoviridae | 790-970x80 | + | Helical | ? | Sensitive |
| Flaviviridae | 40-50 | + | Icosahedral | ? | Sensitive |
| Orthomyxoviridae | 80-120 | + | Helical | ? | Sensitive |
| Paramyxoviridae | 150-300 | + | Helical | ? | Sensitive |
| Picornaviridae | 25-30 | - | Icosahedral | 32 | Insensitive |
| Reoviridae | 60-80 | - | Icosahedral | 32,92 | Insensitive |
| Retroviridae | 80-100 | + | Helical | ? | Sensitive |
| Rhabdoviridae | 75x180 | + | Helical | ? | Sensitive |
| Togaviridae | 50-70 | + | Icosahedral | 60 | Sensitive |

Animal viruses have a certain number of capsomeres, protein subunits joined to each other by non-covalent bonds around their DNA and RNA. Capsomeres, in viruses with icosahedral symmetry, come together in a certain order and thus form a protein envelope around the

genome, which is called the capsid. In viruses with helical symmetry, the capsomeres are side-by-side on the viral nucleic acid and attached to the genome. Viruses are divided into three main parts according to their capsid symmetry. It can be listed as icosahedral (cubic) symmetry, Helical symmetry, and complex structure. Most viruses with cubic symmetry do not have an envelope in their nucleocapsid [29,30].

The viral envelope is found in all animal viruses with helical symmetry, and in some viruses with cubic symmetry. The viral envelope is largely composed of lipids. Mature viruses capable of infecting living cells are called virions. Virions that have completed their maturation development in the cell are surrounded by an envelope during development. The source of the envelope is essentially the cell membrane. As the virion leaves the cell, it buds through the membrane and is surrounded by an envelope [31].

The envelope's main job is to carry the virus's antigenic and biological activities. The viral envelope can come from the membrane of the host cell, the Golgi apparatus, the endoplasmic reticulum, or the nuclear membrane. This depends on the type of virus. The chemical make-up of the envelope of a virus is similar to the chemical make-up of the membrane of the cell from which it comes. At the same time, there are proteins on the envelope that are unique to the virus. Another important thing about envelope glycoproteins is that they help the virus attach to the surface of the host cell, stick to it, and get inside the cell [31].

### 1.1.3. Virus Diagnosis

Rapid, user-friendly, and efficient diagnostic techniques for viral detection are urgently needed. The number of viral epidemic diseases has been increasing all over the world in recent years. Although there has been a decrease in virus-related deaths in parallel with this increase, thanks to the variety of therapies developed, the trend in the number of virus outbreaks have been increasing in the last 30 years. Viruses and bacteria are among the diseases that cause the most deaths in this period. In particular, diseases transmitted from person to person and through insects are increasing. For example, in virus outbreaks, while the number of epidemics was below 50 in the 1980s, this number increased to over 1000 in 2010. On the other hand, non-fatal virus outbreaks also negatively affect human life. For example, influenza epidemics often cause long-term societal problems [32]. In addition to

social losses and negative effects on human life, it also causes treatment costs and loss of workforce [33].

Viruses are one of the factors that negatively affect agricultural production as well as affecting human health. It also affects people indirectly through food products. In general, the detection of epidemic diseases in livestock and agricultural plants is an underdeveloped subject in the world, but it is a subject of intense interest [34]. Rapid and precise detection of viruses or bacteria in agricultural animals is of primary importance in the prevention of new epidemics in both animals and humans [35]. Viruses that threaten the health of animals emerge annually, so the struggle made in the previous year is not always effective. The rapid diagnosis of the causative virus, which may cause an epidemic at the moment, is the most important component of the fight before the epidemic begins. Virus diagnosis can be made by detecting the virus directly in the body fluid taken from the area of infection, or by detecting the antibodies produced by the immune system. However, direct virus diagnosis gives faster and more accurate results. Although diagnostic systems are used for viruses of medical importance, there is a need for biosensors that can give results faster and without the need for specialized personnel. For agricultural viruses, virus diagnosis systems that can make the early diagnosis are not widely used.

Using the RNA-guided RNA endonuclease Cas 13a, Qin et al. created an automated point-of-care assay for the identification of Ebola-RNA. The nonspecific refractive products of Cas13a were monitored using a fluorometer of the proper size for in situ identification following automated microfluidic processes to mix and enhance hybridization. They discovered that the identification time for purified Ebola RNA was 5 minutes, and the LOD value was 20 PFU/mL which corresponds to $5{,}45 \times 10^7$ copies/mL [36]. For the simultaneous detection of the H1N1, H3N2, and H9N2 influenza viruses, Zhang et al. devised a microfluidic system based on nucleic acid hybridization in conjunction with a controlled micro magnetic field. The detection limits for these three viruses are, respectively, 0,21 nM, 0,16 nM, and 0,12 nM, and they can be discovered in as little as 80 minutes. The sample volume used was 3 μL [37].

PCR-based detection methods are also available in the literature. Li et al. designed a real-time PCR and online fluorescence identification biosensor. The LOD value of the target molecule was found to be $1{,}0 \times 10^2$ copies/mL and the analysis time for the HBV virus was 30 minutes [38]. Using the Ebola virus as a test subject, researchers created a microfluidic

system for fluorescence measurements in real-time in a continuous flow-reverse transcription PCR apparatus. The chip includes extensive microfluidic channels for propagating PCR solutions in zones with varying temperatures. The solution initially persisted in the reverse transcription section, where complementary DNA was synthesized from RNA, and as it moved through the heat conversion domain, the complementary DNA was amplified and recognized in real-time. The maximum number of RNA copies/L for identification is 10, and the analysis takes 40 to 60 minutes [39]. To identify the nodavirus prevalent in seafood, Lee et al. created a microfluidic chip containing reverse transcription PCR, capillary electrophoresis, and optical fiber for online identification. The limit of identification was found to be 12,5 copies/μl [40].

Bliss et al. came up with a way to separate viruses using PCR and capillary electrophoresis [41]. It took less than 3 hours to do the analysis. Ishii et al. made a microfluidic quantitative PCR (MFQPCR) that can test the safety of food and water by measuring 11 major human viral diseases at the same time. These include the adenovirus, Aichi virus, astrovirus, enterovirus, human norovirus, rotavirus, and sapovirus. The MFQPCR method was tested on river water in Japan that had been contaminated by waste from a factory. The least amount of cDNA/DNA that can be measured is 2 copies/L [42]. Lung et al. made a microfluidic device that uses multiple RT-PCR and reverse dot blocking to identify viruses that can cause different diseases that can be found in animal feeds and animals. For example, these viruses can cause foot-and-mouth disease (FMD), vesicular stomatitis (VS), and swine vesicular disease (SVD). 144 clinical animal samples were used to test how well this method worked [43].

Due to their size, viruses can't be seen with a light microscope. Because of this, there aren't many papers about how to identify viruses optically. Still, some groups have come up with their own ways to deal with this. Interferometric reflectance imaging is one of them. Using this method, Daaboul et al. made a microfluidic chip that can be used with a single particle interferometric reflectance imaging system [44] to find Ebola, Marburg, and Lassa Fever viruses. Again, the same group made a microfluidic system that can find the virus that causes vesicular stomatitis [45].

Using a point-of-care application to find viral infections early is a key part of managing infections [46]. The current COVID-19 pandemic was a good reminder of how important it is to have quick ways to diagnose viruses. Traditional ways to find viruses usually require

highly trained staff and expensive equipment. In fact, screening detection programs can also prevent diseases caused by the Dengue virus, influenza, and the Human Immunodeficiency Virus (HIV) [47]. Since viruses are the smallest infection-causing agents and can't be seen with the naked eye, they are hard to grow. As a result, methods for precise diagnosis that take time to process and are expensive to use everywhere, such as immunodetection (ELISA) or nucleic acid detection (qPCR), were targeted, such as the identification of surface proteins or genome amplification [48]. Because of this, other methods, like lateral flow strip tests, are needed to find viral illnesses quickly and easily.

## 1.2. CORONOVIRUSES

RNA viruses known as coronaviruses may infect both humans and birds. They may lead to serious or minor pulmonary conditions. The common cold is one of the mild varieties. the Nidovirales order's family Coronaviridae. The Coronovirinae and the Torovirinae are the two subfamilies that make up the Coronoviridae family. There are four genera in the coronovirinae family: alpha, beta, gamma, and delta coronaviruses. There are seven human coronaviruses: SARS-CoV, MERS-CoV, and SARS-CoV-2 are beta coronaviruses, while HCoV-229E, HCoV-NL63, HCoV-HKU1, HCoV-OC43, and HCoV-OC43 are alpha coronaviruses. Upper respiratory infections brought on by HCoV-229E, HCoV-NL63, HCoV-HKU1, and HCoV-OC43 are often minor. SARS-CoV, MERS-CoV, and SARS-CoV-2 are more contagious than other viruses. They may cause lower respiratory tract infections, exacerbate symptoms, and sometimes result in fatalities [49]. The taxonomy of Coronaviruses is shown in Figure 1.1. At the end of 2002, SARS-CoV was declared the first global health emergency of the twenty-first century. It was believed that the virus, which killed hundreds of people, had never existed before. About ten years later, in September 2012, the MERS-CoV virus was discovered. It had never previously been seen in either people or animals. The WHO China Country Office most recently learned about instances of pneumonia with unknown causes in the city of Wuhan in China's Hubei Province around the end of December 2019. A novel coronavirus, 2019-nCoV, which has never previously been seen in humans, was named as the disease-causing agent on January 7, 2020. Later, COVID-19 was used to refer to the 2019-nCoV illness. SARS-CoV-2 was given the moniker because the new virus closely resembles SARS-CoV [50].

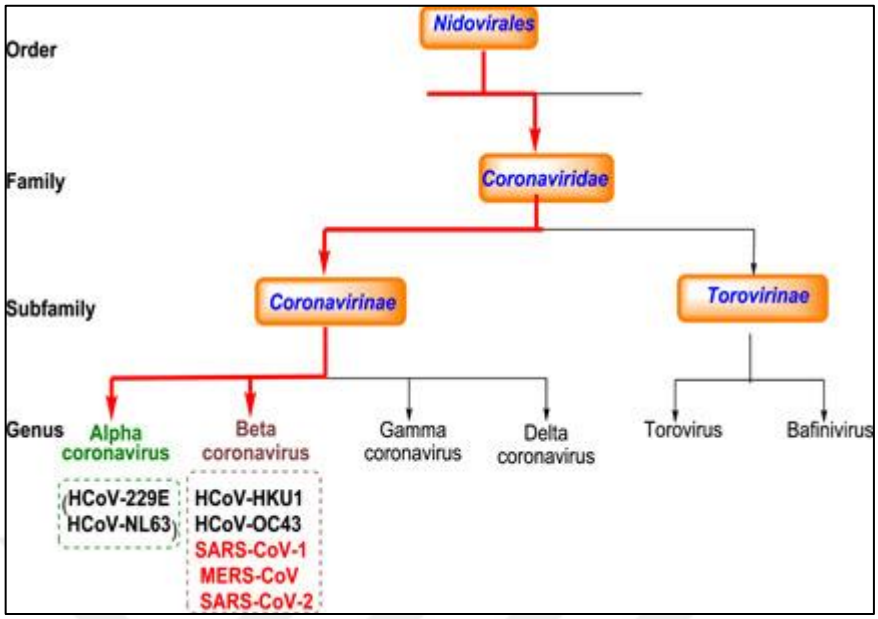


Figure 1.1. Schematic representation of the taxonomy of Coronaviruses [49]

## 1.3. SARS-COV-2: THE MODEL TARGET

Preliminary research on the SARS-CoV-2 virus has shown that the initial source of this new virus may have been wild animals such bamboo rats, raccoons, and snakes sold in the Wuhan city seafood wholesale market.

It is well established that the sources of MERS-CoV and SARS-CoV, respectively, are dromedary camels and civet cats, respectively. Finally, research has shown that certain bat species may be linked to the SARS-CoV-2 virus in humans [51].

SARS-CoV-2 was found in Wuhan, China, and the WHO declared the COVID-19 pandemic on March 11, 2020.

At the NIAID Integrated Research Facility at Fort Detrick, Maryland, SARS-CoV-2 was captured and color-enhanced for transmission electron microscopy (TEM) imaging (Figure 1.2.) [52].

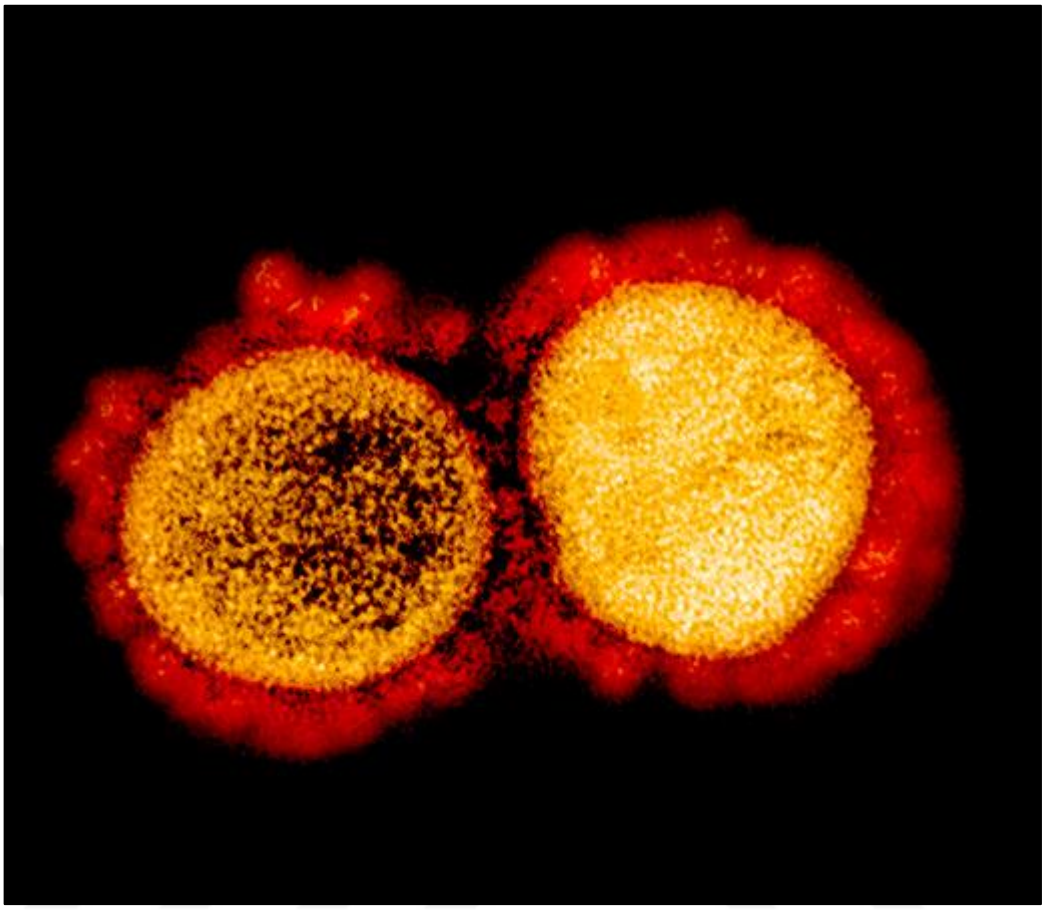

Figure 1.2. Transmission electron micrograph of SARS-CoV-2 virus particles taken from a patient [52]

SARS-CoV-2 may survive outdoors for roughly two hours and is very infectious from an epidemiological perspective. The incubation period after a disease typically lasts between 4 and 8 days, and the quarantine period is at least 14 days long. The SARS-CoV-2 virus poses a serious risk of infection to people of all ages. It is believed that elderly individuals have a higher risk of contracting SARS-CoV-2 [53].

### 1.3.1. Structure of SARS-CoV-2

The coronavirus family includes the sense single-strand RNA virus known as SARS-CoV-2. The complete 29.881 bp SARS-CoV-2 genome (GenBank no. MN908947) has been identified through an RNA metagenomic analysis using next-generation sequencing [54]. The structure of SARS-CoV-2 is shown in Figure 1.3.

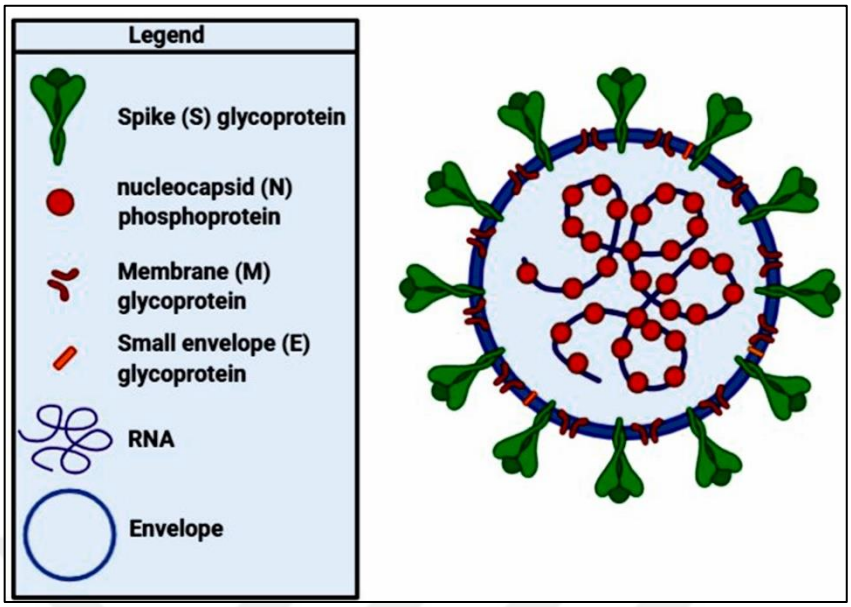


Figure 1.3. Description of SARS-CoV-2 by drawing [55]

29 proteins in total, including 4 structural proteins, 16 nonstructural proteins (Nsp1–16), and 9 accessory proteins, are expressed by SARS-CoV-2 (Figure 1.4.). The genes S (spike), E (envelope), M (membrane), and N all code for structural proteins (nucleocapsid). Accessory proteins are encoded by Open Reading Frame (ORF) 3a, 3b, 6, 7a, 7b, 8, 9b, 9c, and 10 [56]. Only the N protein binds to the RNA genome while the S, E, and M proteins construct the viral envelope. Receptor binding is mediated by the S protein. S1 and S2 subunits are found in glycoproteins referred to as S proteins. Viral infection is catalyzed by the angiotensin receptor 2 (ACE-2) enzyme in the respiratory tract and the S1 subunit of S proteins. The type 1 transmembrane protein ACE-2 is expressed by the host epithelial cell. The fusion is then allowed by the serine protease TGRBSS2, which makes it easier for the virus to enter the cell. Mostly, the e protein directs the assembly and release. The virus's shape is provided by the M protein. The N protein shields RNA. Because of the viral polyproteins ORF1a and ORF1ab, NSPs (NSP1–16) are produced. These proteins participate in transcription, translation, and replication. The primary component of SARS-CoV-2 is RdRp, also known as NSP12, which is crucial for the replication and transcription cycles as well as for the production of viral RNA [57]. NSP12 is thus the main area of attention for the SARS-CoV-2 therapy. NSP9 is a part of the replication complex. It is believed that NSP9 protein dimerization is necessary for viral replication. However, studies have shown that the

interaction between single-stranded nucleic acids (ssDNA and ssRNA) and NSP9 is weak and non-specific [58].

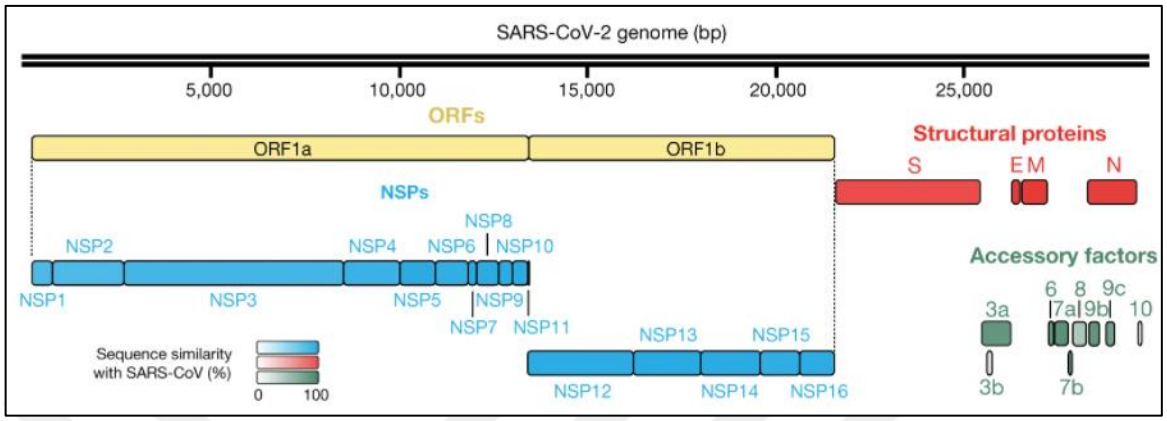


Figure 1.4. SARS-CoV-2 genome annotation [59]

### 1.3.2. Life Cycle of SARS-CoV-2

Angiotensin converting enzyme 2 (ACE2) on ciliated bronchial epithelial cells and type II pneumocytes is the surface receptor for SARS-S CoV-2's glycoprotein. The virus enters these cells in this manner. The S glycoprotein is divided into S1 and S2 subunits. It is simpler for viruses to adhere to their targets when S1 determines the types of cells and the distances between hosts. The S2 component joins the viral and cellular membranes. This permits the virus to undergo endocytosis and enter the cell. The cell surface-associated transmembrane protease serine 2 (TMPRSS2) and cathepsin molecules cleave the trimer S protein when the S glycoprotein attaches to ACE2. Important conformational changes that are required for infection occur next. The early route and the late pathway are the two entrances to a cell's cytoplasm. The virus' membrane and the cell's membrane converge at the cell's surface in the first route. The viral particle enters the cell by endocytosis in the late route before joining the endosomal membrane. The virus initially releases its RNA genome when it enters the cytoplasm. Then, the ORF1a and ORFb genes are translated into pp1a and pp1b, the viral replicase polyproteins. The viral replication and transcription complex is made up of non-structural proteins (nsps), which are then formed from these polyproteins (RTC). Viral genomic RNA is copied in defense-membrane vesicles (DMVs). The viral polymerase produces a number of subgenomic mRNAs by a process known as "discontinuous transcription." The structural proteins of the virus are subsequently produced by the

translation of these mRNAs. The S, E, and M proteins are inserted into the viral envelope in the ER and Golgi intermediate compartments. The genomic RNA and the N protein combine to create a complex (ERGIC). E and M proteins interact with condensates of freshly created genomic RNA and N proteins. This results in the assembly of viral particles. These fresh virus particles are exocytosed out of the infected cells by this procedure. Exocytosis can occur in two different ways: either through the Golgi compartment as in the traditional exocytosis pathway, or through the fusion of deacidified lysosomes with the cell surface membrane (Figure 1.5.) [60].

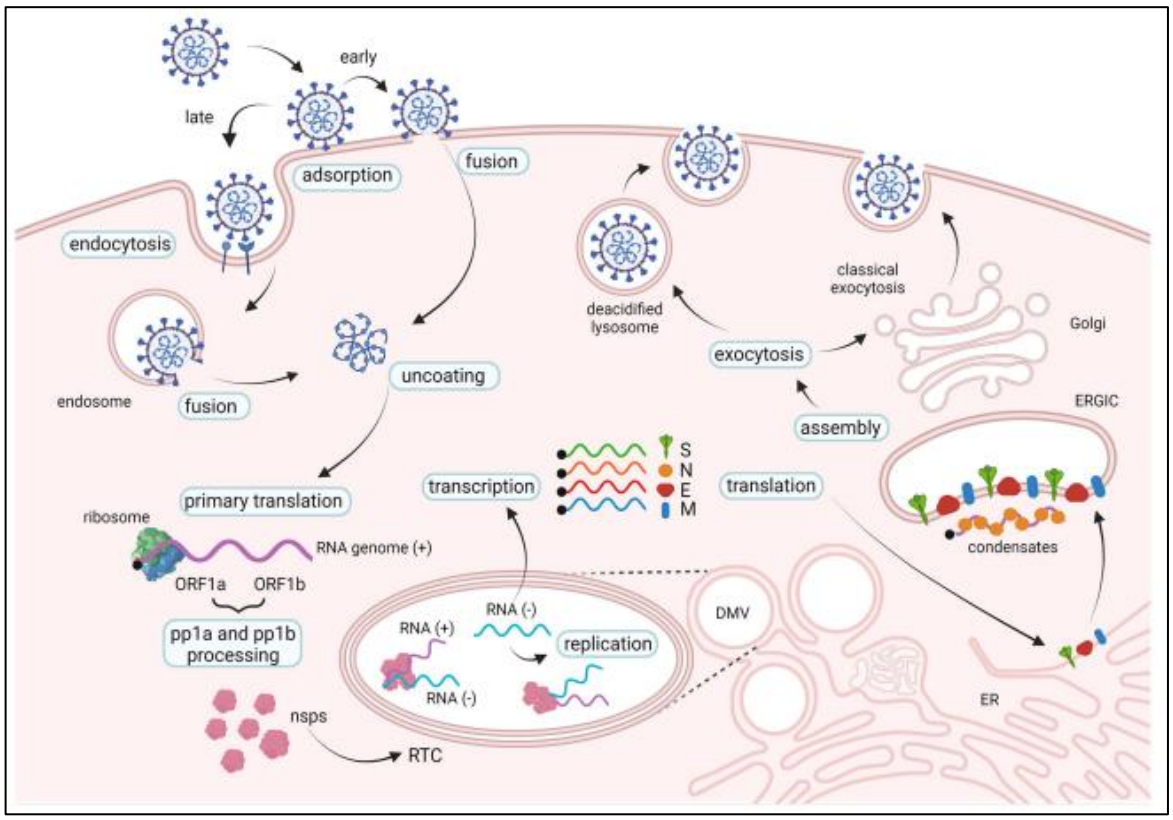


Figure 1.5. SARS-CoV-2 life cycle [60]

### 1.3.3. Covid-19

On February 11, 2020, the World Health Organization (WHO) designated the illness brought on by the SARS-Cov-2 virus as "COVID-19" (coronavirus disease 2019). At the end of 2019, Wuhan, China, reported the first cases of the disease, which then rapidly swept the globe. Beginning in March 2020, when the first positive case was discovered in our nation, this

virus, which spreads quickly, began to exist. It spread quickly and is still having an impact, albeit less so [61].

Signs and symptoms at the start of the disease vary a lot, but many people who have been diagnosed with COVID-19 have had the following symptoms at some point [62].

• Shivering or a fever

• Cough;

• Breathing difficulties or shortness of breath

• Headache;

• loss of taste or smell;

• sore throat;

• congestion and/or runny nose;

• nausea and/or vomiting;

• diarrhea; exhaustion;

• muscle and/or body pains;

Depending on how bad the disease is, the symptoms can be different. For example, COVID-19 patients who are hospitalized more often report shortness of breath than COVID-19 patients who don't need to be hospitalized [62]. People who have COVID-19 often get stomach problems like nausea, vomiting, or diarrhea before their fever and lower respiratory symptoms start. In one study, people often said they had lost the ability to smell or taste, especially in the third group of women and patients who were younger or in their middle years [63].

People who are over 50 years old, have chronic diseases like cancer, COPD, diabetes, or high blood pressure, and are men are more likely to get COVID-19. Children and young adults are more likely to be carriers who don't have any symptoms [64].

WHO has been told about 630.387.858 confirmed cases of COVID-19 around the world, including 6.583.163 deaths [65]. WHO [66] says that there have been a total of 16.919.638

cases in Turkey, with a total of 101.203 deaths. Table 1.3 shows the number of COVID-19 cases and deaths around the world and for each WHO region.

Table 1.3. COVID-19 Situation

| Name | Cases (Cumulative Total) | Cases (Newly Reported in last 7 days) | Deaths (Cumulative Total) | Deaths (Newly Reported in last 7 days) |
|---|---|---|---|---|
| Global | 630.387.858 | 2.068.515 | 6.583.163 | 7.351 |
| Europe | 262.088.023 | 701.470 | 2.122.104 | 2.186 |
| Americas | 180.429.028 | 379.002 | 2.859.144 | 3.414 |
| Western Pasific | 94.824.020 | 926.732 | 277.586 | 1.271 |
| South-East Asia | 60.507.835 | 46.651 | 800.640 | 364 |
| Eastern Mediterranean | 23.168.524 | 11.118 | 348.777 | 62 |
| Africa | 9.369.664 | 3.542 | 174.799 | 54 |

### 1.3.4. Covid-19 and Thalassemia

In the world, β-Thalassemia is the most prevalent inherited disease. The main treatment for β-thalassemia is repeated blood transfusions and iron chelation. In additon, bone marrow transplantation can be used to treat some patients. There are also new treatment researches such as gene therapy. However, in a routine treatment, gene therapy is not used yet. Thalassemia syndromes are divided into transfusion-dependent and non-transfusion-dependent thalassemias. In thalassemia, damage may occur in many organs such as heart,

liver, lung and endocrine organs due to ineffective erythropoiesis, anemia and iron overload [67]. It is also known that there are changes in the natural and adaptive immune system in thalassemia patients. For example, deterioration in neutrophil function/chemotaxis and monocyte/macrophage phagocytic activity, decrease in natural killer and complement system activity, and deterioration in T and B cell functions. These changes in the immune system, together with the comorbidities that can be seen in thalassemias, suggest that there may be a risk and susceptibility to COVID-19, especially in elderly patients [68].

Sezaneh H. et al. looked at how often COVID-19 infection happened and how many people died from it among people with -thalassemia and sickle cell disease from the start of the COVID-19 pandemic to June 15, 2020. COVID-19 is found in 1,34 out of every 100.000 people with -thalassemia every day. But among people with sickle cell disease, the rate of COVID-19 was 17,22 per 100.000 person-day [69].

### 1.3.5. SARS-CoV-2 and Variants

SARS-CoV-2 variations are separated into "Variants of Concern" (VOC) and "Variants of Interest" (VOIs) by the WHO. Unusual occurrences, such as variations in clinical presentation, transmissibility, and disease severity, are brought on by variants. It is referred to be a VOC if these changes are obvious. However, the modifications are referred to as VOI [70] if they are unclear and under study. The WHO recognized five distinct VOCs, which are Alpha, Beta, Delta, Gamma, and Omicron, as shown in Table 1.4. The first instances of the Alpha variant were observed in the UK in September 2020, followed by those of the Beta variant in South Africa in May 2020, the Gamma variant in Brazil in November 2020, the Delta variant in India in October 2020, and the Omicron variant in numerous locations in November 2021 [70].

Table 1.4. SARS-CoV-2 Variants of Concern

| **WHO Label** | **Pango Lineage** | **Earliest Documented Samples** | **Date of Designation** |
|---|---|---|---|
| Alpha | B.1.1.7 | United Kingdom, September 2020 | 18.12.2020 |
| Beta | B.1.351 | South Africa, May 2020 | 18.12.2020 |
| Gamma | P.1 | Brazil, November 2020 | 11.01.2021 |
| Delta | B.1.617.2 | India, October 2020 | 11.05.2021 |
| Omicron | B.1.1.529 | Multiple countries, November 2021 | 26.11.2021 |

The WHO found 8 distinct VOI, including versions of Epsilon, Zeta, Eta, Theta, Iota, Kappa, Lambda, and Mu (Table 1.5.). The first reports of the Epsilon variant came from the USA in March 2020, followed by those for the Zeta variant from Brazil in April 2020, the Eta variant from a number of different countries in December 2020, the Theta variant from the Philippines in January 2021, the Iota variant from the USA in November 2020, the Kappa variant from India in October 2020, the Lambda variant from Peru in December 2020, and the Mu variant from Colombia in January 2021 [71].

Table 1.5. SARS-CoV-2 Variants of Interest

| WHO Label | Pango Lineage | Earliest Documented Samples | Date of Designation |
|---|---|---|---|
| Epsilon | B.1.427, B.1.429 | USA, March 2020 | 05.03.2021 |
| Zeta | P.2 | Brazil, April 2020 | 17.03.2021 |
| Eta | B.1.525 | Multiple countries, December 2020 | 17.03.2021 |
| Theta | P.3 | Philippines, January 2021 | 24.03.2021 |
| Iota | B.1.526 | USA, November 2020 | 24.03.2021 |
| Kappa | B.1.617.1 | India, October 2020 | 04.04.2021 |
| Lambda | C.37 | Peru, December 2020 | 14.06.2021 |
| Mu | B.1.621 | Colombia, January 2021 | 30.08.2021 |

Figure 1.6. shows the emergengence of SARS-CoV-2 over time.

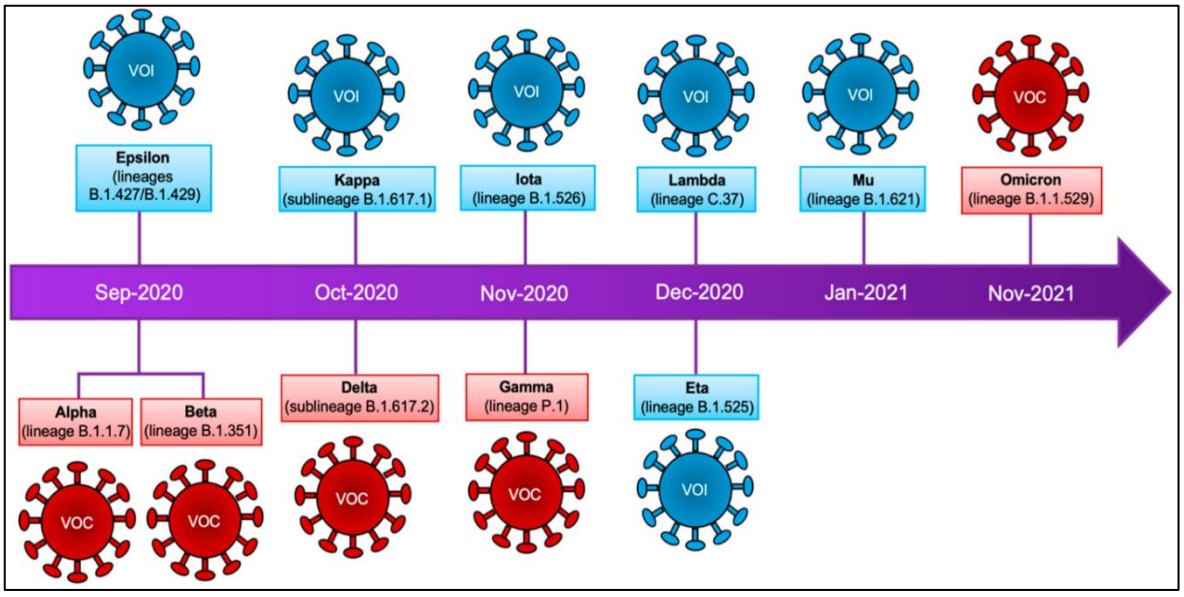


Figure 1.6. Timeline of variants of SARS-CoV-2 [72]

The United States Centers for Disease Control and Prevention (CDC) has created a new group of variants called "Variants of High Consequencies" by adding to the WHO's

definitions of VOC and VOI. This group includes variants in which medical measures are insufficient, response to treatment is decreased, and immune response is evident. However, there is no variant identified in this group, yet.

Considering that variants will have a very important role in determining the future of the epidemic, the importance of preventing human-to-human transmission becomes even more clear. As this transition continues, the probability of new mutations and the emergence of new variants in the virus increases. For this reason, countries allocate resources to the follow-up of variants. For example, USA, follow-up of variants on April 16, 2021, that is, he allocated 1,7 billion dollars for genomic surveillance [73].

### 1.3.6. SARS-CoV-2 and Mutations

RNA viruses often exhibit the greatest mutation rates, ranging from 104 to 106 mutations per base pair [74], since RNA-dependent RNA polymerases (RdRp) cannot check for errors. On the other hand, the coronavirus family of viruses' exoribonuclease (ExoN) domain is known to include a mechanism for detecting errors [75]. Among coronaviruses, the nsp14-ExoN is likewise well recognized for being relatively stable [76]. Therefore, a modest rate of mutation was anticipated at the beginning of the virus's dissemination. However, more than 6 million viral genomes have been logged by the Global Initiative on Sharing All Influenza Data (GISAID) during the last two years [77].

The spike protein was discovered to have undergone its initial mutation a few months after the SARS-CoV-2 epidemic [77]. This could be the case since there are so many illnesses that can spread globally. Additionally, Gribble et al. conducted studies to demonstrate that nsp14-ExoN may be crucial for RNA recombination activities during viral replication, which might result in genetic alterations [76].

A three-part protein called the spike glycoprotein penetrates the membrane. It is the primary protein and the major target of diagnosis and therapy since it explains the pathophysiology of the virus and how it selects its host [78]. Therefore, any alteration to the S protein has the potential to alter the bacteria's pathogenicity and virulence. Adaptive changes to the S protein may further facilitate the virus's ability to propagate, infect the host, and evade the host immune system [79]. One of the first mutations discovered, D614G increases the quantity

of S-proteins on the surface of the virus, making it more contagious [80]. Glycine replaces aspartic acid at position 614 (D614) in this mutation (G614). The variations of Alpha, Beta, Delta, Gamma, and Omicron may all include this mutation, which is also highly frequent [79]. However, due to their great conservation and moderate rate of change, the M and E proteins are also crucial screening indicators for coronavirus infection [81]. All coronaviruses have a similar N gene. Because it changes less often than the S-protein, it is also more stable [82]. The ORF1a/b gene is in charge of maintaining and duplicating the viral genome and produces non-structural proteins (nsp1–16) [83]. In order to boost viral replication or treatment resistance, adaptive mutations in the ORF1a/b gene are also known to increase the virus's risk. The function of a protein may also be negatively altered by mutations in other proteins that interact with it [79].

Table 1.6 lists the potentially dangerous mutations on the spike glycoprotein, M, E, and N proteins, non-structural proteins, and accessory proteins for the Alpha, Beta, Delta, Gamma, and Omicron variants [84].

Table 1.6. Mutations on structural proteins or non-structural proteins for Variants of Concerns (VOCs)

| | **B.1.1.7 (Alpha)** | **B.1.351 (Beta)** | **P.1 (Gamma)** | **B.1.617.2 (Delta)** | **B.1.1.529 (Omicron)** |
|---|---|---|---|---|---|
| **Spike** | H69del, V70del, Y144del, N501Y, A570D, D614G, P681H, T716I, S982A, D1118H | D80A, D215G, L241del, L242del, A243del, K417N, E484K, N501Y, D614G, A701V | L18F, T20N, P26S, D138Y, R190S, K417T, E484K, N501Y, D614G, H655Y, T1027I, V1176F | T19R, E156del, F157del, R158G, L452R, T478K, D614G, P681R, D950N | A67V, H69del, V70del, T95I, G142del, V143del, Y144del, Y145D, N211del, L212I, G339D, S371L, S373P, S375F, K417N, N440K, G446S, S477N, T478K, E484A, Q493R, G496S, Q498R, N501Y, Y505H, T547K, D614G, H655Y, N679K, P681H, N764K, D796Y, N856K, Q954H, N969K, L981F |
| **Nucleocapsid** | D3L, R203K, G204R, S235F | T205I | P80R, R203K, G204R | D63G, R203M, D377Y | P13L, E31del, R32del, S33del, R203K, G204R |
| **Envelope** | | P71L | | | T9I |
| **Membrane** | | | | I82T | D3G, Q19E, A63T |
| **Orf1a** | T1001I, A1708D, I2230T, S3675del, G3676del, F3677de | T265I, K1655N, K3353R, S3675del, G3676del, F3677del | S1188L, K1795Q, S3675del, G3676del, F3677del | | K856R, S2083del, L2084I, A2710T, T3255I, P3395H, L3674del, S3675del, G3676del, I3758V |
| **Orf1b** | P314L | P314L | P314L, E1264D | P314L, G662S, P1000L | P314L, I1566V |
| **Orf3a** | | Q57H | S253P | S26L | |
| **Orf7a** | | | | V82A, T120I | |
| **Orf8** | Q27*, R52I, Y73C | | E92K | D119del, F120de | |
| **Orf9b** | | | | T60A | P10S, E27del, N28del, A29del |

### 1.3.7. SARS-Cov-2 and Vaccines

There are many platforms being used to produce COVID-19 vaccines. These include viral vector vaccines (replicative and non-replicative), recombinant protein [protein subunit and virus like particle (VLP)] vaccines, nucleic acid-based DNA and mRNA vaccines, and complete viron vaccines (live attenuated, inactivated) [85].

SARS-CoV-2 is grown in cell culture to create inactivated vaccines, which are subsequently treated with chemicals to prevent the virus from proliferating. The dormant virus is often combined with an adjuvant, such as aluminum, to boost the immune response. Inactive vaccinations are administered intramuscularly. You require a biosafety level 3 facility to manufacture them. The SARS-CoV-2 inactivated vaccine will trigger the immune system to fight additional viral components in addition to the spike protein. The majority of COVID-19 vaccinations now in use were produced in China and India. The Sinovac firm created the Coronavac vaccine in this manner. Because the body cannot produce additional inactivated vaccines, they must be administered more than once [85,86].

Live attenuated (attenuated) vaccines are created by genetically altering the wild-type virus or subjecting it to adverse conditions so that it loses its capacity to spread disease but retains its capacity to immunize people. This weaker virus replicates itself in the recipient's body to elicit an immune response, but it does not really cause illness. It is well known that the live attenuated COVID-19 vaccination enhances cellular and humoral protection against several attenuated virus components. Another advantage of live attenuated vaccines is that they may be administered nasally. This may prevent the virus from entering by making the upper respiratory tract's mucosa immune. However, there are additional security issues with live attenuated vaccines, such as the potential for the virus to revert to its wild-type state or combine with it. In preclinical and clinical development are a number of live attenuated COVID-19 vaccines [87, 88].

RNA vaccines are vaccines for SARS-CoV-2 that represent a completely new vaccine approach. While the Pfizer/BioNTech (BNT-162b2) vaccine was the first mRNA vaccine approved for use in humans, it is a technology that has been trialled for more than 20 years to develop vaccines against cancer and other infections in humans. In addition, Moderna vaccine is mRNA vaccine. In the SARS-CoV-2, the vaccine consists of mRNA encoding the

spike protein. The mRNA delivered to the cell is read here and spike proteins are synthesized. Instead of giving viral protein to the body as a vaccine, genetic material is given to synthesize the protein in question. It is delivered in a lipid nanoparticle (LNP) that surrounds the mRNA molecule to protect the easily degraded RNA. Once inside the cell, lipases in the cell break down the LNP structure and the mRNA becomes free in the cytoplasm. The spike protein synthesized in the cell by reading the codes in the mRNA goes out of the cell and creates the desired immunity by stimulating both humoral (antibody) and cellular (T cell) immunity. The mRNA remains in the cell cytoplasm and never enters the nucleus. Therefore, it does not interact with or integrate with the recipient's DNA and is degraded in the cytoplasm within 72 hours. Since mRNA is easily degraded, it must be stored at very low temperatures [89].

In vector vaccines, RNA is introduced into the body by putting it into living or non-living vectors such as adenovirus. Thus, it is aimed that the RNA in question produces the desired proteins and those proteins stimulate the immune system [87].

In replicative vector vaccines, replicative vectors are produced from attenuated virus strains. Replicative vectors stimulate the immune system more strongly because they have the ability to replicate in vaccinated individuals. For this reason, the immunity they create is stronger than non-replicative vector vaccines[90].

Nonreplicative vector vaccines are designed to express the intended immune target viral protein using non-replication vectors. Adenovirus is most commonly used in viral vector vaccines. Pre-existing immunity to the vector which can reduce the immunogenicity of the vaccine is a disadvantage of vector vaccines Sputnik-V and Oxford/AstraZeneca (AZA-1222) vaccines are examples of viral vector vaccines [91].

Viral proteins make up recombinant protein vaccines. Protein subunit vaccinations often concentrate on the virus's spike protein or receptor-binding component. To make these vaccinations more effective, immunostimulating adjuvants could be required. When a virus-like particle (VLP) is employed in vaccinations, empty virus shell antigens are used. Due of their absence of genetic material, they are not infectious. They can develop a robust immunity, but it is challenging to produce them. Recombinant spike proteins, recombinant receptor binding domains, and virus-like particle (VLP) vaccines are among the recombinant COVID-19 vaccines currently under development [87, 92].

Only 254 of 416.900 recipients of the Pfizer-BioNTech vaccine who received a double dose were found to have SARS-CoV-2 infection when the effectiveness of alpha variant vaccines was investigated [93]. All of these patients recovered only mildly from the infection. Similarly, the effectiveness of Oxford-AstraZeneca, Novovax and Moderna vaccines on alpha variant has been reported to be similar to their effectiveness on the original virus [94,95,96]. Globally, 12.943.741.540 vaccine doses were administered. 5.444.421.268 persons were vaccinated with at least one dose and 4.988.424.268 persons were fully vaccinated according to WHO [97]. In Turkey, % 93,34 of population over 18 years old received first dose of vaccines and % 85,67 of population received second dose of vaccines. Totally, 152.520.042 first second and third doses were applied [98].

### 1.3.8. SARS-CoV-2 Detection

Fast viral detection technologies were required during the COVID-19 pandemic since conventional methods of detecting viruses often call for costly equipment and highly experienced personnel. Better imaging and detection techniques are urgently required as shown by the rapid worldwide spread of COVID19, which was brought on by the SARS-CoV-2 virus, and the delayed and often inaccurate testing. Computer tomography (CT), single photon emission computer tomography (SPECT), and positron emission tomography are all used for virus imaging (PET) [99]. These procedures are expensive, inaccurate, and, in the case of CT, can only identify viral infections that have obvious symptoms, such as pneumonia or observable lung lesions. In order to diagnose COVID19, CT has therefore been used as a supplemental technique in recent years [100]. Enzyme-linked immunosorbent assays (ELISA) or reverse-transcription polymerase chain reactions (RT-PCR) are often used with immunofluorescence to detect infections and viruses. Currently, RT-PCR is the most effective method for locating SARS-CoV-2, but it is a multistep procedure that requires purification, nucleic acid amplification, and fluorescence detection. The procedure requires a skilled operator, takes a long time, often yields false-negative findings, and is difficult to locate in areas with limited resources. As a result, the assay created for this research can compete with all of these methods. Since viruses are very tiny infectious organisms that cannot be seen with the human eye, finding and cultivating them is difficult. Because accurate diagnostic methods like immunodetection (ELISA) or nucleic acid detection (PCR)

are costly and take time to implement globally [101], the two aims are surface proteins or genome amplification.

There are several COVID-19 diagnostic approaches in use right now, as well as constant advancements and developments such point-of-care (POC) diagnostic kits and biosensors. The several diagnostic techniques for identifying SARS-CoV-2 are shown in Figure 1.7. [102].

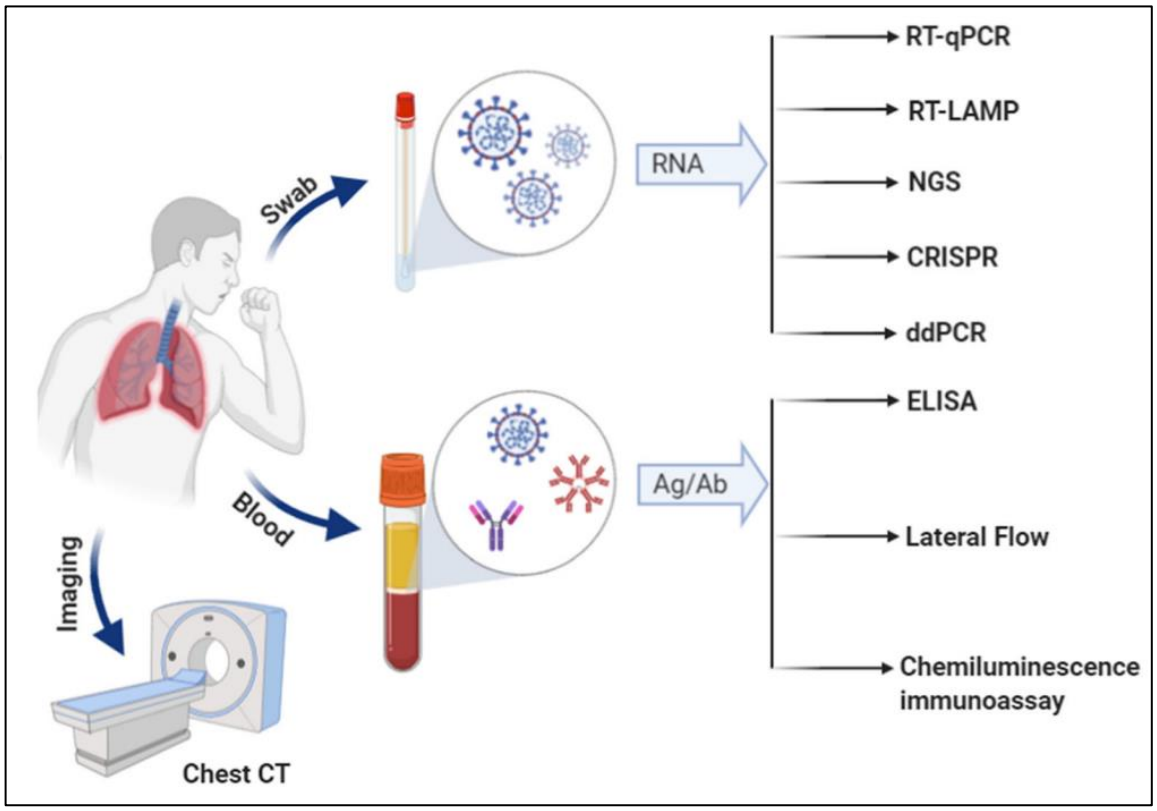


Figure 1.7. Diagnostic methods SARS-CoV-2 [102]

There are currently three ways to diagnose SARS-CoV-2: computed tomography imaging of the chest, virus RNA identification, or immunoassay of blood antibodies produced after infection. The SARS-CoV-2 viral RNA is often discovered using nucleic acid hybridization or PCR methods. First, a swab sample is obtained. Several molecular methods, including reverse transcriptase real-time PCR (RT-PCR), loop-mediated isothermal amplification-based assay (RT-LAMP), next-generation sequencing (NGS), clustered regularly interspaced short palindromic repeats (CRISPR), and droplet digital PCR, can be used to detect SARS-CoV-2 after it has been introduced. The gold standard during the Covid-19

epidemic was RT-PCR. Blood samples are also used for serological assays such as ELISA, Lateral Flow, and Chemiluminescence Immunoassay. The most used technique in immunology and serology for identifying viral antibodies or antigens is ELISA [102].

RT-PCR-dependent detection has mostly been used to find virus genomes because it is a very reliable method. Large-scale monitoring is hard to do with this technology because of how long the process takes, how low the viral load is, how inaccurate the samples are, and how specialized workers and complicated equipment are needed. This can lead to false-negative results.

The Centers for Disease Control and Prevention (CDC) and WHO [103] say that urgent cases of SARS-CoV-2 should be tested quickly. A quick diagnosis is needed to stop the spread and limit the number of people who get sick. Because of this, other quick tests have been made. Here, a mesoporous silica nanoparticle-based biosensor was supposed to be made by focusing on the SARS-CoV-2 genome's NSP12, NSP9, and E genes. This was done to get around some problems with RT-PCR.

A generic detection approach based on the direct detection of viral nucleic acid was developed in this work using CoV-2 viral RNA as a proof-of-concept model for all RNA viruses.

The majority of the time, clinical samples from the upper respiratory tract were tested for the presence of SARS-CoV-2 using nasopharyngeal swab collections [104]. With this technique, 45,5% of nasopharyngeal swabs and 71,3% of lower respiratory tract swabs yielded positive findings, but none in the urogenital tract. Because it is a highly dependable approach, RT-PCR was used. Since swab samples were treated before PCR, the findings' accuracy was not very excellent. The technique itself is a challenging operation that can only be completed by skilled laboratory personnel in order for the test to be effective and to prevent errors with the samples. Although RT-PCR is a reliable method for detecting SARS-CoV-2 [103], the CDC and WHO have been working to develop accurate assays that are simple to use and comprehend. A prompt diagnosis is required to halt the spread and reduce the number of cases. These features have enabled the development of several innovative techniques for diagnosing SARS-CoV-2. Here, we demonstrate that, despite the limitations of RT-PCR, mesoporous nanoparticles may be employed to create a biosensor that can rapidly and precisely detect SARS-CoV-2.

Applications of nanotechnology in the medical field have had a considerable influence on diagnostic and monitoring instruments. To perform the test and avoid sample errors, the technique itself is a challenging process that requires the assistance of trained laboratory professionals. The CDC and WHO have pushed for the development of rapid, simple-to-use tests that are reliable for diagnosing SARS-CoV-2 despite the fact that RT-PCR is a powerful method for detecting SARS-CoV-2 [103]. An early diagnosis is essential to halt transmission and control the progress of the disease. As a consequence of these variables, many SARS-CoV-2 diagnostic techniques have recently been created. Here, we show a mesoporous nanoparticle-based biosensor for rapidly and precisely detecting SARS-CoV-2 despite a number of issues with RT-PCR. For bacteria in food specimens, on environmental samples, and in vivo utilizing animal-infection models with Staphylococcus aureus, antibiotic delivery using aptamer-gated mesoporous silica has been reported [105–109]. Similar to this, mesoporous apertures that may house infections were closed off by DNA probes. The limit of detection (LOD) for Listeria monocytogenes using lateral flow biosensors based on aptamer-gated mesoporous silica was fewer than 100 cells in this setting, according to a recent research [110]. Another example uses a mesoporous silica-based solution biosensor with nuclease-sensitive oligonucleotide probes to directly detect S. aureus in blood samples [111]. Additionally, it has been said that single-stranded DNA probes have been utilized to detect mutations in a variety of targets, such as ions, mRNA, and genomic DNA [112–114]. We previously discussed the use of DNA probe-gated mesoporous silica nanoparticles in a nanosensor for the detection of thalassemia mutations [115]. Similar results by Ribes et al. [116] suggest that micro RNA (miRNA) may be detected by oligonucleotide-gated silica nanoparticles at 0,25 pM. The researchers immobilized probe DNA sequences corresponding to miRNA-145 to cover the mesopores of silica nanoparticles that were fluorescent in their study.

When used in clinical and scientific contexts, fluorescence-based sensing and imaging offers special advantages such high sensitivity, high temporal resolution, the availability of biocompatible imaging agents, and the fact that it is noninvasive [117]. The most popular kind of sensors nowadays are fluorescence-based optical biosensors [118]. This is due to the market's availability of various fluorescence probes, premium optical fibers, and complementary optical equipment. Fluorescence is an inexpensive and accessible instrument since it doesn't need much electricity to start working. A smartphone-sized gadget was used

in a research to take photographs of fluorescent nanoparticles and viruses. It must overcome issues like photobleaching, artifacts brought on by the orientation of transition dipoles, and the difficulty of multiple target molecules emitting visible fluorescence signals before it can be utilized to detect viruses [119].

The intensity, energy transfer, lifespan, and quantum yield of fluorescent biosensors may all be used to detect viruses [120]. Forster resonance energy transfer is often employed in these biosensors to identify small interactions (10 nm) between an analyte and a fluorophore (FRET). By using FRET, radiation from a donor is absorbed and transmitted to an acceptor without releasing any radiation [121]. FRET microscopy is a helpful technique for imaging and detecting in the biological sciences as a result of recent advancements in FRET research and optical technology [122].

Depending on the wavelengths at which the sensors are activated and the time at which they emit light, the fluorescence emission from those sensors may either be upconverted or downconverted. When the wavelength of the radiation is less than the wavelength of the excitation, upconversion occurs (antiStokes shift). Autofluorescence may be decreased, sample penetration can be made deeper, the signal-to-noise ratio can be raised, and biosensing can be made more chemically and physically stable by converting near-infrared excitation wavelengths to shorter visible wavelengths. The most typical kind of linear fluorescence is down conversion. Longer wavelengths than those utilized to excite the light are created using fluorescent light. In this investigation, down conversion fluorescence was employed.

A colorimetric test with sufficient specificity for the N-gene (nucleocapsid phosphoprotein) of SARS-CoV-2 was created using gold nanoparticles and capped by thiol-modified antisense oligonucleotides. The quantity of virus injected may have an impact on how well it performs, however it showed promise for the selective and visual naked-eye diagnosis of COVID-19 (10 minutes) [123]. When the target RNA sequence of SARS-CoV-2 was present, thiol-modified antisense oligonucleotide-capped gold nanoparticles clumped together more and the surface plasmon resonance altered (SPR). Additionally, the RNA strand and the RNA-DNA hybrid might be separated using RNaseH. As a result, additional gold NPs would condense and precipitate out in the solution. At a LOD of around 0,18 ng L1, the test was utilized to determine how effectively it could distinguish MERS-CoV viral RNA from SARS-CoV-2 viral RNA. This research demonstrated that SARS-CoV-2 may be

distinguished and seen using simple experimental techniques. The test used in this research outperforms similar assays in that it provides data straight from swab samples while maintaining the same degree of sensitivity.

Graphene nanostructures, organic conjugated polymer nanoparticles, carbon dots (CDs), and other light-emitting substances known as fluorophores are only a few examples of the fluorophores used in fluorescence-based optical biosensors [124]. QDs are very tiny particles (1–10 nm in all three dimensions) having distinctive optical and electrical characteristics. They are also known as "colloidal semiconductor nanocrystals." Due to quantum confinement, the wavelengths of QD emission may be altered from the ultraviolet to the near-infrared. Quantum yield, photostability, the capacity to alter the wavelength of their emissions, Stokes shift, and the shape of their absorption and emission profiles are just a few of the reasons that QDs outperform small molecule organic dyes. They are now among the materials for fluorescence sensing that have received the most research. Numerous research have examined their potential as fluorescence biosensors. For instance, single viruses have been tracked in a lab environment using this material's strong photoluminescence, wide emission spectrum that can be tailored for size, and photochemical stability. To create azido-derivatized NIR QDs that could be dissolved in water and were used to monitor and photograph the avian influenza H5N1 pseudotype, Pan et al. swapped out the hydrophobic ligands that naturally occur in quantum dots with multidentate polymer ligands with imidazole pendant groups [117]. Water-soluble QDs were applied to the virus particles using biorthogonal chemistry, a chemical technique that doesn't obstruct normal biological functions. By tagging the animals, it was feasible to monitor viral respiratory illnesses without endangering the animals. A bionic test was developed in another research to identify thrombin activity, a marker for conditions including thrombosis, hemophilia, atherosclerosis, and inflammation. This test is based on peptide-modulated CdTe QD aggregation, in which the surface charge of CdTe QDs is controlled by the hydrolysis of a thrombin substrate peptide [125]. However, the majority of QDs include hazardous compounds, which poses a significant threat to their in vivo long-term toxicity. As a result, new environmentally friendly light-emitting nanomaterials have been created, including carbon dots and conjugated polymer nanoparticles (CP NPs) [126]. It is more difficult to visualize these things, albeit [127]. In this investigation, a fluorophore compound was utilized as a reporter molecule.

It is crucial to learn as soon as possible about COVID-19. In order to lessen the likelihood of serious issues, it is generally vital to acquire a diagnosis as soon as feasible. The majority of the time, severe COVID-19 infections are associated with potentially fatal risk factors including age and immunological status. For instance, those who are older or have weakened immune systems are more susceptible to significant health issues. A very high risk of developing a serious illness from COVID-19 exists in those who take medications that impair their immune systems or who are receiving treatment for cancer. A moderate risk of illness exists in people over 65, as well as those who already have diabetes, renal disease, or asthma. In order to prevent the condition from becoming worse and preserve lives, medical care must begin immediately [128].

## 1.4. AIM OF STUDY

The objective of this research was to develop a biosensor based on a DNA probe that could quickly and accurately identify the NSP12, NSP9, and E genes of the SARS-CoV-2 genome from samples obtained from the nose and throat. The viral RNA in the samples binds to DNA oligonucleotide probes that are affixed to the surface of mesoporous silica nanoparticles that are loaded with fluorescein molecules in this procedure. Due to the hybridization and release of fluorescein molecules from the target RNA region in the samples and the probe oligonucleotides, the fluorescence signal is produced (Figure 1.8.).

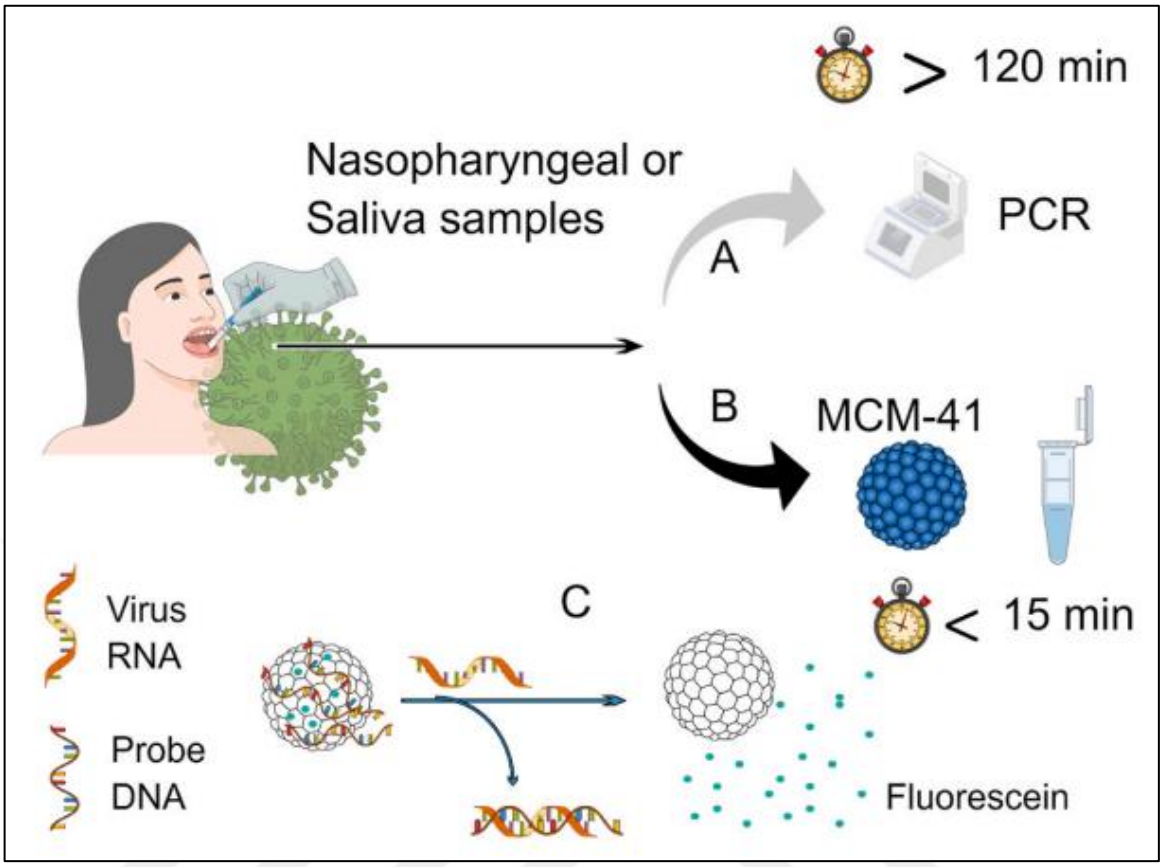


Figure 1.8. Comparing the approach for SARS-Cov-2 detection put out in this thesis with the conventional PCR-based method. (A) RT-PCR can be used to process samples from Cov-2-infected individuals by converting viral RNA to cDNA, which is then applied to the PCR amplification of particular areas. (C) Infected patients' nasopharyngeal swab samples were used to quickly identify the virus using a molecular diagnostic biosensor

# 2. MATERIALS

## 2.1. INSTRUMENTS

The following are the tools used in this study:

- Precision Balance (Ohaus)
- Orbital Shaker (Alfagen)
- Ultrasonicator (Isolab)
- Centrifuge (Labnet Prism$^{TM}$ Microcentrifuge)
- Zetasizer (Malvern Nano ZS)
- FTIR (Thermo Scientific, NicoletTM iS50 FTIR- OMNIC 0.9, ATR).
- Fluorescence Microplate Reader (Thermo Scientific)
- Transmission electron microscopy (TEM) (JEM 2100 Plus Electron Microscope, Jeol)

## 2.2. EQUIPMENT

The following list of laboratory tools was used in this study:

- Automatic pipettes 1000 µl, 200 µl, 20 µl, 10 µl and their tips
- Polypropylene Centrifuge Tubes 50 ml, 15 ml, 1,5 ml
- 96-well plate

## 2.3. CHEMICALS

- MCM-41 type (hexagonal) mesoporous silica nanoparticles (Sigma-Aldrich)
- 99,8% Acetic Acid Glacial (Sigma-Aldrich)

- Ethanol Absolute (Sigma-Aldrich)
- (3-Aminopropyl)triethoxysilane (APTES)
- Fluorescein
- Phosphate Buffered Saline (PBS)

The DNA or RNA molecules were created by Sentromer (Istanbul, Turkey). Table 2.1 contains a list of the hybridization probes used in the experiments. The complementary DNA molecules are the positive strand of SARS-CoV-2 RNA, whereas the probe oligonucleotides are the complementary sequences to SARS-CoV-2 RNA.

Table 2.1. Sequences of the hybridization probes and oligonucleotides utilized in this study

| **Probe** | **Sequences** |
|---|---|
| $NSP12_{PROBE}$ | 5'- TAC CGG CAG CAC AAG ACA TCT -3' |
| $NSP12_{COMP}$ | 5'- AGA UGU CUU GTG CTG CCG GUA -3' |
| $E_{PROBE}$ | 5'-CGA AGC GCA GTA AGG ATG GCT AGT GT-3' |
| $E_{COMP}$ | 5'-ACA CUA GCC AUC CUU ACU GCG CUU CG-3' |
| $NSP9_{PROBE}$ | 5'- CCT ACC TCC CTT TGT TGT GTT GTA GTA AGC TAA CGC AT-3' |
| $NSP9_{COMP}$ | 5'- UG GCG UUA GCU UAC UAC AAC ACA ACA AAG GGA GGU AGG -3' |

The University of Health Sciences Kartal Dr. Lutfi Kirdar City Hospital's ethical committee gave its approval to this study under reference number 2021/514/202/45. The Declaration of Helsinki was followed when conducting the study. All patient samples were taken using blind sampling (no names).

# 3. METHODS

## 3.1. CHARACTERIZATION OF MCM-41 NANOPARTICLES

In this study, MCM-41 type of mesoporous silica nanoparticles was used. First of all, the characterization of this nanoparticle was done by using different techniques.

### 3.1.1. Transmission Electron Microscope (TEM)

Firstly, 0,00001 g MCM-41 powder were weighed. 10x, 100x and 1000x MCM-41 particles were prepared inside PBS. MCM-4 particles were sonicated for 10 minutes and filtered. 10 µl sterile water was added onto front part of TEM grid waited for 2 minutes then water was taken with filter paper. Again, 10 µl sterile water was added onto front part of TEM grid waited for 2 minutes then water was taken with filter paper. After that, sample was applied by drop-casting method onto copper carbon grid and waited until dry (Figure 3.1.). Transmission electron microscopy (TEM) analysis was done at 120 mV.

Figure 3.1. The grid preparation for the TEM characterization with MCM-41 nanoparticles

In addition, MCM-41 particles were also prepared in ethanol with ultrasonically processed for 10 minutes and filtered. Transmission electron microscopy (TEM) analysis was done at 120 mV (JEM 2100 Plus Electron Microscope, Jeol).

### 3.1.2. Dynamic Light Scattering (DLS)

A zeta sizer was used to figure out the hydrodynamic radius and zeta potential of the nanoparticle (Malvern Nano ZS). Sample tubes were sonicated for 15 minutes before the zeta sizer was used to measure them. For the DLS study, the sample was put in a sizing cuvette that could be thrown away. For all of the data processing, the viscosity of the solution, the refractive index of the particle, and the refractive index of the solution are all set to 0,8872 cp, 0,20, and 1,330 respectively. For each measurement, 15 runs were done, and each run took 30 s. The three measurements were taken three times for each sample to figure out how far off the measurements were (45 runs for each sample). All DLS measurements showed that there was only one peak. For optimization, phosphate-buffered saline (PBS) solutions were used to measure MCM-41 nanoparticles at different pH and temperature levels. Then, fluorescein was added to MCM-41 nanoparticles, which were topped with a probe made from one of three gene sequences (NSP9, NSP12, or E). After putting probes on the surface of the nanoparticles and making them stay there, the size of these probe-capped nanoparticles was measured by DLS in PBS solution at different pH and temperature levels to find the best conditions for synthesis. So, the nanoparticles were made at 25$^{o}$C and a pH of 7,4 for the all-synthetic probe-releasing tests and the patient swap sample tests. So, 0,05 g of MCM-41 nanoparticles were mixed in PBS with a pH of 7,4, and the mixture was then looked at to plot the intensity vs. the size of the nanoparticles. The software on the instrument figured out automatically the average hydrodynamic diameter and zeta potential of the silica nanoparticles' surfaces.

### 3.1.3. Fourier Transform Infrared Resonance (FTIR)

0,05 g of MCM-41 powder was weighed in a tube. The tube was covered with aluminum foil. Then, 1 ml of 95% ethanol which also included 5% and 1 mM of acetic acid was added and mixed on shaker for 1 hour at room temperature. For FTIR analysis, 10 µl sample was taken from the tube after 1 hour incubation, and measurement was done. After that, 30 µl of 3% (3-Aminopropyl) triethoxysilane (APTES) was added to the mixture and then incubated all night under mixing. To find NH- group addition on nanoparticles, FTIR analysis was again applied after the amine functionalization (NicoletTM iS50 FTIR- OMNIC 0.9, ATR).

### 3.1.4. Brunauer-Emmett-Teller (BET) Analysis

BET analysis was carried out to investigate the size of the mesopores of the synthesized silica nanoparticles and surface area determination (Micromeritics -TriStar II Plus).

## 3.2. PREPARATION OF PROBE-GATED SILICA NANOPARTICLES

### 3.2.1. Synthesis of Amino Grafted MCM-41 Particles

At room temperature, 0,05 g of MCM-41 powder was mixed with 1 ml of 95% ethanol that had 5% and 1 mM of acetic acid in it. This was done for an hour. The mixture was given 30 µl of 3% (3-Aminopropyl) triethoxysilane (APTES), and it was left to sit overnight while being stirred. During the 5 minutes of centrifugation (14.000 rpm), the solution was washed three times with 1X PBS (0,01 M phosphate-buffered saline; NaCl-0,138 M; KCl-0,0027 M; pH 7,4). After the last centrifugation, this tube was dissolved in 1 ml of PBS and marked as B1 (Figure 3.2.).

### 3.2.2. Loading with Fluorescein

The 10 µl of amino-modified nanoparticles from the B1 tube were dissolved in 190 µl of 1X PBS (pH:8) (Figure 3.2.). The 100 µM fluorescein sodium salt was then added to the dissolved nanoparticles. All night, the mixture was kept while being stirred.

Figure 3.2. The synthesized fluorescein probe gated MCM-41 nanoparticles (B1 Tubes)

### 3.2.3. Capping with Synthetic SARS-CoV-2 Probes

Last, 2 µl of 1 µM SARS-CoV-2 complementary sequences (E probe, NSP12 probe, and NSP9 probe) were attached to the fluorescein-loaded silica nanoparticles in the PBS buffer (Table 2.1). The four tubes with the different probes were put on the shaker at room temperature and left there all night.

1. Tube = 10 µl from B1 + 190 µl PBS + 2 µl Fluorescein solution + NSP12 probe

2. Tube= 10 µl from B1 + 190 µl PBS + 2 µl Fluorescein solution + NSP9 probe

3. Tube = 10 µl from B1 + 190 µl PBS + 2 µl Fluorescein solution + E probe

4. Tube (Control) = 10 µl from B1 + 190 µl PBS + 2 µl Fluorescein solution + NSP12 probe

With 100 µl (1X) PBS buffer, the particles were thoroughly washed three times during centrifugation (14.000 rpm, 5 min.). From the differences in the spectra of the starting and final concentrations, the probe's entrapped fluorescein quantities were calculated (Excitation 460, emission 520 nm).

## 3.3. RELEASE ASSAY WITH SYNTHETIC COMPLEMENTARY PROBES

To cause the outflow of fluorescein molecules, the target RNA sequence (NSP12comp, NSP9comp, or Ecomp) mixture dissolved the probe-capped fluorescein-loaded mesoporous silica nanoparticles (Table 1). To do this, after the last centrifugation of the washing step, supernatants were thrown and 100 µl complementary probe solution (CP mixture), which was prepared by adding 15 µl NSP12comp or NSP9comp or Ecomp into 1485 µl PBS, was added according to the below procedure and pellet is dissolved.

1. Tube= 10 µl from B1 + 190 µl PBS + 2 µl Fluorescein solution + NSP12 probe+CP (NSP12comp)

2. Tube= 10 µl from B1 + 190 µl PBS + 2 µl Fluorescein solution + NSP9 probe + CP (NSP9comp)

3. Tube= 10 µl from B1 + 190 µl PBS + 2 µl Fluorescein solution + E probe + CP (Ecomp)

4. Tube (Control)= 10 µl from B1 + 190 µl PBS + 2 µl Fluorescein solution + NSP12 + CP (NSP9comp)

These four tubes were rotated at 14.000 rpm for one minute. They filled a 96-well plate with 50 µl of supernatants. Each tube was filled with 50 µl of the CP mixture. The tubes were spun in the same manner once they had been incubating for 4 minutes. The supernatant was then added to each well in an amount of 50 µl. Each tube was filled with 50 µl of the CP mixture. The incubation periods of 1, 5, 15, 30, 45, and 1 hour all followed the same procedure. It was determined how much fluorescence was present in the supernatant (460 nm for excitation and 520 nm for emission) (Thermo Scientific, Varioscan Fluorescence Microplate Reader). The correlation between the number of fluorescein molecules released and the passage of time demonstrated the cumulative release of fluorescein. The experiment was repeated three times (n = 3).

## 3.4. PATIENT SAMPLE COLLECTION AND TESTING FOR SARS-COV-2 WITH RT-PCR

Nasopharyngeal/oropharyngeal swab samples were taken from 43 people who had COVID-19 symptoms or a history of contact and went to the emergency room of Kartal Dr. Lütfi Kırdar City Hospital in 2021. Patients ranged in age from 24 to 62, and 31 of them were women. Using the gold standard RT-PCR method, the SARS-CoV-2 genome was looked at in samples. Swabs made of sterile synthetic fiber and plastic shafts were used to take samples from the combined nasopharynx and oropharynx. These samples were sent to a PCR laboratory within four hours. The COVID-19 PCR Laboratory at Kartal Dr. Lütfi Kırdar City Hospital used the Bio-Speedy® SARS-CoV-2 Emerging Plus kit and the vNAT® Viral Nucleic Acid Buffer from Bio-eksen, Turkey, to find SARS-CoV-2.

The Bio-Speedy® SARS-CoV-2 Emerging Plus kit has a single-stage reverse transcription and RT-qPCR test for detecting the quality of SARS-CoV-2 RNA. This kit focuses on the Orf1ab and N gene regions that are the same for all SARS-CoV-2 variants. It can also identify the Alpha variant by the N D3L mutation, the Delta variant by the S L452R mutation, and the Gamma and Mu variants by the S E484K mutation. Forward and reverse primers for Orf1ab and N gene regions are shown in Table 3.1 [129].

Table 3.1. Primers for Orf1ab and N genes

| Target gene | Forward Primer | Reverse Primer |
|---|---|---|
| Orf 1ab | 5’-CTA GGA CCT CTT TCT GCT CA-3’ | 5’-ACA CTC TCC TAG CAC CAT CA3’ |
| N gene | 5’- CCT CTT CTC GTT CCT CAT CA-3’ | 5’-CCT GGT CCC CAA AAT TTC CT-3’ |

The sample tube was spun for 15 seconds at its fastest speed as directed by the kit's instructions. Then, a microcentrifuge tube was filled with 100 µL of vNAT® Viral Nucleic Acid Buffer [130].

The vNAT® buffer is used to safely remove viral nucleic acids from samples taken from the respiratory system. Real-time RT-PCR may begin 5 minutes after the sample is inserted thanks to the vNAT® component. The SARS-CoV-2 envelope and nucleocapsid are destroyed by polyethyleneimine-coated tetradecyl dimethyl benzyl ammonium chloride-based nanoparticles (NP) and tween-20 in vNAT®, releasing the genome. Guanidinium thiocyanate, NaN3, and NP in vNAT® prevent the released genomes from being altered. In order to counteract the negative effects of PCR inhibitors, BSA is utilized as a PCR facilitator in vNAT® [131].

100 µL of fluids from the lungs were placed in this tube with vNAT®, which was then spun for 15 seconds at its highest speed. The tube was allowed to rest at room temperature for five minutes. Last but not least, the 200 µL mixture is prepared for real-time RT-PCR [130]. The reagents and template from the sample-vNAT® buffer combination are to be added to the qPCR tubes in the order listed in Table 3.2, according to the real-time RT-PCR methodology. The qPCR machine was then equipped with qPCR tubes and programmed to execute the Table 3.3 program below [130].

Table 3.2. Real Time PCR Reaction Set-up

| **Component** | **Reaction** |
|---|---|
| 2X Prime Script Mix | 5 µl |
| Emerging Oligo Mix | 2,5 µl |
| Template Nucleic Acid | 2,5 µl |
| TOTAL REACTION VOLUME | 10 µl |

Table 3.3. Real Time PCR Program

| Cycle Number | Temperature | Duration |
|---|---|---|
| 1 | 52 | 3 min |
| 1 | 95 | 10 sec |
| 5 | 95 | 1 sec |
| | 60 | 12 sec |
| 35 | 85 | 1 sec |
| | 60 | 1 sec |
| | FAM/HEX/ROX/CY5/CY5.5 Read | |

The samples were stirred for 15 seconds in the presence of vNAT® buffer to identify ORF 1 ab, the SARS-CoV-2 N gene, and the RNase P gene. Using a pipette, the sample-buffer mixture was next added to the RT-PCR amplification mixture. A negative control and a positive control were used in each RT-PCR experiment. Results with a cycle threshold (Ct) under 32 were deemed to be favorable. There were 12 negative and 31 positive SARS-CoV-2 tests. The average CT value for positive samples ranged from 12,9 to 30,4.

## 3.5. HYBRIDIZATION-TRIGGERED FLUORESCEIN SIGNAL TEST

The biosensor developed by probe-gated mesoporous silica nanoparticles was tested with human swab samples. 43 swab samples were collected and diagnosed by gold standard RT-PCR to compare with the biosensor results. Before using the hybridization-triggered fluorescein signal test technique, the swab samples were diluted in dH2O at a ratio of $1:10^3$

with an incubation time of 15 minutes always employed. The Varioskan LUX- Fluorescence Microplate Reader from Thermo Scientific was used to measure the fluorescein molecules the nanoparticles produced (Excitation 460, emission 520 nm).

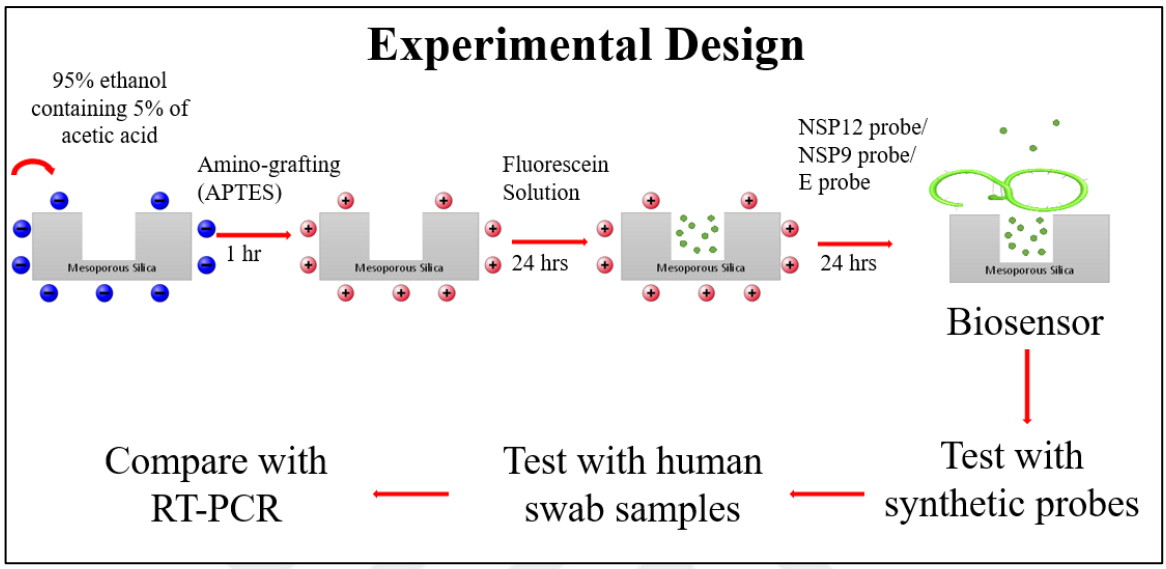


Figure 3.3. Experimental Design. MSNPs were modified by APTES and loaded by fluorescein as a reporter molecule and capped with NSP12, NSP9 or Gene E probe. Then, firstly, the probe gated MSNPs were tested with the synthetic complementary probes in PBS. Second, human swab samples either tested by RT-PCR in clinics or tested by probe gated MSNPs. The positive and negative samples detected by two methods, the novel biosensor developed in this thesis and gold standart RT-PCR were compared

As a summary of the experimental design, mesoporous silica nanoparticles (MSNPs) were firstly mixed with ethanol containing acetic acid. This caused a negative charge on the particles. APTES was added to MSNPs and after 1-hour incubation, nanoparticles became positively charged. Then, fluorescein solution was added as a reporter molecule and incubated all night. One of the three probes (NSP12 gene, NSP9 gene, Gene E) was added and again incubated all night. So, after these steps, a biosensor has been developed. The biosensor was firstly tested with synthetic complementary probes in a physiological buffer solution. Then it was tested with human swab samples and the results were compared with RT-PCR results as a gold standard method (Figure 3.3.).

The Sensitivity, accuracy, and specificity of biosensor were calculated according to Equations (3.1.), (3.2.), and (3.3.).

$$Sensitivity = \frac{True\ Positives}{True\ Positives + False\ Negatives}\ x100 \quad (3.1.)$$

$$Accuracy = \frac{True\ Positives + True\ Negatives}{Total\ Sample} x100 \quad (3.2.)$$

$$Specificity = \frac{True\ Negatives}{True\ Negatives + False\ Positives} x100 \quad (3.3.)$$

# 4. RESULTS

Mesoporous silica nanoparticles are the basis for synthesizing target-responsive fluorescent assay. First, the mesoporous silica nanoparticles were obtained by following a sol-gel procedure for particles with desired mesopores which were loaded with fluorescein molecules as reporter agents and capped with virus-specific oligonucleotide probe sequences. The prepared SARS-CoV-2 responsive fluorescent nanoparticles were used to design a detection assay.

## 4.1. OPTIMIZATION OF THE SYNTHESIS OF MCM-41 SILICA NANOPARTICLES

For the optimization of the synthesis of fluorescein loaded probe gated MCM-41 silica nanoparticles the synthesis protocol performed at different temperature conditions. The average diameter of nanoparticles were measured at 10$^{o}$C, 15$^{o}$C, 20$^{o}$C, 25$^{o}$C, 30$^{o}$C and 40$^{o}$C by using DLS. However, according to the DLS results the particles were very polydisperse for cumulated analysis and aggregated at 10$^{o}$C, 15$^{o}$C, 30$^{o}$C and 40$^{o}$C as shown in Figure 4.1. Up to 15$^{o}$C, the particles demonstrated similar diameters below 2000 nm. Reaching the temperature to 30$^{o}$C, the particles showed slightly higher size with over 2000 nm. At 40$^{o}$C conditions, the particles had almost 3000 nm average diameter size.

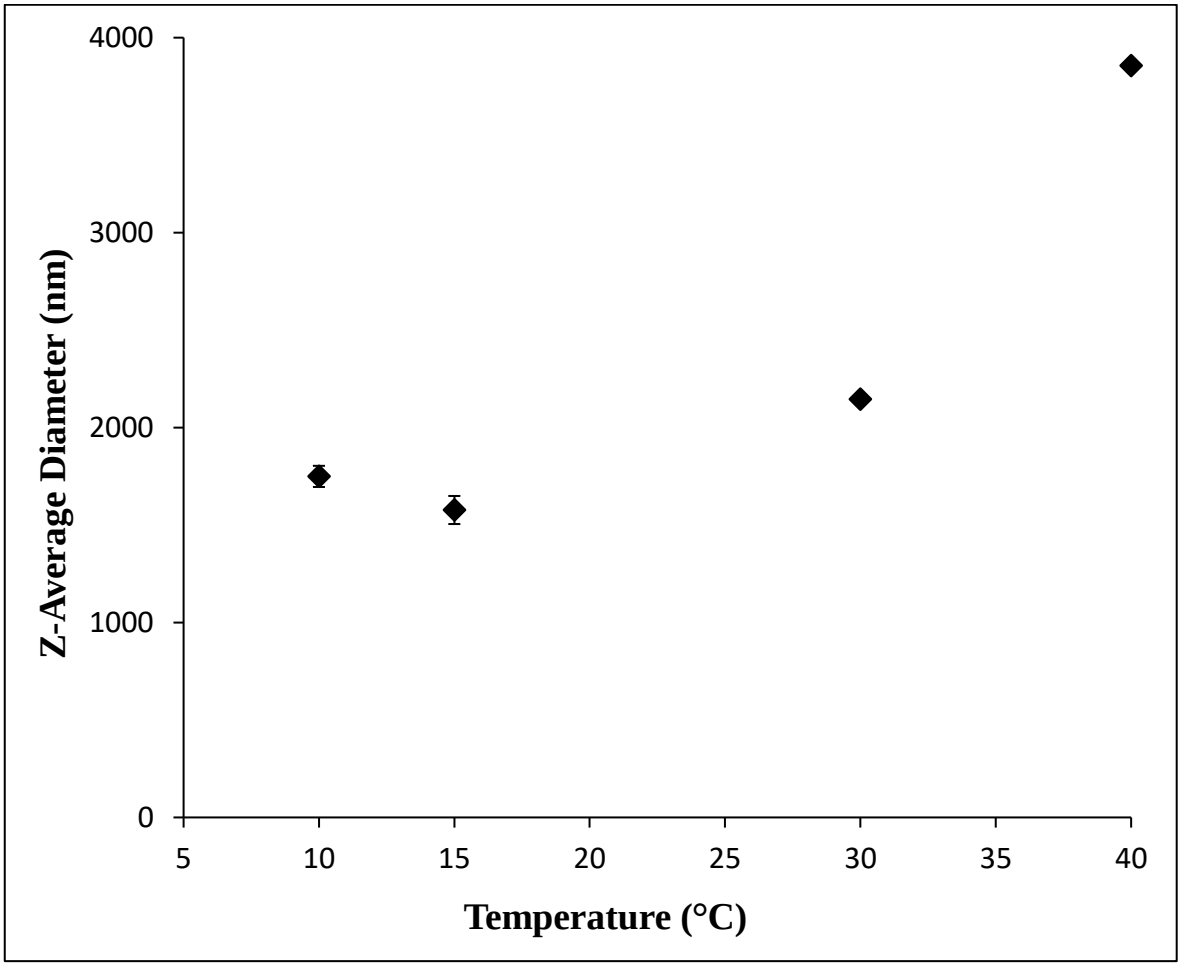


Figure 4.1. The effect of temperature on MCM-41 particle size. The nanoparticles synthesized at 10ºC, 15ºC, 30ºC and 40ºC were aggregated

The optimization for the synthesis of fluorescein loaded probe gated MCM-41 silica nanoparticles were performed under different pH conditions. The average diameter of nanoparticles were measured at pH 5, 6, 7, 8, 9 and 10 by using DLS. However, according to the DLS results the particles were very poly-disperse for cumulated analysis and aggregated at pH 5, 6, 8, 9 and 10 as shown in Figure 4.2.

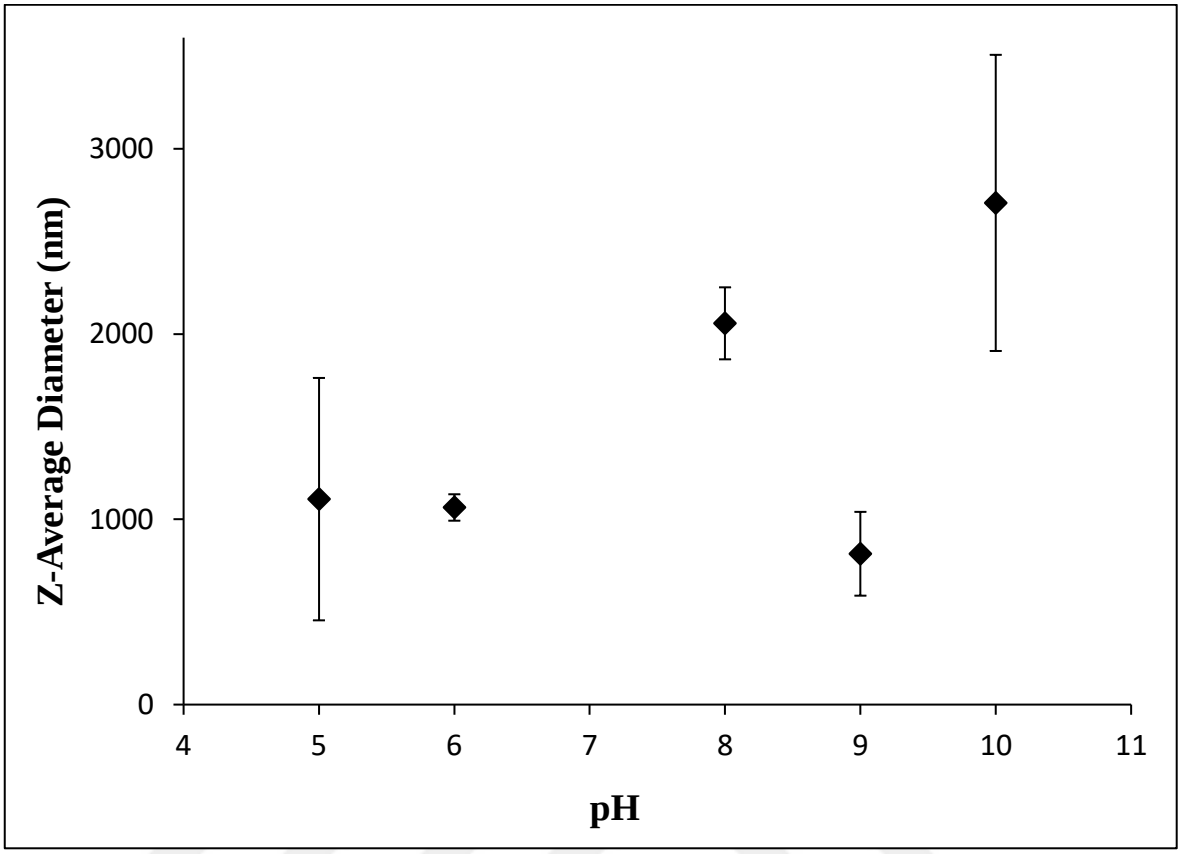


Figure 4.2. The effect of pH on MCM-41 particle size. The nanoparticles synthesized at Ph 5, 6, 8, 9 and 10 were aggregated

The average size of particles were around 1000 nm at acidic pH values. The sizes were similar at pH of 5 and 6 (Figure 4.2.). At slightly basic pH (pH=8), the size of the particles increased to 2000 nm. At pH 9, the average size of the particles reduced to levels of acidic values at 700 nm, but increasing pH to 10 increased the particle sized to highest level at 2700 nm.

Similar pH optimization analysis were performed after probe capping protocol with one of the three COVID-19 probes (NSP12 gene, NSP9 gene, Gene E). The probe gated nanoparticles synthesized at Ph 5, 6, 8, 9 and 10 were also aggregated as shown in Figure 4.3., 4.4. and 4.5. The optimum temperature for the synthesis is determined as between 20-25 and pH was determined as 7.0.

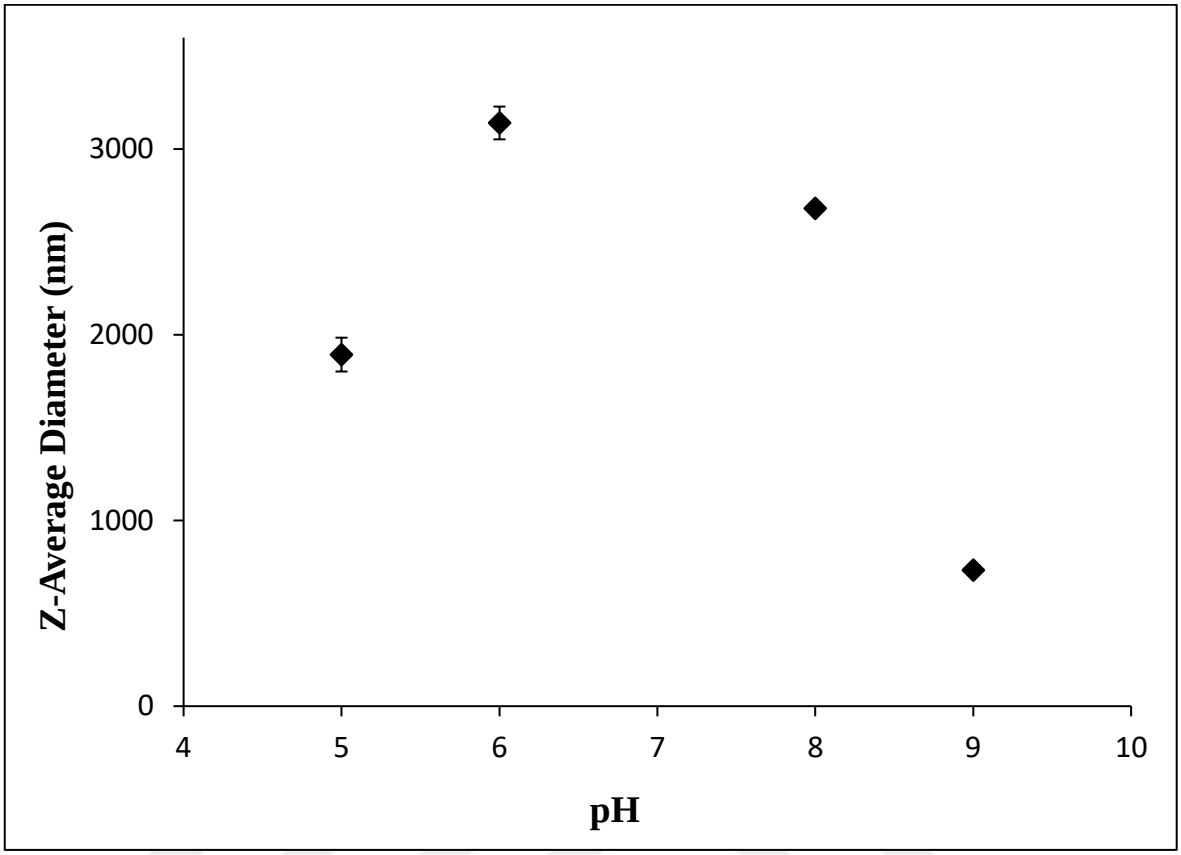


Figure 4.3. The effect of pH on MCM-41+Egene probe size. The Egene probe gated nanoparticles synthesized at Ph 5, 6, 8 and 9 were aggregated

Figure 4.3. is the average sizes of particles with E gene probe at a range of pH values between 5 and 9. At acidic pH 5, the average size is 2000 nm and the size reaches a peak value of 3200 nm at pH 6. Then, increasing pH to basic values at 8 reduces the average size to 2700 nm. The basic pH value of 9 resulted in the lowest average value for E gene probe functionalized particles at 1000 nm of diameter.

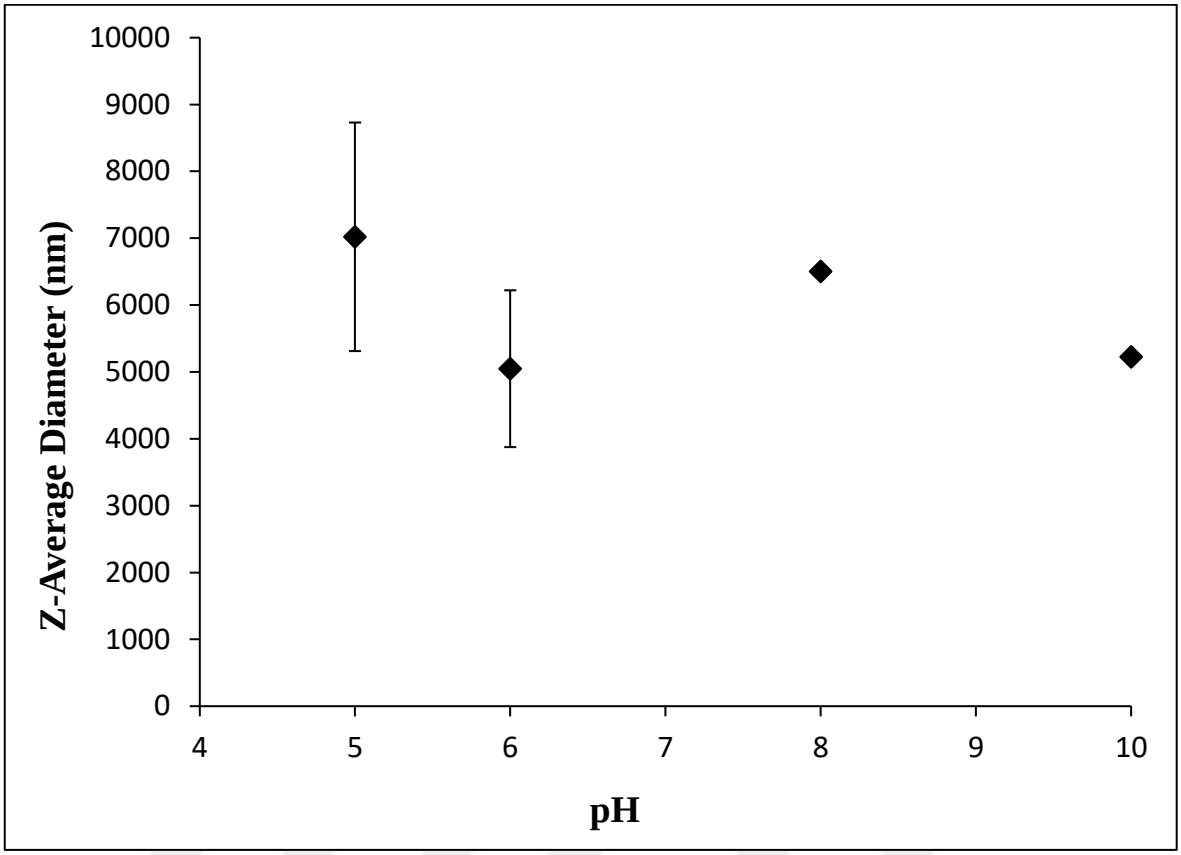


Figure 4.4. The effect of pH on MCM-41+NSP9probe size. The NSP9 probe gated nanoparticles synthesized at Ph 5, 6, 8 and 10 were aggregated

When probe was NSP9 gene probe, the pH changes were not affected by pH shifts (Figure 4.4.). The pH values 5, 6, 8 or 9 resulted in average particle sized between 5000 and 7000 nm. NSP9 gene probe covered particles had average size of 7000 nm at pH 5, reduced to 5000 nm at pH 6, It was 6000 nm at pH 8 and 5200 nm at pH 9.

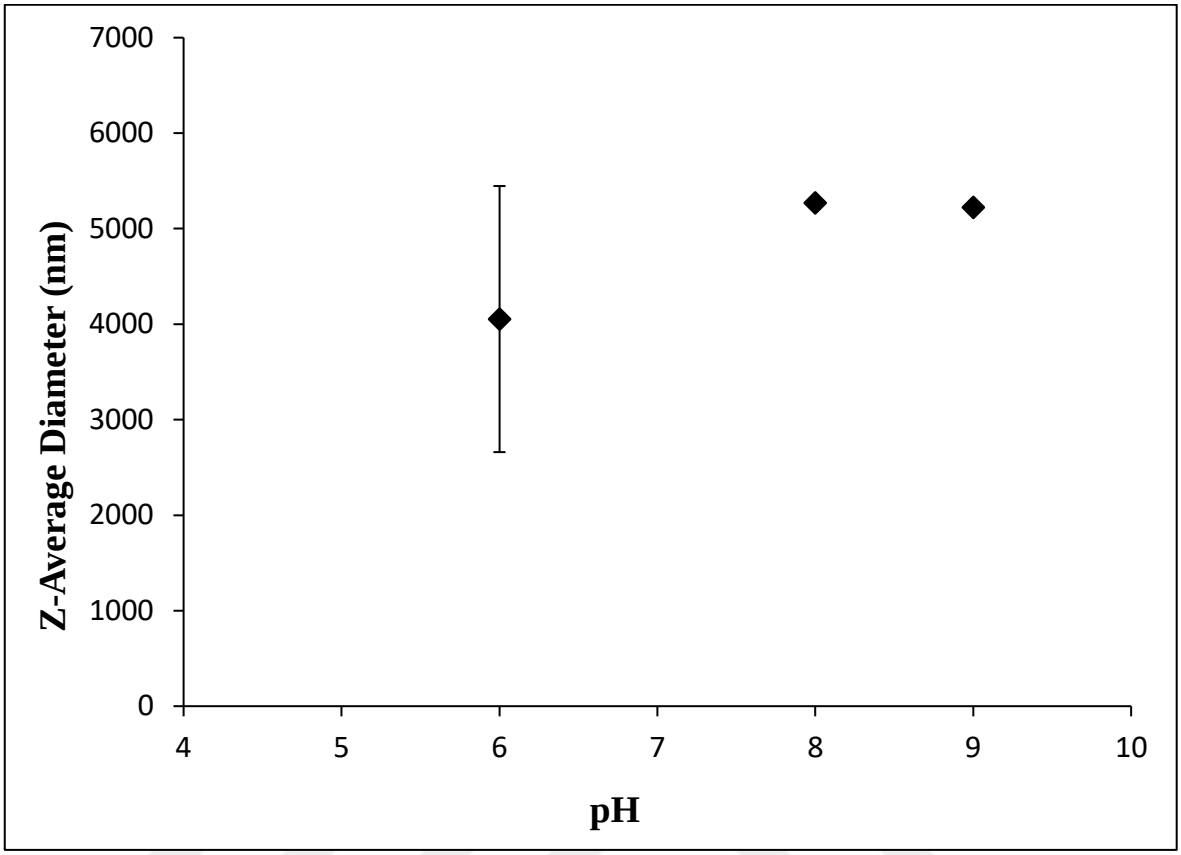


Figure 4.5. The effect of pH on MCM-41 and NSP12 gene probe size. The NSP12 gene probe gated nanoparticles synthesized at Ph 6, 8 and 9 were aggregated

Figure 4.5. presents average particle sized changes for NSP12 gene probe functionalization. At acidic pH 6, the size was lowest at 4000 nm. Increasing pH to basic level of 8 increased the average particle size to 5000 nm and increasing pH to 9 did change the size.

## 4.2. CHARACTERIZATION OF SILICA NANOPARTICLES

MSNPs and DNA probes were used to make probe-capped MSNPs that can show if three target viral genome regions are present. The mesoporous silica nanoparticles were made using a bottom-up sol-gel method that involved the hydrolysis and condensation of silicon precursors, followed by aging, drying, and calcination.

### 4.2.1. Transmission Electron Microscopy

According to TEM scans, the particles displayed an irregular, spherical shape with some aggregation (Figure 4.6.A.). The ordered array of the hexagonal shape of mesopores can be observed in the close-up TEM image (Figure 4.6.B.).

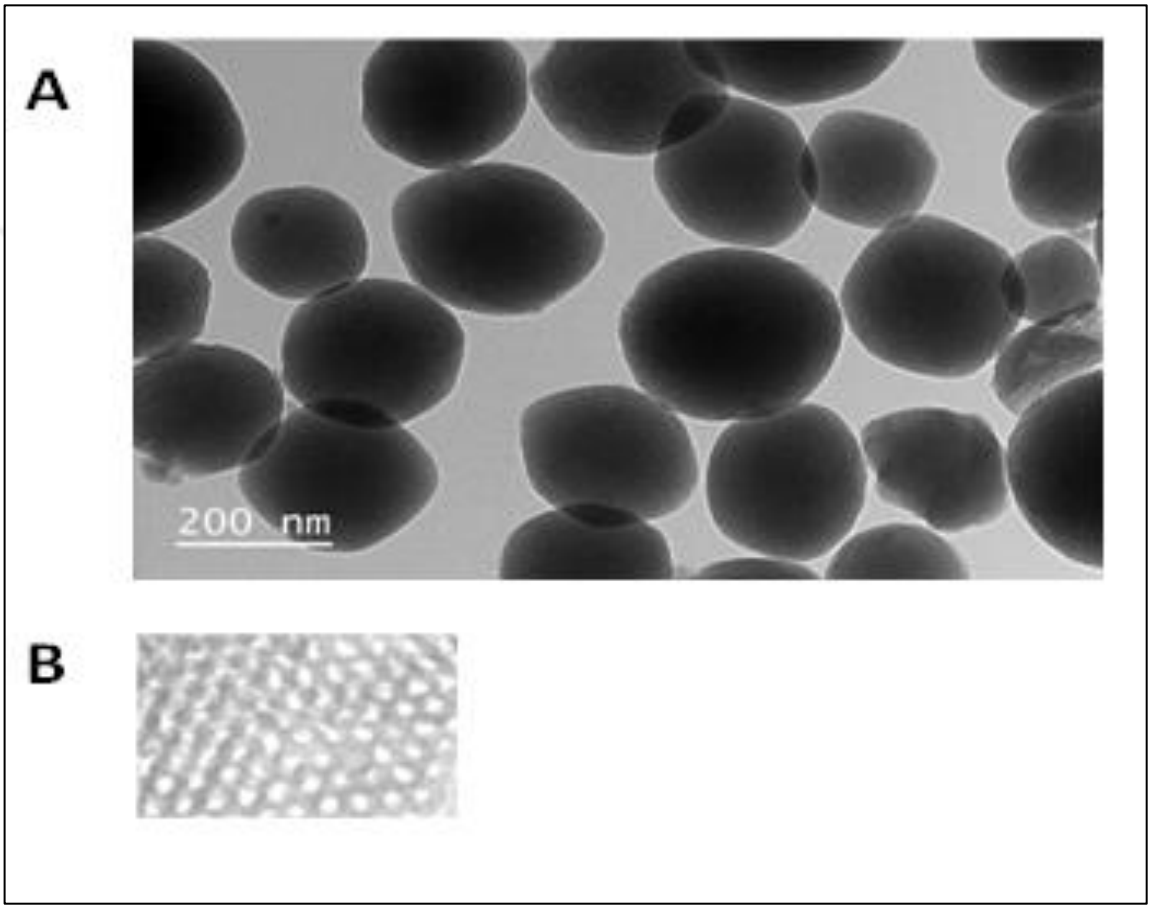


Figure 4.6. MCM-41 nanoparticle characterization using (A) and (B) TEM

The nanoparticle's hydrodynamic size was determined to be 264 ± 11 nm by using DLS (Figure 4.7.). In addition, the zeta potential was also measured by using the electrophoretic light scattering (ELS) technique. It was found to be -23,4 mV at 20°C in PBS. The surface of the nanoparticles was then salinized using APTES to graft amine groups onto them. The amination raised the nanoparticle’s potential to 34,3 mV.

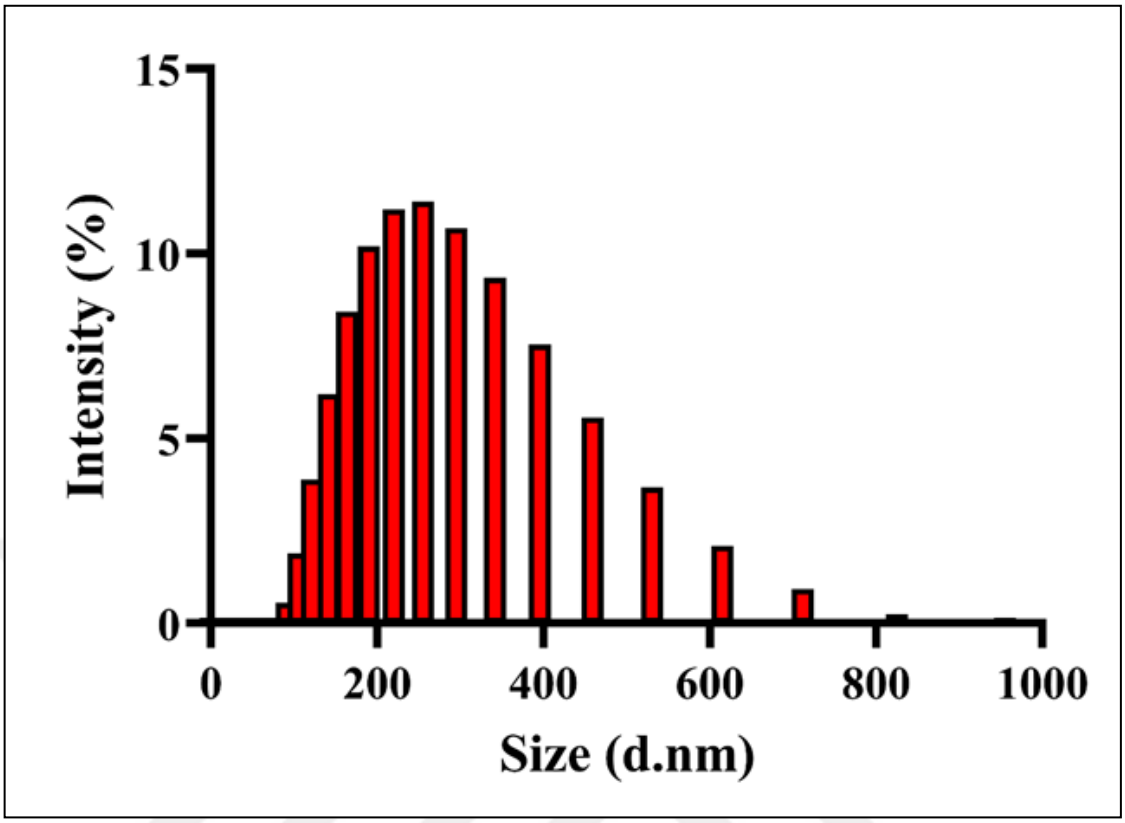


Figure 4.7. Silica nanoparticle characterization using DLS

The average particle diameter of the particles by the hydrodynamic model increased at a small proportion to 265 ± 9 nm upon probe attachment (data not shown). However, there was no statistically meaningful shift with probe attachment. However, after probe attachment to aminated nanoparticles by covalent bonds, the particles' potential dropped to 31,6 mV, representing the negative charge added by probe immobilization.

### 4.2.2. Fourier Transform Infrared Resonance Spectroscopy

To check amine group addition on the nanoparticle, FTIR analysis was applied. FTIR analysis produced peaks at 3293,54 cm-1 and 650 cm-1, confirming the functionalization of the amine group (Figure 4.8.).

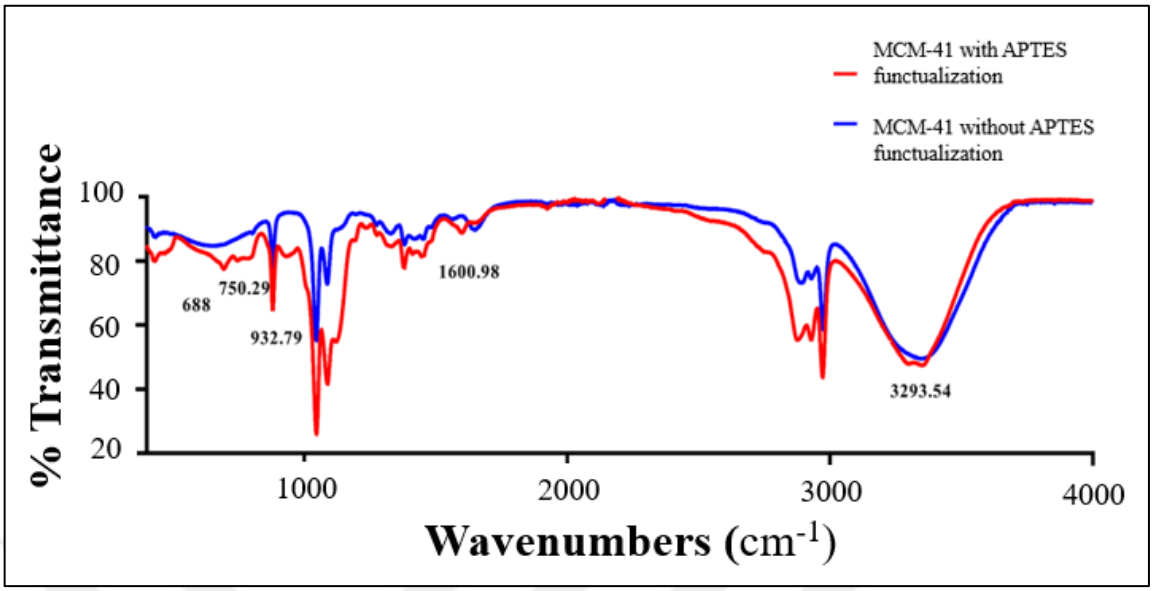


Figure 4.8. Silica nanoparticle characterization using FTIR analysis

### 4.2.3. Brunauer-Emmet-Teller Analysis

The size of the mesopores of the synthesized silica nanoparticles was further investigated by BET analysis. Figure 4.9. is the result of the BHJ desorption method of nitrogen gas. The blue line shows the distribution of mesopores with an average diameter (peak value) of 2,833 nm. The red line is the volume for each pore diameter. The average pore volume was 1,033 cc/g. The surface area of the mesopores was estimated as 1.245,649 $m^2/g$.

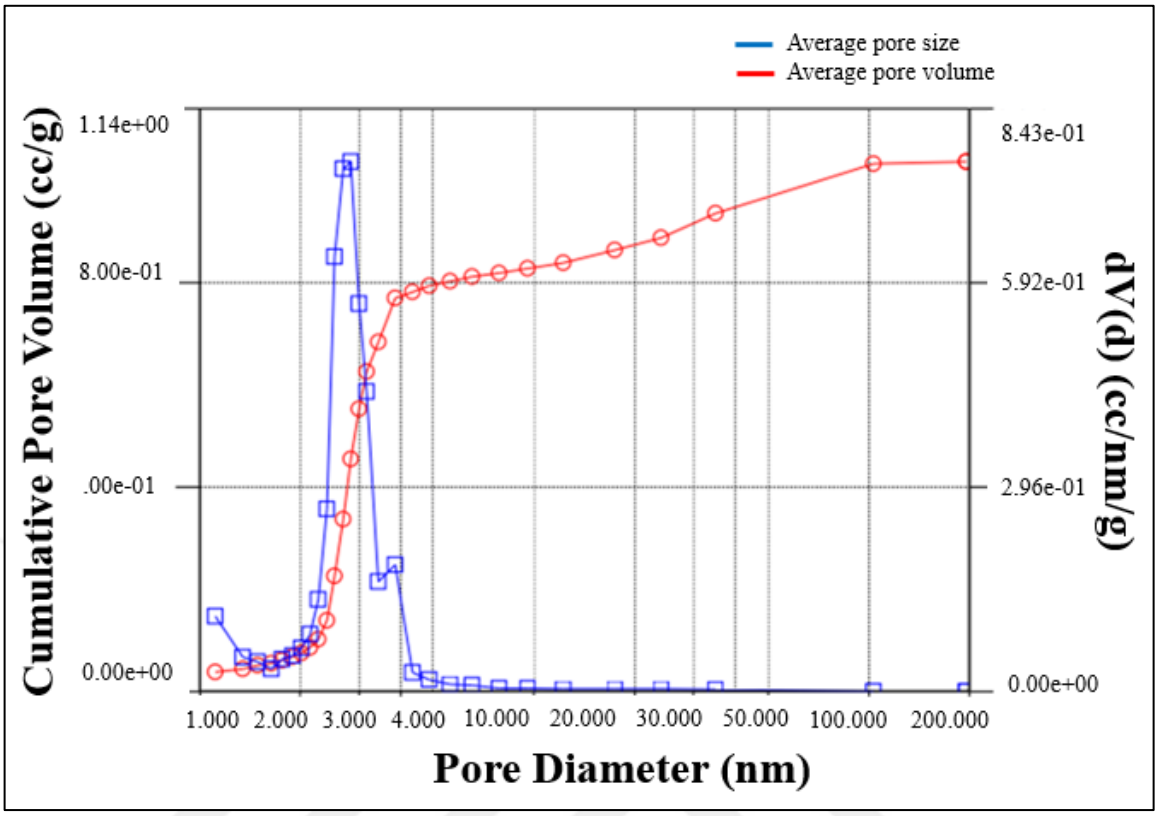


Figure 4.9. BET analysis is used to describe silica nanoparticles

### 4.2.4. Determination of entraped flourecence level in the nanoparticle

Standart concentrations for the florecence were prepared and were used to determine the entrapment of the flourecence in MSNPs. There was a lineer relation between the amount of flourecence (microM) and the meaured relative flousence amount as seen in Figure 4.10. There was also a lineer relation between the amount of loaded flourecence and the meaured relative flousence amount.

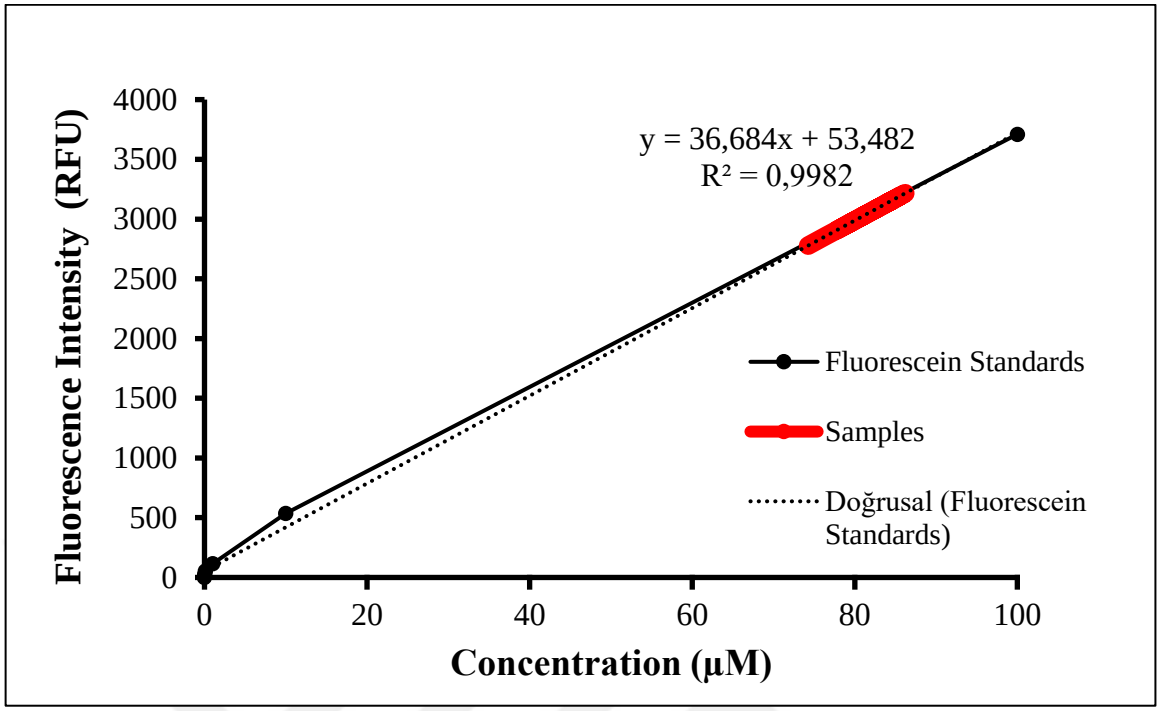


Figure 4.10. Reletive Flourecence intensity of flourecence loaded MSNPs Determination of The Number of Probes Fixed on The Nanoparticle Surface

### 4.2.5. Determination of the number of probes fixed on the nanoparticle surface

FAM labelled probes were used to determine the number of one of the COVID-19 gene probes (NSP12, NSP9, Gene E) fixed on the mesaphorus slica nanoparticle surface. There was a lineer relation between the amount of FAM labelled probe (microM) and the meaured relative flousence amount as seen in Figure 4.10. The probe capping afficiany was similar for all probes.

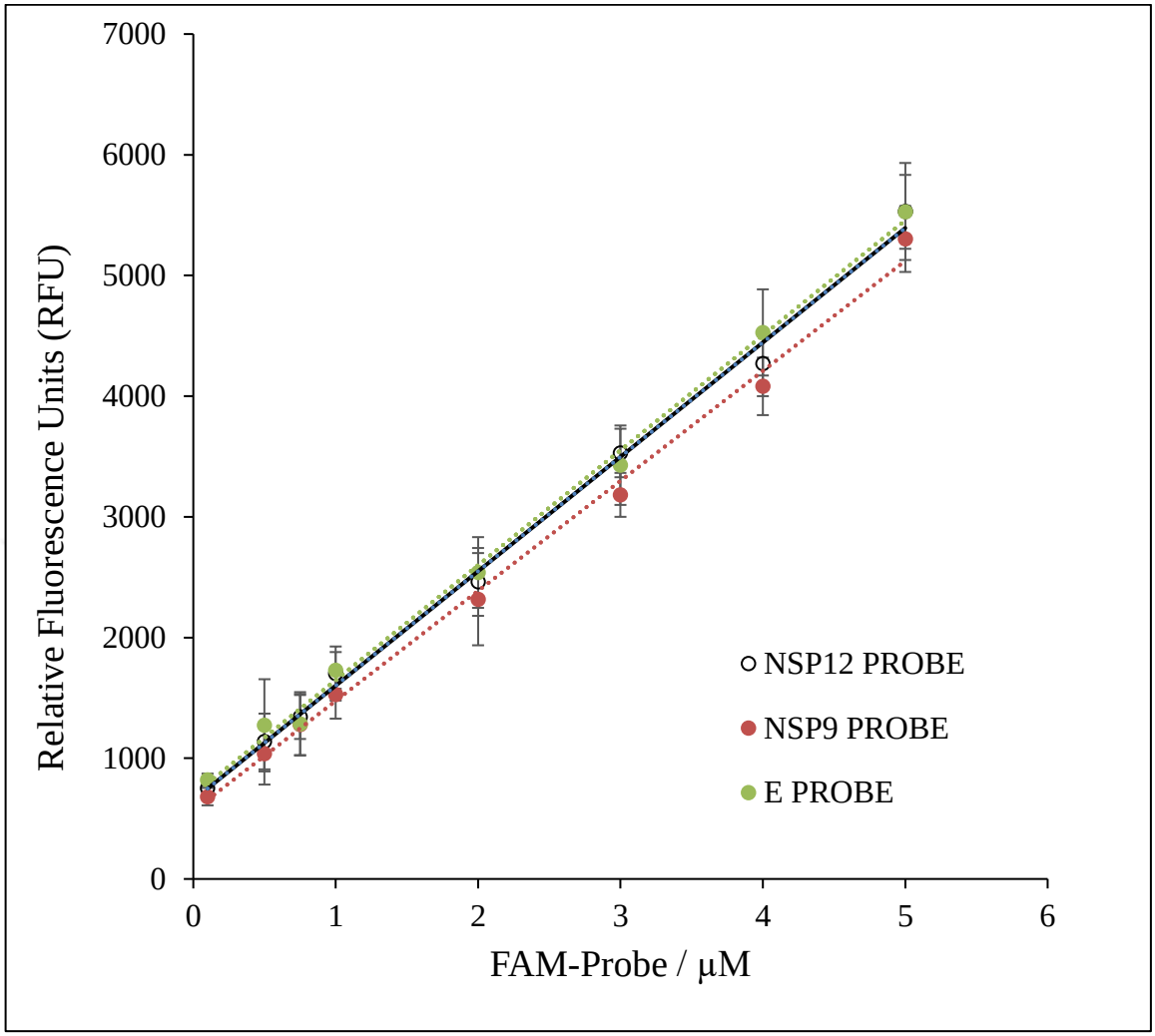


Figure 4.11. Calibration curve for FAM-labelled probes

The number of probes fixed on the nanoparticle surface was determined by a standard curve shown in Figure 4.11. for each probe by using the following linear equations (4.1.), (4.2.) and (4.3.):

$$E\ GENE\ PROBE: Y = 952{,}24X + 694{,}99 \qquad R^2=9963 \quad (4.1.)$$

$$NSP9\ GENE\ PROBE: Y = 911{,}27x + 564{,}1 \qquad R^2=9961 \quad (4.2.)$$

$$NSP12\ GENE\ PROBE: Y = 947{,}8X + 653{,}09 \qquad R^2=9966 \quad (4.3.)$$

## 4.3. THE CONTROLLED RELEASE PERFORMANCE OF DIFFERENT PROBES (NSP12, NSP9, AND E GENE PROBES) CONJUGATED WITH FLUORESCEIN-LOADED MCM-41 BY USING SYNTHETIC PROBES

After applying APTES to the amine groups on the surface of the MCM-41 nanoparticles (NP), the reporter fluorescein (FL) molecules were added. By forming an electrostatic interaction between the negatively charged oligonucleotides and the positively charged silica surface, the probes were then employed to cap the ends of the oligonucleotides. As a result, fluorescein molecules were entrapped in porous silica nanoparticles that were prevented from migrating by the probe's ssDNA sequences. The positive strand of SARS-CoV-2 RNA is the complementary DNA oligonucleotides. The SARS-CoV-2 RNA and probe DNA have the same sequence, although they run in different directions. The nanoparticles have 26 nmol/g of DNA probes, according to a fluorescence assay.

The number of fluorescein agents trapped in mesopores of silica nanoparticles was determined from the difference between before and after the entrapment procedure, and it is calculated as 8,3 ± 1,2 μmol mg-1.

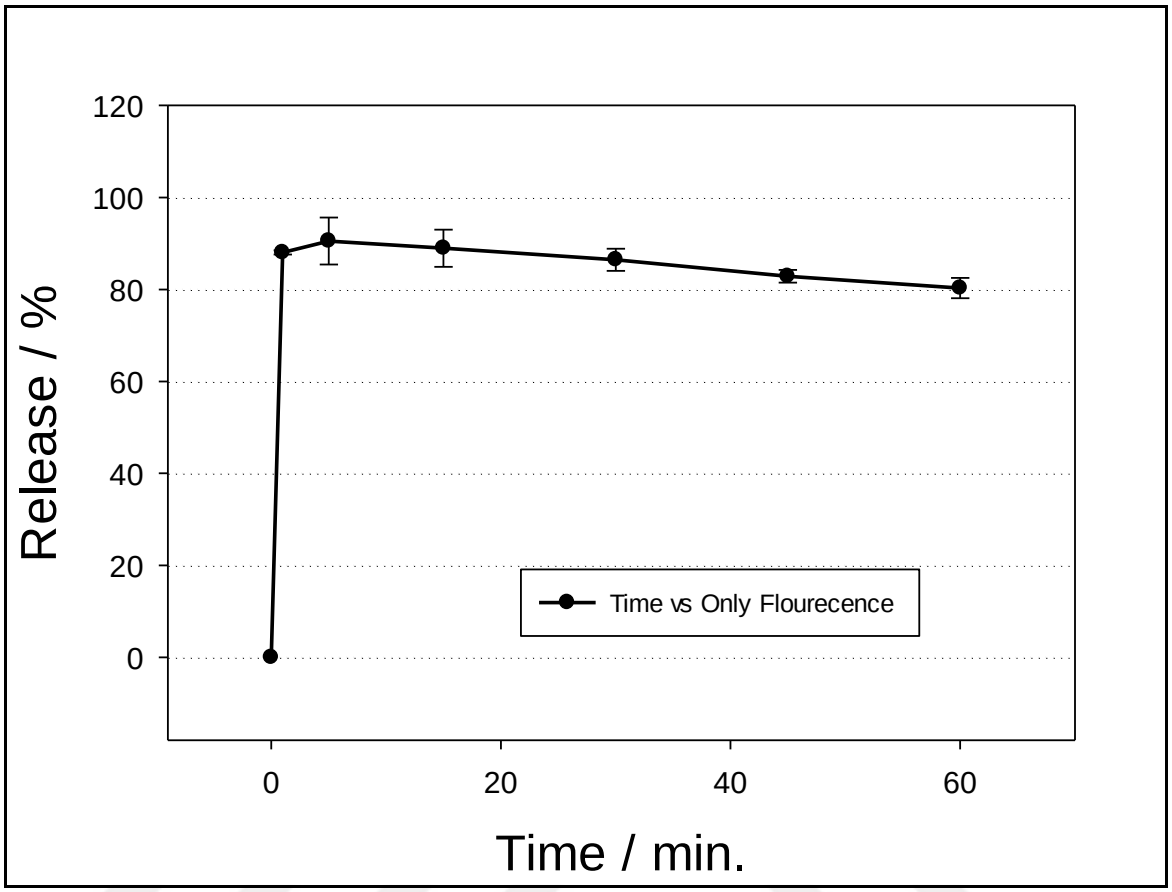


Figure 4.12. Cumulative Releasing of Fluorescein from MSNPs without capping in PBS

When there is no capping, the fluorescein entrapped in to MSNPs were released directly in PBS without specific target or control (Figure 4.12.). Using synthetic oligonucleotides, signaling MSNPs coated for certain probes were developed and assessed for every target area (NSP12, NSP9, and E gene). The fluorescein releasing according to time patterns with synthetic oligonucleotides complementary to probes are shown in Figure 4.13., 4.14. and 4.15.

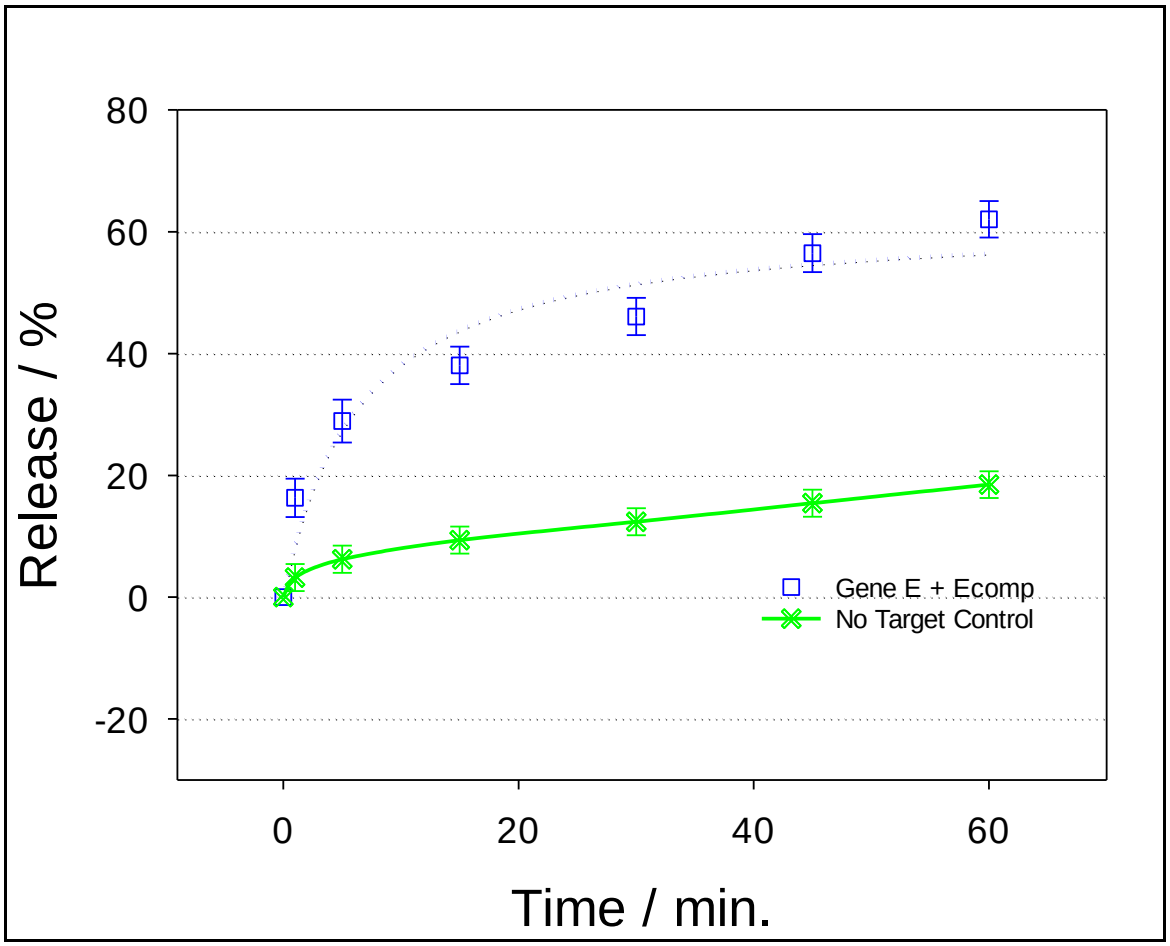


Figure 4.13. Cumulative Releasing of Fluorescein from MSNPs capped with E Gene probe after added its complementary and MSNPs capped with E Gene without target in PBS

Up to 60 minutes of fluorescence signal monitoring was done during probe-target oligonucleotide hybridization. The fluorescein molecules inside the mesopores in the NSP12 probe-gated MSNPs were quickly released from the nanoparticles when the target sequence (NSP12comp) was added to the assay fluid as seen in Figure 4.14. Similar to the NSP12 probe, combinations of NSP9 probe and NSP9comp or Gene E probe and Gene Ecomp also demonstrated an abrupt increase in fluorescence signal, but at slower rates as seen in Figure 4.13. and 4.14. compared to NSP12 probe. Only a little quantity of fluorescein was released when the probe-gated MSNPs left in PBS alone in 60 minutes without target (Figure 4.13., 4.14., and 4.15.).

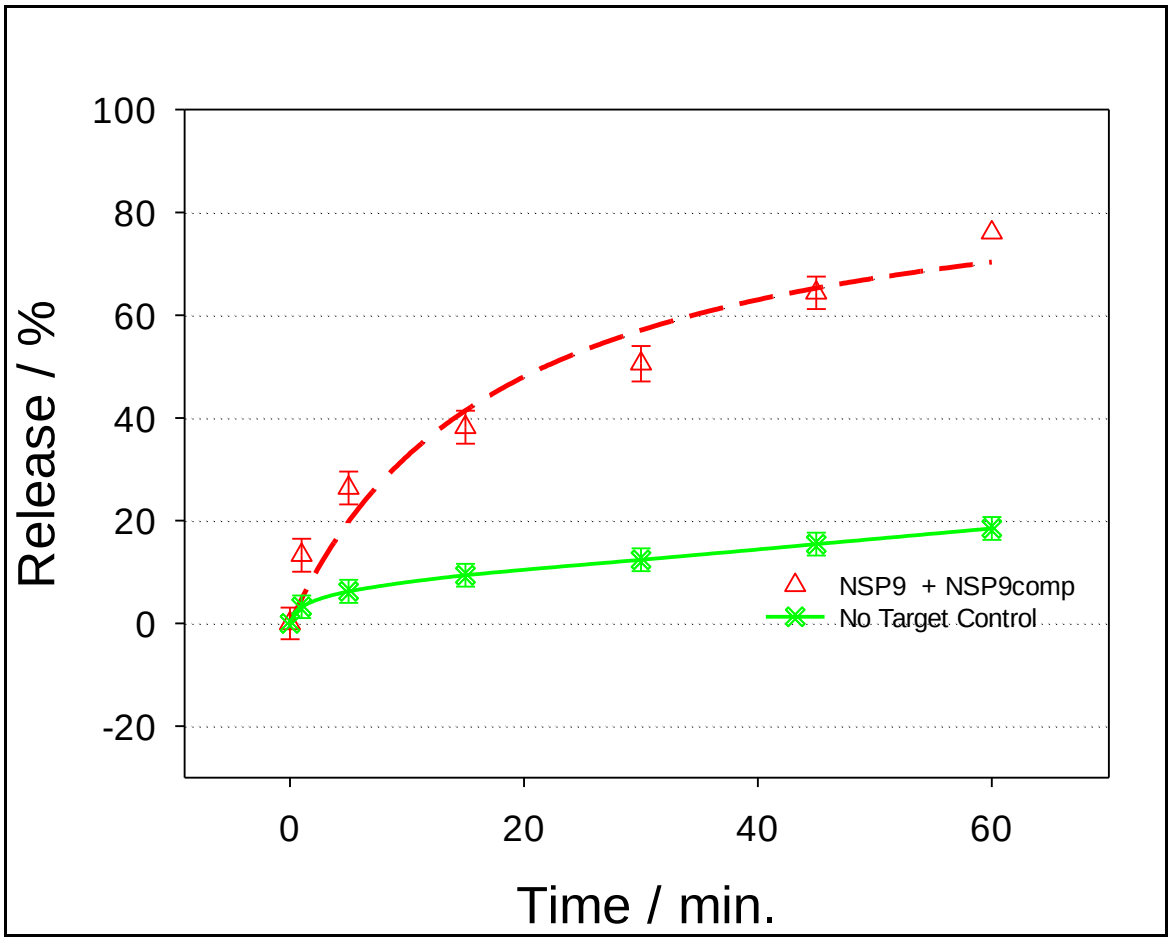


Figure 4.14. Cumulative Releasing of Fluorescein from MSNPs capped with NSP9 Gene probe after added its complementary and MSNPs capped with NSP9 Gene without target in PBS

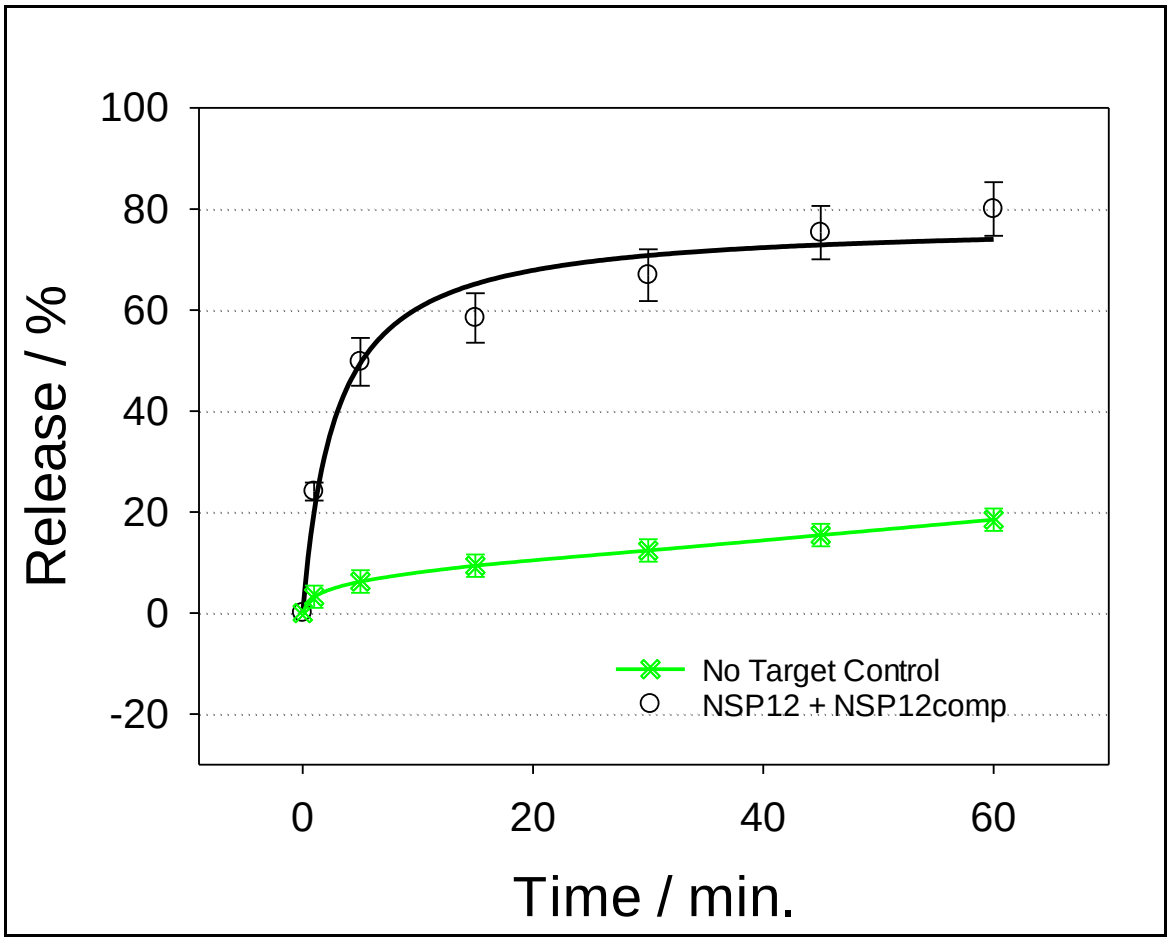


Figure 4.15. Cumulative Releasing of Fluorescein from MSNPs capped with NSP12 Gene probe after added its complementary, MSNPs capped with NSP12 Gene without target in PBS

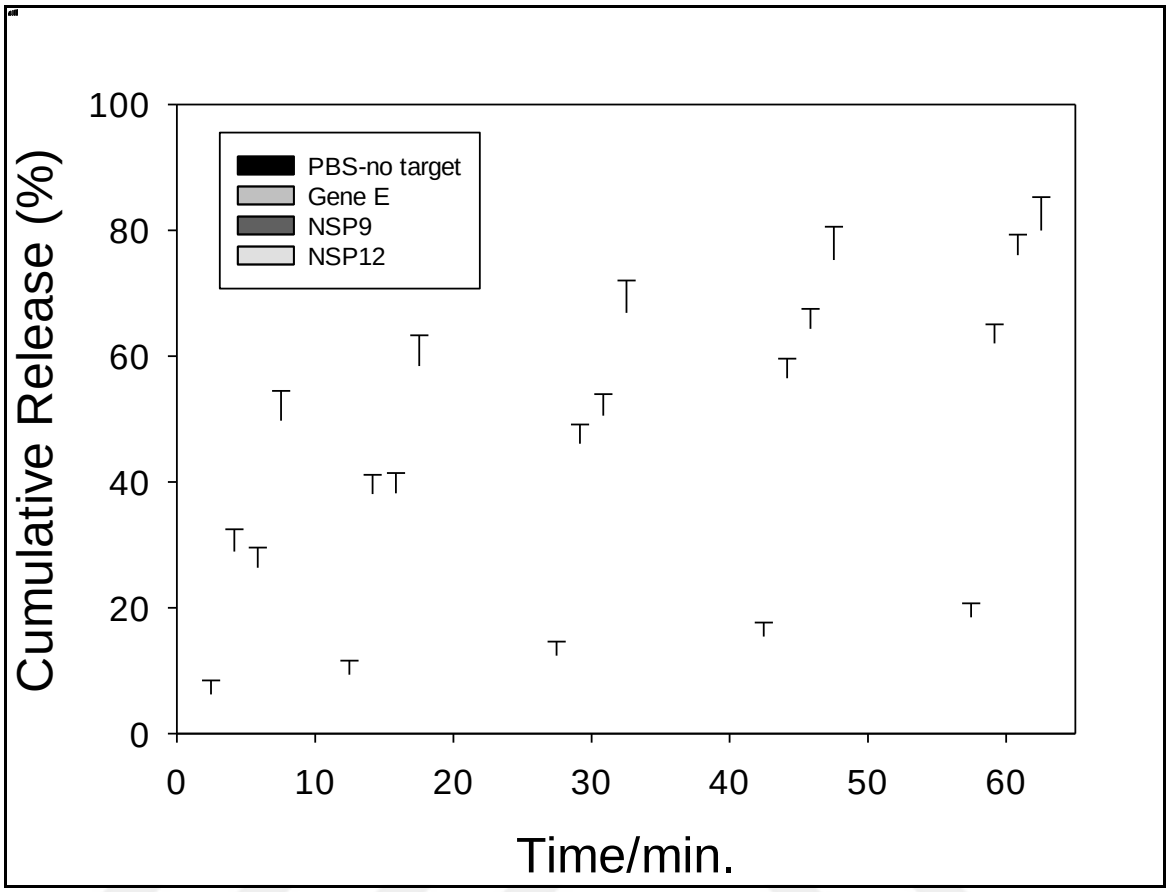


Figure 4.16. Cumulative Releasing of all gene probes with their complementary sequences

The comparison of cumulative release profiles up to 60 minutes of three probes were shown in Figure 4.16. After 5 minutes, there was a statistically significant difference between the probe gated nanoparticle system with all of the different probe conjugates and the no target control (only PBS). The other time points were also similar, statistically, the maximum cumulative release of E Gene probe, NSP9 Gene probe and NSP12 Gene probe was increased compared to no target control (PBS) after 15 minutes, 30 minutes and 60 minutes. The minimum time point which can be selected for the applications was 5 minutes and the probe gated nanoparticle system was responding similarly for both designs using either E Gene probe, NSP9 Gene probe and NSP12 Gene probe. To continue and decide the optimum time point we check the release kinetics of all probes (Figure 4.16.).

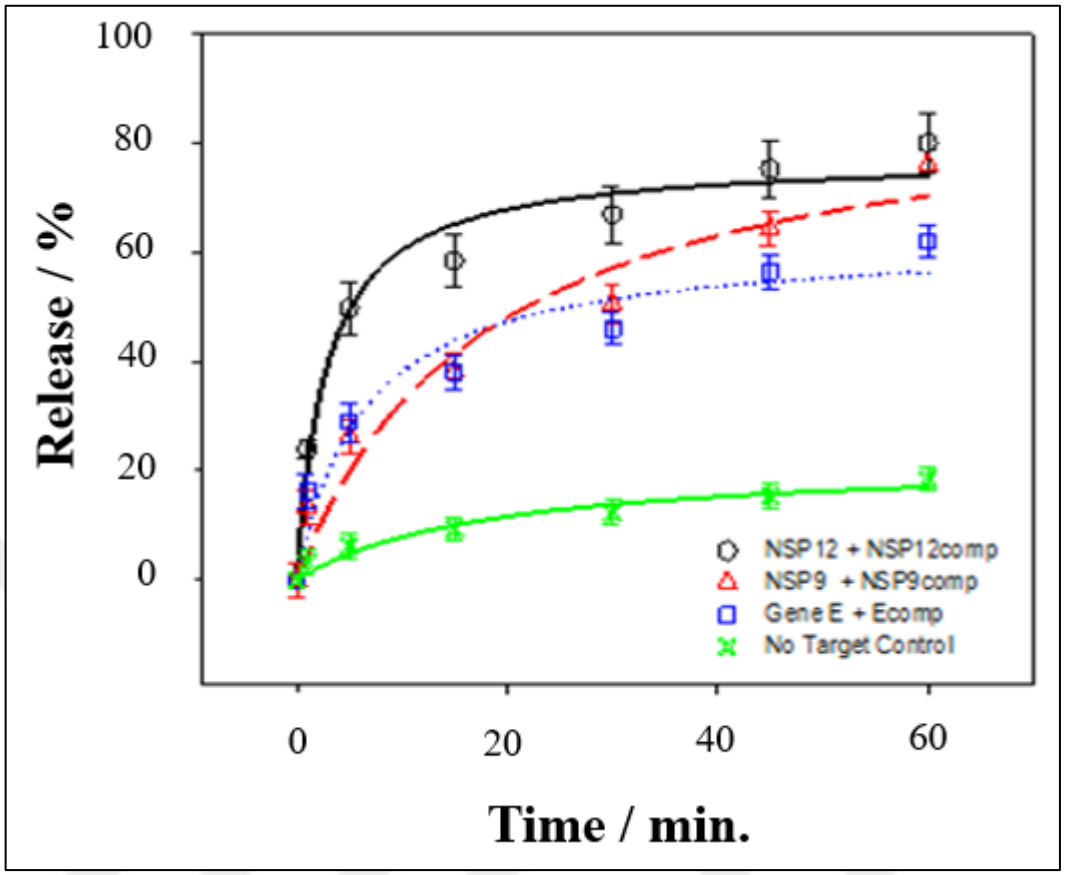


Figure 4.17. Probe-capped MSNPs Release Profiles

In Figure 4.17., the comparison cumulative release profiles in 60 minutes of three probes were shown. Precise hybridization and swift fluorescein release occurred when the NSP12 probe and NSP12comp were used. Similar to the NSP12 probe, combinations of NSP9 probe and NSP9comp or E Gene probe and E Gene comp also demonstrated an abrupt increase in fluorescence signal, but at slower rates as seen in Figure 4.17. compared to NSP12. Following the complementary RNA sequence, 66,11% of the fluorescein from the NSP12 probe-MSNPs was released in a period of 15 minutes. Only 9,07% of the control mixture was released during the same period. NSP9 probe and Gene E probe release less fluorescein under the same conditions with their corresponding target sequences at 39,27% and 41,2%. The release of fluorescein for NSP12 leveled flat at around 70,2% with minimal increase up to 60 minutes to 72,3%. NSP9 showed a different profile with a more significant increase from 49,1% at 20 minutes to 68,8% in 60 minutes. Gene E showed a similar profile to NSP12 with 54,7% at 20 minutes and a slight increase to 58,2% at 60 minutes.

To decide the optimum application time point, three probe-target pairings were compared for fluorescein release amount in PBS having different complementary concentrations (0,0005 nM, 0,1 nM, 0,5 nM, 100 nM, 500 nM, 1000 nM) at 5, 15 and 30 minutes. The cumulative fluorescence release results of NSP12 probe-MSNPs in PBS having different NSP12comp concentrations (0,0005 nM, 0,1 nM, 0,5 nM, 100 nM, 500 nM, 1000 nM) incubated 5, 15 or 30 minutes were showed the maximum fluorescence release for lower concentrations of targets compared to the NSP9 probe-MSNPs or E gene probe-MSNPs. Generally in all optimization experiments the NSP12 probe showed the strongest fluorescence and NSP12 probe was therefore utilized in the intricate investigations for analytical parameters.

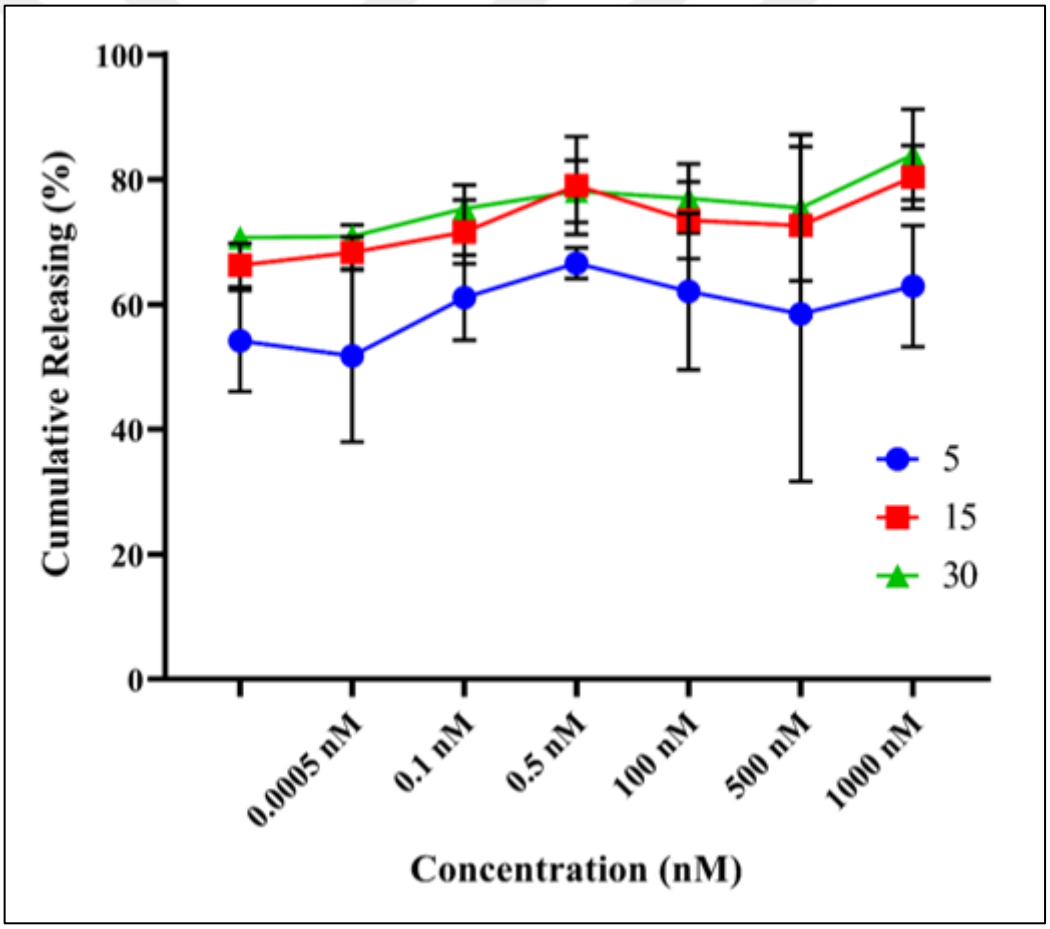


Figure 4.18. Different concentrations of NSP12 complementary sequences

The cumulative fluorescence releasing amount of NSP12 gene probe gated MSPNs, different NSP12comp concentrations (0,0005 nM, 0,1 nM, 0,5 nM, 100 nM, 500 nM, 1000 nM) were showed in Figure 4.18. at different time points (5, 15 and 30 minutes). The fluorescence

release amount after 5 minute incubation was a bit lower than 15 minutes or 30 minutes incubations. However, the fluorescence release amount after 15 minutes or 30 minutes incubation was not different from each other and thus, the experiments were optimized at 15 minutes.

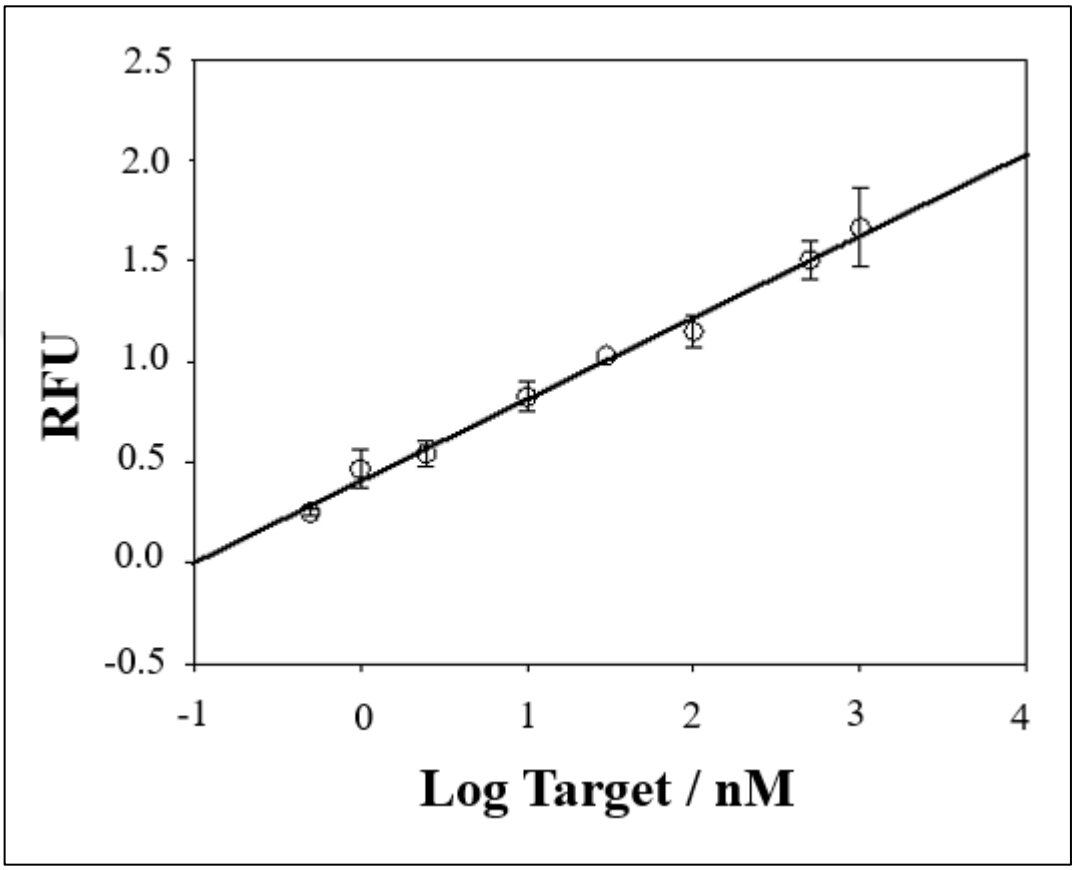


Figure 4.19. Target-response curve for an experiment using the NSP12 gene probe after a 15 minutes incubation

The concentration of target and relative fluorescence unit relation tested with NSP12 gene probe gated MSPNs was showed in Figure 4.19. At 15 minutes incubation time, it is determined that the probe concentrations (0,0005 nM, 0,1 nM, 0,5 nM, 100 nM, 500 nM, 1000 nM) were linearly correlated with the amount of fluorescence signal between 100 fM and 1 M. (Figure 4.19.). The least squares method is used to fit a regression line with the formula y = mx + c. Given that not all data points fall exactly on the line, the line maps the best correction. The limit of detection is then calculated using the three-sigma limit (3σ) approach (LOD). A statistical calculation known as the 3σ technique refers to data that is three standard deviations or less from the mean. It is calculated using the formula LOD =

3,3x / S, where S is the calibration curve's slope and is the response's standard deviation. The LOD was thus set at 48 fM.

## 4.4. THE CONTROLLED RELEASE PERFORMANCE OF PROBES CONJUGATED WITH FLUORESCEIN-LOADED MCM-41 BY USING DIFFERENT COMPLEMENTARY COMBINATIONS OF SYNTHETIC PROBES

To test the unspecific binding and flourence releasing due to unspecific binding to the different gene locations in virus, artificially, different combinations of the complementaries such as NSP12 gene complementary and E gene complementary or NSP12 complementary and NSP9 complementary were tested with NSP12 gene probe, E gene probe or NSP9 gene probe gated MSNPs. The minumum release due to unspecific binding occured with NSP12 gene probe gated MSPNs compared to other conjugations. Only a little quantity of fluorescein was released when the NSP12 probe and NSP9comp target were combined in PBS, but precise hybridization and swift fluorescein release occurred when the NSP12 probe and NSP12comp were used (Figure 4.20.). In addition, similar results were obtained with other combinations. Little quantity of fluorescein was released when the NSP12 probe and Ecomp target were combined in PBS, but precise hybridization and swift fluorescein release occurred when the NSP12 probe and NSP12comp were used (Figure 4.21.).

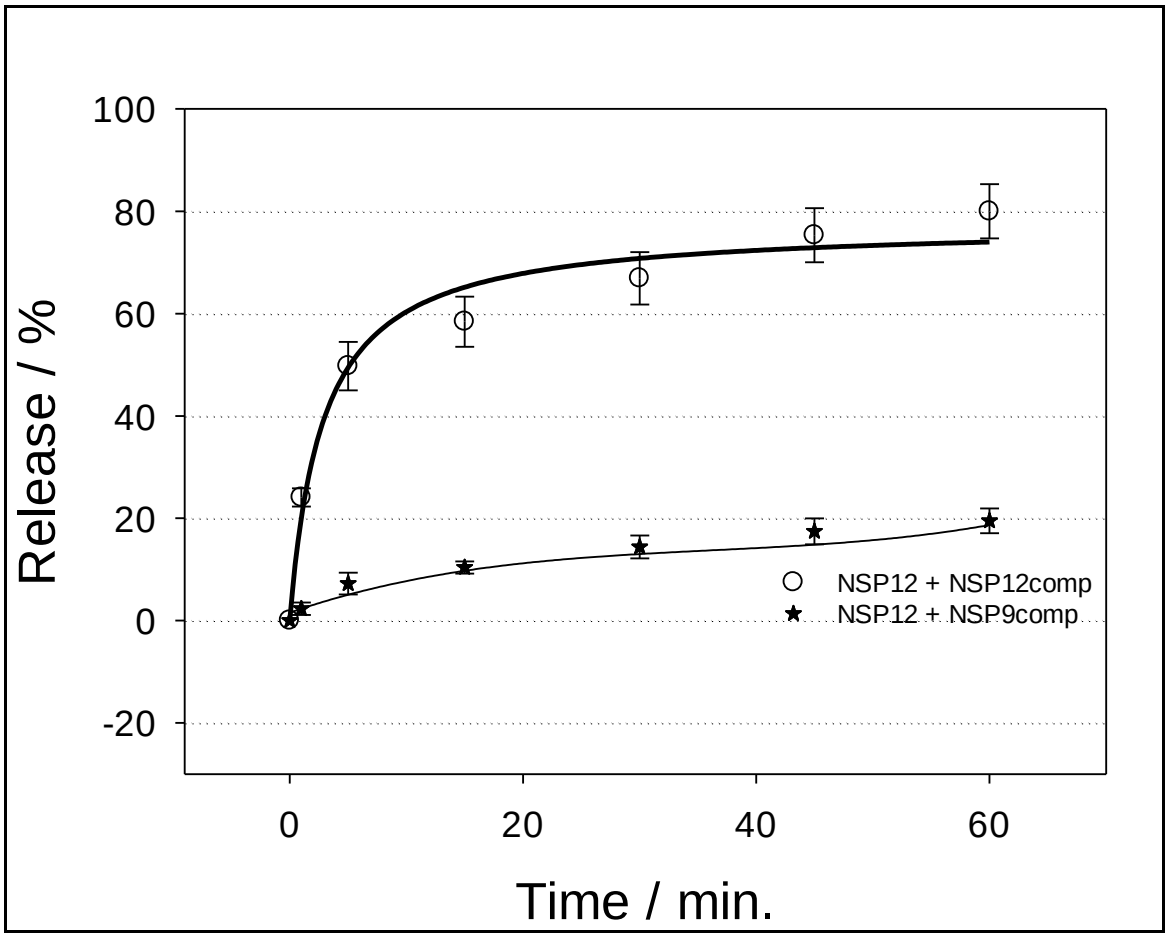


Figure 4.20. Cumulative releasing of NSP12 probe-gated MCM-41 by using NSP12 gene complementary and NSP9 gene complementary

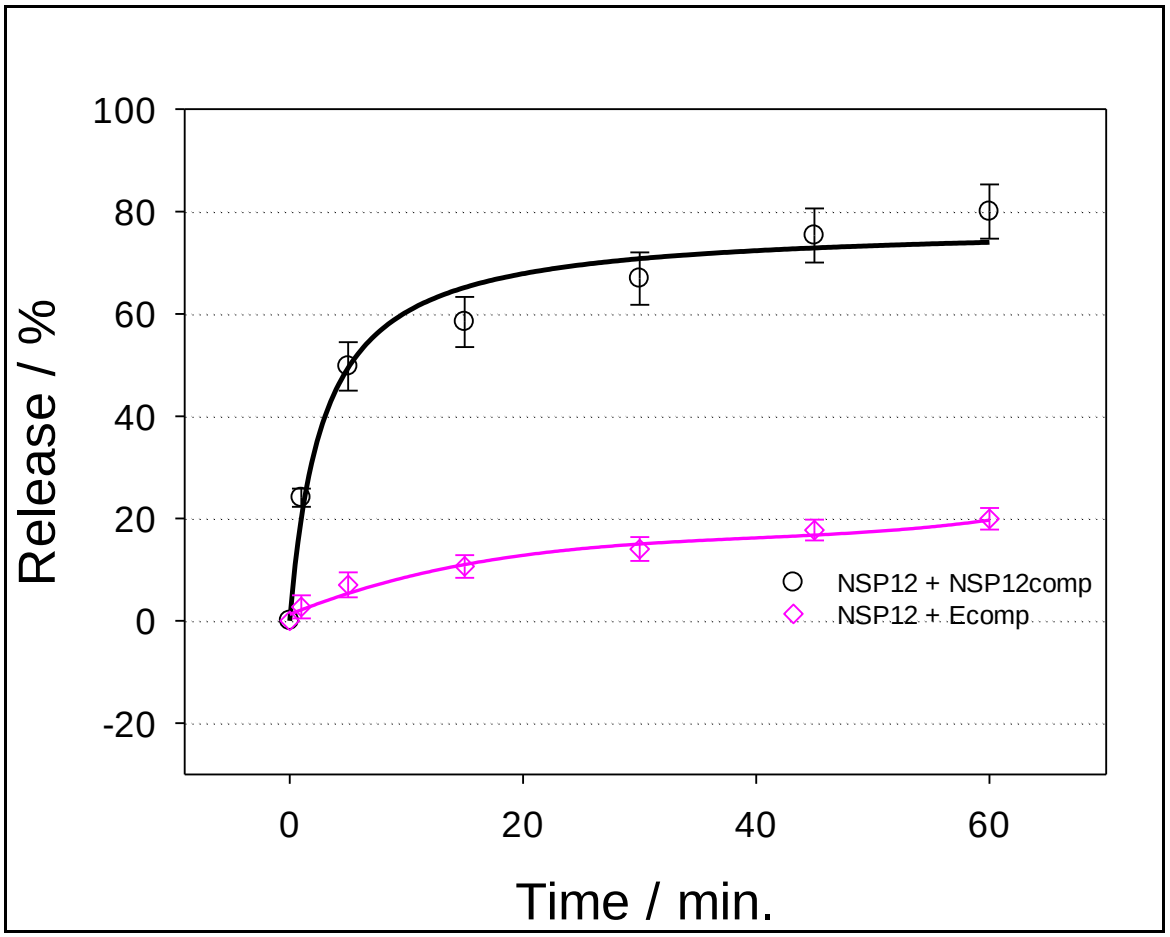


Figure 4.21. Cumulative releasing of NSP12 probe-gated MCM-41 by using NSP12 gene complementary and E gene complementary

## 4.5. TESTING WITH HUMAN SWAB SAMPLES

Finally, patient samples were used to assess the probe-capped MSNPs. The gold standard RT-PCR as well as the probe-gated MSNP biosensor described in this study were used to analyze a total of 43 samples. RT-PCR was used to make the diagnosis in 31 SARS-CoV-2 positive and 12 SARS-CoV-2 negative patients. For biosensor testing, swab collections were taken and immediately placed in RNA preservation buffer, which was subsequently diluted $1{:}10^3$ times in water, then samples were directly used for the assay. After 15 minutes as an assay time, fluorescent signals were measured.

All the synthesized probe gated MSNPs (NSP12 probe-MSNP, NSP9probe-MSNP or Egene probe-MSNP) were tested with patients samples to find the optimum conjugation form. For this purpose first, randomly selected 10 positive and 10 negative samples were tested with

probe gated MSNPs. According to these results (Table 4.1.), sensitivity and specificity were calculated as 30% and 60%, respectively for Egene probe-MSNP. Sensitivity and specificity were calculated as 90% and 0%, respectively for NSP9 probe-MSNP (Table 4.2.).

Table 4.1. The tested 10 positive and 10 negative Patient Samples with Egene probe-capped MSNPs or NSP9 probe-capped MSNPs

| **Genes** | **Clinical positive samples with RT-PCR** | **Clinical negative samples With RT-PCR** | **Positive Samples detected with NP based method** | **Negative Samples detected with NP based method** | **Sensitivity** | **Specificity** |
|---|---|---|---|---|---|---|
| E Gene | 10 | 10 | 3 | 6 | 30% | 60% |
| NSP9 Gene | 10 | 10 | 9 | 0 | 90% | 0% |

Table 4.2. The sensitivity and specifity calculations of tested 10 positive and 10 negative Patient Samples with Egene probe-capped MSNPs or NSP9 probe-capped MSNPs

| **Egene probe MSNP** |
|---|
| $Sensitivity\ of\ Egene\ probe\ MSNP = \frac{3}{3+7}\ x100 = 30\%$ |
| $Specificity\ of\ Egene\ probe\ MSNP = \frac{6}{6+4} x100 = 60\%$ |
| **NSP9 probe MSNP** |
| $Sensitivity\ of\ NSP9\ probe\ MSNP = \frac{9}{9+1}\ x100 = 90\%$ |
| $Specificity\ of\ NSP9\ probe\ MSNP = \frac{0}{0+10} x100 = 0\%$ |

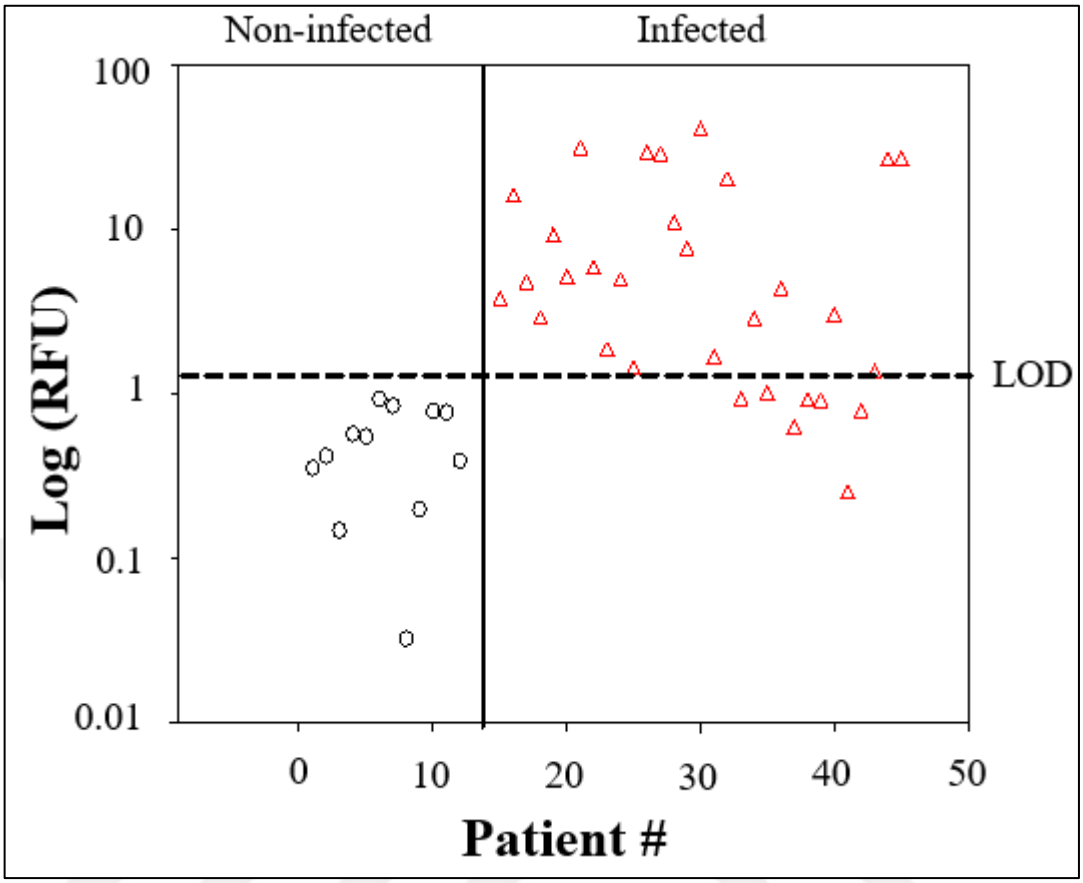


Figure 4.22. The tested Patient Samples with NSP12 probe-capped MSNPs

The relative fluorescence measurements of tested Patient Samples with NSP12 probe-capped MSNPs were showed in Figure 4.22. The average signal was 0,286 RFU, and all of the relative fluorescent signals from the RT-PCR negative samples (n=12) were below 0,926 RFU. At 1,354 RFU, all RT-PCR negative patients samples were detected as “true negative” with also NSP12 probe-capped MSNPs. Therefore, the LOD of 1,354 RFU was chosen as the cutoff value for assessing whether a sample is positive or negative (Figure 4.22.). The new biosensor created in this thesis indicated that 24 of the 31 patients had been identified as SARS-Cov-2 positive, while the other patients had been reported as healthy (NSP12 probe-capped MSNPs). According to these results, sensitivity, accuracy, and specificity were calculated below by using formulas described in methods as 77%, 84%, and 100%, respectively (Table 4.3.).

Table 4.3. The sensitivity, accuracy and specifity calculations of tested 31 positive and 12 negative Patient Samples with NSP12 probe-capped MSNPs

| **NSP12 probe MSNP** |
| --- |
| $Sensitivity\ of\ NSP12\ probe\ MSNP = \frac{24}{24+7}\ x100 = 77\%$ |
| $Accuracy\ of\ NSP12\ probe\ MSNP = \frac{24+12}{43} x100 = 84\%$ |
| $Specificityof\ NSP12\ probe\ MSNP = \frac{12}{12+0} x100 = 100\%$ |

# 5. DISCUSSION

Two different processes were used to create amino-modified mesoporous silica nanoparticles: co-condensation of APTES and TEOS and post-synthetic grafting of 3-aminopropyltriethoxysilane (APTES) onto calcined MSNP. Particles made using the grafting method were used in this study. In order to learn more about the textural characteristics and the preservation of the mesoporous structure following functionalization by grafting technique, calcined and amino-modified MSNP was evaluated by DLS and BET studies.

The particle sizes were first studied at different temperature and pH values for their stability. The synthesized MCM-41 particles were observed to aggregate with increasing temperature to 40°C. The size was similar at or below room temperature (Figure 4.1.). Silica particles are notoriously known for aggregation at different conditions. In our conditions (PBS buffer and specific concentrations), aggregation was easily observed for average size of synthesized particles.

The size of silica particles is affected by temperature, pH, and electrolyte concentrations in a wider range that has been researched at the low-volume scale. This is due to the common belief that temperature plays a significant role in particle shape. The range of temperatures examined in this study was from 15°C to 40°C. The lower and upper bounds were selected based on the size distribution. A comparison of particle sizes based on DLS is shown in Figure 4.1. Figure 4.1. shows that the highest temperature made the particles more amorphous and clumped together, while temperatures below room temperature made the particles smaller and better shaped. Some writings [132] said the same thing [133].

Another important parameter in the average size of MCM-41 particles is the pH value. To employ nanoparticles in bioinspired applications, agglomeration-resistant nanoparticles are necessary. Using DSL measurements, the ability of nanoparticles to agglomerate in liquid phase was explored (Figure 4.1., 4.2., 4.3., 4.4., 4.5.). As shown in the figures, the average particle size estimated by DLS for sample MCM-41 was affected by temperature and pH, depending on the kind of probe. The results indicate that there was a partial agglomeration of MCM-41-probe particles in the solution. This might be explained by the fact that

negatively charged oligonucleotide probes cause MCM-41 probe particles distributed in acidic or basic liquids to interact less or more with other particles.

Due to the negative surface charges on both DNA and the silica substrate, the electrostatic contact between them is poor [133]. The electrostatic attraction between DNA and absorbents must be reduced in order for DNA to be absorbed. To improve their ability to absorb and release substances, mesoporous silica materials have undergone several modifications. Mono-, di-, and tri-amino functional groups were applied to the inner surfaces of a mesoporous silica material by Choi et al. The findings amply revealed that this mesoporous material could bind DNA by establishing electrostatic interactions [134]. Jiang et al. developed a very efficient alternate method to extract DNA from Fe3+-immobilized silica particles by constructing a salt bridge [135]. The Gu group used chaotropic salt solution to increase DNA adsorption into magnetic mesoporous silica nanoparticles by shielding negatively charged species [136]. However, any chaotropic salt that is left behind after purification could impede subsequent procedures [137]. To alter how DNA adheres to silica beads, people have employed an electrical switch [138]. The quantity of DNA molecules that were adsorbed was impacted by the pH shift. On silica particles, DNA adsorption and desorption have been the subject of much research. MCM-41 and modified MCM-41 molecular sieves have been the subject of much investigation because they may be utilized as adsorbents to remove catalysts, environmental contaminants, and catalyst supports. However, only a few studies have shown the ability of MCM-41 with metal ions to bind DNA. To make the surface charge of silica more similar to DNA oligonucleotides in this work, amino groups were added.

When the pH of a solution was changed from 2 to 6, as in a typical study [139], DNA desorption efficiency went up by a lot. The rate of recovery was different at pH levels between 6 and 8. As the pH went up even more, DNA desorption dropped by a huge amount. So, the pH of the eluent has a big effect on how well DNA desorbs, and all of the samples tested showed that the best recovery happened at pH 6. To learn more about how DNA and particle surfaces interact, the effect of salt content on how DNA desorbs was looked into more. DLS measurements were used in this study to see how many of these things were happening together.

WHO has called it a pandemic because it has spread all over the world (WHO). So, finding viruses quickly became a key part of figuring out how to stop the disease from spreading.

The COVID-19 vaccine was released at the beginning of 2021, but although the execution of major vaccination efforts, the overall containment of the pandemic is still made difficult by the quickly increasing number of virus mutations [140]. Also, effective treatments aren't always easy to get, and diagnostic screening techniques that work for large groups are needed to stop Covid-19 from happening again in the coming months. Therefore, the need for quick, simple, and effective diagnostic techniques for SARS-CoV-2 identification is still very important. More virus pandemics are also projected in the coming times. It was demonstrated in this work that these issues could be resolved by creating a design using fluorescein-filled and nucleic acid probe-covered silica nanoparticles. It might be possible to determine someone's SARS-CoV-2 infection using this design. Based on the fluorescein that mesoporous MCM-41 silica nanoparticles release when they hybridize with complementary SARS-CoV-2 RNA and DNA probes, the system functions. In order to identify the viral signaling system, this detection method uses oligonucleotide probes to capture fluorescent molecules inside mesoporous silica nanoparticles. The fluorescein molecules in the mesopores are examined to directly detect the viral genome RNA in the nasopharyngeal swab collections after the probes covering the nanoparticle surface have been removed by hybridization.

The fluorescent signal was seen after mixing the probe and target oligonucleotides for 60 minutes. The fluorescein molecules in the mesopores of the probe-covered MSNPs were released from the nanoparticles as soon as the target RNA sequence was added to the assay mixture. The NSP12 probe and NSP12comp target hybridized flawlessly and released fluorescein quickly, whereas the NSP12 probe and NSP9comp target only released a small amount of fluorescein. Similar to what happened with the NSP12 probe, when the NSP9 probe was combined with NSPcomp or the Gene E probe was combined with Gene Ecomp, the fluorescence signal went up a lot. After a complementary RNA sequence, 66,11% of the fluorescein in the NSP12 probe-MSNPs was let out in 15 minutes. In the same amount of time, only 9,07% of the control mixture came out. Given that the rate of hybridization depends on the sequence, the variations in the amounts of fluorescein released may be the result of different levels of hybridization between probes and targets [141]. When compared to control studies, a 15-minutes test period gives off a signal that can't be found in other studies. After 15 minutes, NSP12 had the strongest fluorescence signal of the three probe-target pairs.

When the test method was used linearly between 100 fM and 1 M, the fluorescence signal was linked to the amount of NSP12comp. All three techniques have a 48 fM limit of detection (LOD). A DNA probe-DNA target assay that relies on the MSNPs that the probe covers has been discussed in prior research [115]. Using a fluorescence method identical to the one used in this investigation, a single nucleotide mutation causing thalassemia was identified. MSNPs that show the presence of a target were designed to show when RNA target sequences are found in nasopharyngeal samples.

While COVID-19 is mostly disseminated by persons who already have symptoms, SARS-CoV-2 is typically transferred from person to person. CoV-2, like other respiratory viruses, is often transmitted by coughing and sneezing droplets. Transmission by aerosols is also a possibility, particularly in crowded public spaces where many individuals are sharing infections. People who don't exhibit any symptoms carry the virus around 80% of the time [142]. Close connections with family, friends, colleagues, and other individuals account for the majority of the spread. You may become ill from viruses that are inside of objects or on surfaces. The frequency of this kind of contact is unclear, however. Typically, the incubation period lasts between three and seven days, and symptoms may appear two weeks after contracting the virus. Because diagnostic biomarkers may be utilized to monitor the virus's progression, they enable the precise diagnosis of SARS-CoV-2 infections. The first or early stage of infection, which happens when the patient becomes infected, and the second stage of infection, which starts antibody production, are the two main stages of infection. Laboratory tests like quantitative polymerase chain reaction (qPCR), computed tomography (CT) of the chest, and serology tests are often used to find the wide range of COVID-19 symptoms. The assay system that was made for this study could be used as an alternative way to quickly find infections.

Point-of-care (POC) biosensors, such as chip-based and paper-based biosensors, have undergone extensive development in an effort to replace conventional assays for the POC detection of infectious diseases [143,144]. Low-cost, simple-to-use POC biosensors that can take a sample and provide a result are in high demand due to the growing need for quick testing to address the current pandemic. These biosensors can find nucleic acids or proteins in samples of sputum, swabs of the throat, or blood. They make it possible to test outside of a lab or in less-developed countries where there may not be a lot of highly educated staff or high-tech infrastructure. Even though these tests are needed to fight the pandemic, they can't

be used in clinical settings yet because of a number of problems. The best point-of-care (POC) biosensor should be able to make quick decisions to stop the spread of COVID-19 and meet the ASSURED criteria (affordable, sensitive, specific, user-friendly, rapid and reliable, equipment-free, and deliverable to end users) [145, 146]. All of the ASSURED criteria are met by the test that was made here. The assay is cheap because it is mostly made of inexpensive materials like oligonucleotide, fluorophore, and silica. The test is accurate (Figure 4.22.). The test can be done easily in a test tube, so it is easy to use. The results of the test are ready in 15 minutes, which is fast. It only needs a small, portable reader with fluorescent lights. The test can be taken to the place where it will be used.

One of the hardest parts of making good biosensors is figuring out how to pick up a very small signal that happens between biological species [147]. To solve the problem, nanoparticles can be used as labels to get a big boost in the signal that is easy to spot. Attaching gold or silver nanoparticles (NPs) and quantum dots to a specific DNA/bio-recognition probe makes it possible to analyze and label these nanoparticles [148]. This could have a synergistic effect because of the nano-labeling effects, which make the electrochemical signal much stronger and allow the development of labeled biosensing techniques that are both sensitive and selective [149]. Current research is focusing on using the attractive physicochemical properties of nanoscale materials (especially their optical, electrical, magnetic, and opto-magnetic properties) to develop nano-enabled biosensing methods for the specific detection of viruses, especially MERS-CoV, SARS-CoV, and SARS-CoV-2 [150]. The development of these biosensors based on nanomaterials to find SARS-CoV-2 has been limited, though. These methods can be used instead of PCR-based testing for COVID-19 because they are easy to use, cost-effective, respond quickly, and can diagnose in real time. These nanomaterial-enabled biosensors mostly use nucleic acid and protein (antigen/antibody) to detect SARS-CoV-2. However, contamination of these highly sensitive bio-receptors has kept them from being 100% accurate, and ultrasensitive, fast, and portable SARS-CoV-2 sequence detection methods are in high demand. For example, the CRISPR-Cas12 method or nanomaterial-based biosensors based on the aerosol mediated diagnostic method have the advantages of being fast, sensitive, and not affecting the sample [151, 152]. Scaling up these detection technologies is very important. In the lab, these biosensors have shown an acceptable level of stability, reaction time, sensitivity/selectivity, and selectivity/sensitivity [153]. The performance of biosensing devices made from

nanomaterials can be affected by a number of factors, such as the properties of the target antigen, protein, or antibody, the properties of the nanomaterial, and the properties of other important biomolecules [153]. Along with these kinds of studies, this work helps solve the above biosensing problems by linking the release of fluorescent cargo to the analyte (a virus) through a nucleic acid gate system.

The examined biosensors fall short of the WHO criterion of 97% for identifying negative samples [154]. This research isn't much different in that regard, in fact. However, this may be due to the uncertainty surrounding sample collection, which falls beyond the purview of this investigation. By selecting biorecognition components that exclusively bind to the target analytes and avoid reacting with molecules unrelated to the target, this problem may be resolved. Additionally, instead of the WHO guideline of 80%, the actual positive rates of the biosensors varied from 46,2% to 100%. Surface modification methods may be used to increase the sensor site's surface area and improve the sensor's sensitivity to low concentrations of bioanalytes [154]. These methods of performance improvement were used in this research.

A biosensor typically functions by a sample or target analyte binding to the bioreceptor, followed by a transducer that converts the information from the biorecognition into a number that can be measured. In this work, an RNA fragment from the virus that hybridized with a DNA probe was used as the target analyte in a test that used DNA probes. Because it might be challenging to identify biological analytes based only on their physical characteristics, labeling approaches have been devised to increase the quantitative signal by attaching a second molecule to immobilized target molecules, viruses, or cells [155]. The immobilized bioreceptors on the chip will bind to the tagged pathogens or proteins they are searching for when analytes are introduced into the sensing region. Examples of biosensing labels include enzymes, fluorescent tags, and dye molecules. A variety of bioreceptor-target coupling mechanisms have been identified, including complementary DNA (cDNA)-DNA hybridization, enzyme-substrate catalysis, and antibody-antigen binding. The gating assay is also a biosensing system that uses a label, but it uses a fluorescent signal instead.

The labels force the selection and replacement of specialized reagents, which might disrupt the assay and, in certain situations, make final detection challenging. Chemistry labeling may also be costly and time-consuming. Thus, several intriguing efforts at biosensing devices that employ unlabeled or unmodified biomolecules (label-free biosensing) and use

natural molecular features, such as molecular weight and RI, for sensing have been made [156]. The necessity for low, nonspecific binding and a large signal when the target attaches are issues with label-free detection, however [157, 158]. However, its advantages might outweigh its drawbacks provided the target analyte concentration and surface adsorption are high enough to permit detection. For instance, by streamlining assays, cutting down on the time and number of procedures required, and eliminating experimental uncertainty, it may provide real-time analysis. The gating assay presented here eliminates the majority of the issues brought on by chemical changes but may still provide powerful signals.

The sensing transduction signals in an optical biosensing platform are often based on minute variations in the refractive index that take place when biomolecules bind to stationary bioreceptors. The ultimate sensitivity and specificity of the biosensor are heavily influenced by the immobilized molecules and how easy the target analyte may access them. A very sensitive biorecognition layer must be present on the transducer's surface for a label-free biosensor to function. Because of this, optimizing the sensing surfaces and the techniques used to make them biofunctional is a key part of any accurate, sensitive, label-free biosensor. Because there are so many different target molecules and biosensor applications, it is very hard to come up with a universal surface biofunctionalization method. Because of this, the method must be designed for each specific surface. For instance, the anti-Zika NS1 mouse monoclonal antibody (mAb) 6B1 produced by the Centers for Disease Control and Prevention is made to interact with the surface in graphene-based field effect biosensing (FEB) (CDC). The possibility of using polyethylene glycol (PEG) to prevent proteins from adhering to silicon-based biosensor surfaces has also been investigated. This is because PEG creates a durable barrier that blocks interactions between unrelated molecules. Because it is more difficult to achieve the appropriate sensitivity and limit of detection (LOD) without raising the concentration of the target analyte, label-free biosensing is more challenging than label-based biosensing. A variety of variables affect whether labeled or unlabeled approaches are more efficient in detecting illnesses like SARS-CoV-2. Gating systems fall halfway between labeled systems and labelless systems in this regard.

The limit of detection is the deciding factor for a viable POC that can replace laboratory-based detection techniques for a highly sensitive optical biosensor that can detect SARS-CoV-2, labeled or unlabeled. the most sensitive optical biosensors that could serve as the

foundation for a point-of-care detection system that is quick and sensitive. In this study, a gating assay that makes a fluorescent signal was described.

By soaking MSNP-probe in a PBS solution, fluorescein was first added as a guest molecule to examine how the amino MSNP-DNA probe system functions during hybridization. The hole was plugged with probe ssDNA. The tube was spun and repeatedly washed with PBS to get rid of the extra dye. Then, in PBS, the amino MSNP-fluorescein particles were dispersed to assess how well they controlled release. Figure 4.17. demonstrates that a very distinct and potent hybridization-operable gating effect was discovered when the maximum fluorescein absorbance was tracked over time. A quick release occurs quickly when comparable target sequences are provided. When non-target sequences are used, there is hardly any release, demonstrating the effectiveness of the cap and the ability of the target sequence to alter the release rate. The rate of release is target-dependent, which is consistent with how the MSNP system functions, which depends on a reversible change in conformation between hybridized complexes and probes for the release of guest molecules. We believed that the gate-like structure created in the closed state would be large enough to block the 2-nm diameter pore and prevent fluorescein molecules from leaving since the diameter of the ssDNA and intramolecular helix regions is approximately 2,0 nm. In fact, we discover that altering the DNA's structure may not be as difficult as it initially appears. A DNA strand, for instance, may fold into a variety of various helix configurations. To determine the precise mechanisms at work, more research will be required, but that is outside the purview of this investigation. The pores were well-covered by the packing of ssDNA when the folded domains were hybridized into a double-stranded form with a cross-sectional diameter of 2,0 nm at pH 8, but the hybridized form is rigid and linear, which changed the capped pores and made dye molecules leak out. These findings proved conclusively that we could use probe ssDNA to seal the pore system of the MSNP before releasing the molecules by hybridizing the probe DNA in the presence of the target sequence. The relatively slow liberation processes observed can be explained by the fact that dye release is regulated by diffusion, which contrasts with the fast capping/uncapping reaction based on the conformational shift of probe DNA.

# 6. CONCLUSION

The recent SARS-CoV-2 pandemic has demonstrated the importance of sensitive and prompt diagnosis. Therefore, the aim was to develop a quick molecular diagnostic biosensor that can detect SARS-CoV-2 directly with samples taken from the nose and throat of human subjects. In this thesis, mesoporous MCM-41 type of silica nanoparticles (MSNPs) were used. Firstly, characterization studies were done by different techniques. To determine microstructure of nanoparticles, TEM was used. DLS to determine particle size and BET to determine pore size were used. After that, MSNPs were loaded by fluorescein and capped by specific gene sequences probes which are three target (NSP12, NSP9 and Egene) regions selected from SARS-CoV-2 genome immobilized on the surface of the nanoparticles. The novel biosensor developed in this thesis based on fluorescein releasing from MSNPs during hybridization between a conjugated complementary single strand oligonucleotide and SARS-CoV-2 RNA samples. This biosensor was firstly tested with synthetic oligonucleotides and it was also optimized in different pH and temperature conditions. The optimum target detection time was determined as 15 minutes. The basic pH damaged the structure of probe-gated MSNPs Every release experiment was repeated three times (n = 3). The results showed that the NSP12 probe displayed the strongest fluorescence signal within 15 minutes. The fluorescein molecules inside the mesopores in the NSP12 probe-gated MSNPs were quickly released from the nanoparticles when the target sequence (NSP12comp) was added to the assay fluid compared to NSP9 gene and E gene oligonucleotide MSNPs conjugates. Therefore, NSP12 probe was therefore utilized in the intricate investigations for analytical parameters. Then, the biosensor was tested with human swab samples. The limit of detection with experiments using patient samples was 1,4, Relative Fluorescence Units with 84% accuracy.

As a conclusion, in this thesis, a novel method based on nucleic acid-gated silica nanoparticles to detect SARS-CoV-2 in 15 minutes directly from patient swab samples was developed. Compared to RT-qPCR, the biosensor correctly identified SARS-CoV-2 RNA in 84% of the samples. Since the prototype assay design has advantages over current market products in that it is quick and easy to use, it may be chosen for the identification of SARS-CoV-2 and other specific determinations.

## REFERENCES


1. Berche P. The enigma of the 1889 Russian flu pandemic: A coronavirus? *La Presse Médicale*. 2022;51(3):104111.

2. Centers for Disease Control and Prevention [cited 2022 24 October]. Available from: https://www.cdc.gov/flu/pandemic-resources/1918-commemoration/1918-pandemic-history.htm

3. Al Hajjar S., McIntosh K. The first influenza pandemic of the 21st century. *Ann Saudi Med*. 2010;30(1):1-10.

4. Centers for Disease Control and Prevention [cited 2022 25 October]. Available from: https://www.cdc.gov/flu/pandemic-resources/2009-h1n1-pandemic.html

5. Xu RH, He JF, Evans MR, Peng GW, Field HE, Yu DW, et al. Epidemiologic clues to SARS origin in China. *Emerg Infect Dis*. 2004;10(6):1030-7.

6. Dhama K, Khan S, Tiwari R, Sircar S, Bhat S, Malik YS, et al. Coronavirus Disease 2019-COVID-19. *Clin Microbiol Rev.* 2020;33(4):e00028-20.

7. Yi Y, Lagniton PNP, Ye S, Li E, Xu R-H. COVID-19: what has been learned and to be learned about the novel coronavirus disease. *Int J Biol Sci*.. 2020;16(10):1753-66.

8. Yang W, Cao Q, Qin L, Wang X, Cheng Z, Pan A, et al. Clinical characteristics and imaging manifestations of the 2019 novel coronavirus disease (COVID-19): A multi-center study in Wenzhou city, Zhejiang, China. *J Infect.* 2020;80(4):388-93.

9. Lu H, Stratton CW, Tang YW. The outbreak of pneumonia of unknown etiology in Wuhan, China: The mystery and the miracle. *J Med Virol.* 2020;92(4):401-2.

10. Gorbalenya AE, Baker SC, Baric RS, de Groot RJ, Drosten C, Gulyaeva AA, et al. The species Severe acute respiratory syndrome-related coronavirus: classifying 2019-nCoV and naming it SARS-CoV-2. *Nat Microbiol.* 2020;5(4):536-44.

11. Wu JT, Leung K, Leung GM. Nowcasting and forecasting the potential domestic and international spread of the 2019-nCoV outbreak originating in Wuhan, China: a modeling study. *Lancet.* 2020;395(10225):689-97.

12. Zhu N, Zhang D, Wang W, Li X, Yang B, Song J, et al. A Novel Coronavirus from Patients with Pneumonia in China, 2019. *N Engl J Med.* 2020;382(8):727-33.

13. Lai CC, Shih TP, Ko WC, Tang HJ, Hsueh PR. Severe acute respiratory syndrome coronavirus 2 (SARS-CoV-2) and coronavirus disease-2019 (COVID-19): The epidemic and the challenges. *Int J Antimicrob Agents.* 2020;55(3):105924.

14. Guan WJ, Ni ZY, Hu Y, Liang WH, Ou CQ, He JX, et al. Clinical Characteristics of Coronavirus Disease 2019 in China. *N Engl J Med.* 2020;382(18):1708-20.

15. Shereen MA, Khan S, Kazmi A, Bashir N, Siddique R. COVID-19 infection: Origin, transmission, and characteristics of human coronaviruses. *J Adv Res.* 2020;24:91-8.

16. Ciotti M, Ciccozzi M, Terrinoni A, Jiang WC, Wang CB, Bernardini S. The COVID-19 pandemic. *Crit Rev Clin Lab Sci.* 2020;57(6):365-88.

17. Lwoff A. The concept of virus. *J Gen Microbiol.* 1957;17(2):239-53.

18. Ruska E. The development of the electron microscope and electron microscopy. *Bioscience Reports.* 1987;7(8):607-29.

19. Duffy S, Shackelton LA, Holmes EC. Rates of evolutionary change in viruses: patterns and determinants. *Nat Rev Genet.* 2008;9(4):267-76.

20. Cornman RS, Boncristiani H, Dainat B, Chen Y, vanEngelsdorp D, Weaver D, et al. Population-genomic variation within RNA viruses of the Western honey bee, Apis mellifera, inferred from deep sequencing. *BMC Genomics.* 2013;14:154.

21. Gibbs AJ, Gibbs MJ. A broader definition of 'the virus species'. *Arch Virol.* 2006;151(7):1419-22.

22. Koonin EV, Senkevich TG, Dolja VV. The ancient Virus World and evolution of cells. *Biol Direct.* 2006;1:29.

23. Sevvana M, Klose T, Rossmann MG. Principles of Virus Structure. *Encyclopedia of Virology*. 2021:257-77.

24. Krupovic M, Koonin EV. Multiple origins of viral capsid proteins from cellular ancestors. *Proc Natl Acad Sci U S A.* 2017;114(12): E2401-e10.

25. Acheson NH. Fundamentals of Molecular Virology. *John Wiley and Sons, Inc*, 2007.

26. Fauquet CM, Fargette D. International Committee on Taxonomy of Viruses and the 3,142 unassigned species. *Virol J.* 2005;2:64.

27. Fenner F, Maurin J. The classification and nomenclature of viruses. *Arch Virol.* 1976;51(1):141-9.

28. Murphy FA, Gibbs EPJ, Horzinek MC, Studdert MJ. *Veterinary Virology*. USA: Elsevier; 1999.

29. Horne RW, Wildy P. Symmetry in virus architecture. *Virology*. 1961;15:348-73.

30. Jana AK, May ER. Structural and dynamic asymmetry in icosahedrally symmetric virus capsids. *Curr Opin Virol.* 2020;45:8-16.

31. Luteijn RD, Praest P, Thiele F, Sadasivam SM, Singethan K, Drijfhout JW, et al. A Broad-Spectrum Antiviral Peptide Blocks Infection of Viruses by Binding to Phosphatidylserine in the Viral Envelope. *Cells*. 2020;9(9).

32. WHO. World health statistics 2015 [cited 2022 5 June]. Available from: http://www.who.int/gho/publications/world_health_statistics/2015/en/.

33. Molinari NA, Ortega-Sanchez IR, Messonnier ML, Thompson WW, Wortley PM, Weintraub E, et al. The annual impact of seasonal influenza in the US: measuring disease burden and costs. *Vaccine*. 2007;25(27):5086-96.

34. Gattani A, Singh SV, Agrawal A, Khan MH, Singh P. Recent progress in electrochemical biosensors as point of care diagnostics in livestock health. *Anal Biochem*. 2019;579:25-34.

35. Neethirajan S, Tuteja SK, Huang S-T, Kelton D. Recent advancement in biosensors technology for animal and livestock health management. Biosens Bioelectron. 2017;98:398-407.

36. Qin P, Park M, Alfson KJ, Tamhankar M, Carrion R, Patterson JL, et al. Rapid and Fully Microfluidic Ebola Virus Detection with CRISPR-Cas13a. *ACS Sens*. 2019;4(4):1048-54.

37. Zhang RQ, Hong SL, Wen CY, Pang DW, Zhang ZL. Rapid detection and subtyping of multiple influenza viruses on a microfluidic chip integrated with controllable micro-magnetic field. *Biosens Bioelectron*. 2018;100:348-54.

38. Li L, Miao B, Li Z, Sun Z, Peng N. Sample-to-Answer Hepatitis B Virus DNA Detection from Whole Blood on a Centrifugal Microfluidic Platform with Double Rotation Axes. *ACS Sens*. 2019;4(10):2738-45.

39. Fernández-Carballo BL, McBeth C, McGuiness I, Kalashnikov M, Baum C, Borrós S, et al. Continuous-flow, microfluidic, qRT-PCR system for RNA virus detection. Anal Bioanal Chem. 2018;410(1):33-43.

40. Lee UN, Su X, Guckenberger DJ, Dostie AM, Zhang T, Berthier E, et al. Fundamentals of rapid injection molding for microfluidic cell-based assays. Lab Chip. 2018;18(3):496-504.

41. Bliss CL, McMullin JN, Backhouse CJ. Rapid fabrication of a microfluidic device with integrated optical waveguides for DNA fragment analysis. *Lab Chip*. 2007;7(10):1280-7.

42. Ishii S, Kitamura G, Segawa T, Kobayashi A, Miura T, Sano D, et al. Microfluidic quantitative PCR for simultaneous quantification of multiple viruses in environmental water samples. *Appl Environ Microbiol*. 2014;80(24):7505-11.

43. Lung O, Fisher M, Erickson A, Nfon C, Ambagala A. Fully automated and integrated multiplex detection of high consequence livestock viral genomes on a microfluidic platform. *Transbound Emerg Dis*. 2019;66(1):144-55.

44. Daaboul GG, Lopez CA, Chinnala J, Goldberg BB, Connor JH, Ünlü MS. Digital Sensing and Sizing of Vesicular Stomatitis Virus Pseudotypes in Complex Media: A Model for Ebola and Marburg Detection. *ACS Nano*. 2014;8(6):6047-55.

45. Lopez CA, Daaboul GG, Vedula RS, Ozkumur E, Bergstein DA, Geisbert TW, et al. Label-free multiplexed virus detection using spectral reflectance imaging. *Biosens Bioelectron*. 2011;26(8):3432-7.

46. Shrivastav AM, Cvelbar U, Abdulhalim I. A comprehensive review on plasmonic-based biosensors used in viral diagnostics. *Commun Biol*. 2021;4(1):70.

47. Cheng MS, Toh C-S. Novel biosensing methodologies for ultrasensitive detection of viruses. *Analyst*. 2013;138(21):6219-29.

48. Kevadiya BD, Machhi J, Herskovitz J, Oleynikov MD, Blomberg WR, Bajwa N, et al. Diagnostics for SARS-CoV-2 infections. *Nat Mater*. 2021;20(5):593-605.

49. Pillaiyar T, Wendt LL, Manickam M, Easwaran M. The recent outbreaks of human coronaviruses: A medicinal chemistry perspective. *Med Res Rev.* 2021;41(1):72-135.

50. Gralinski LE, Menachery VD. Return of the Coronavirus: 2019-nCoV. *Viruses*. 2020;12(2):135.

51. Wang D, Hu B, Hu C, Zhu F, Liu X, Zhang J, et al. Clinical Characteristics of 138 Hospitalized Patients With 2019 Novel Coronavirus-Infected Pneumonia in Wuhan, China. *JAMA*. 2020;323(11):1061-1069.

52. The Biologist Features Focus on SARS-CoV-2 [cited 2022 28 October]. Available from: https://thebiologist.rsb.org.uk/biologist-features/focus-on-cov-sars-2

53. Lipsitch M, Swerdlow DL, Finelli L. Defining the Epidemiology of Covid-19 - Studies Needed. *N Engl J Med.* 2020;382(13):1194-1196.

54. Chen L, Liu W, Zhang Q, Xu K, Ye G, Wu W, et al. RNA based mNGS approach identifies a novel human coronavirus from two individual pneumonia cases in 2019 Wuhan outbreak. *Emerg Microbes Infect*. 2020;9(1):313-9.

55. Bakhshandeh B, Jahanafrooz Z, Abbasi A, Goli MB, Sadeghi M, Mottaqi MS, et al. Mutations in SARS-CoV-2; Consequences in structure, function, and pathogenicity of the virus. *Microb Pathog*. 2021;154:104831.

56. V'Kovski P, Kratzel A, Steiner S, Stalder H, Thiel V. Coronavirus biology and replication: implications for SARS-CoV-2. *Nat Rev Microbiol.* 2021;19(3):155-70.

57. Gao Y, Yan L, Huang Y, Liu F, Zhao Y, Cao L, et al. Structure of the RNA-dependent RNA polymerase from COVID-19 virus. *Science*. 2020;368(6492):779-82.

58. Sutton G, Fry E, Carter L, Sainsbury S, Walter T, Nettleship J, et al. The nsp9 replicase protein of SARS-coronavirus, structure and functional insights. *Structure*. 2004;12(2):341-53.

59. Gordon DE, Jang GM, Bouhaddou M, Xu J, Obernier K, White KM, et al. A SARS-CoV-2 protein interaction map reveals targets for drug repurposing. Nature. 2020;583(7816):459-68.

60. Pizzato M, Baraldi C, Boscato Sopetto G, Finozzi D, Gentile C, Gentile MD, et al. SARS-CoV-2 and the Host Cell: A Tale of Interactions. *Front. Virol*. 2022;1:815388.

61. Uğraş Dikmen A, Kına HM, Özkan S, İlhan MN. COVID-19 Epidemiyolojisi: Pandemiden Ne Öğrendik. *J Biotechnol and Strategic Health Res.* 2020;1(Özel Sayı):29- 36.

62. Centers for Disease Control and Prevention [cited 2022 2 November]. Available from: https://www.cdc.gov/coronavirus/2019-ncov/symptoms-testing/symptoms.html

63. Feray Aycan Yılmaz. SARS-CoV-2 Virüsünün Neden Olduğu COVID-19 Pandemisi Döneminde Servisimizde Takip Edilen Hastaların Epidemiyolojik, Klinik, Laboratuvar ve Tedavi Yanıtlarının Değerlendirilmesi. Tıpta Uzmanlık Tezi, Sağlık Bilimleri Üniversitesi 2021.

64. Du Z, Xu X, Wu Y, Wang L, Cowling BJ, Meyers LA. Serial İnterval of COVID-19 Among Publicly Reported Confirmed Cases. *Emerg Infect Dis*. 2020;19: 26 (6).

65. World Health Organization Covid-19 Overview Homepage [cited 2022 9 November]. Available from: https://covid19.who.int/

66. World Health Organization Covid-19 Region Euro Country [cited 2022 9 November]. Available from: https://covid19.who.int/region/euro/country/tr

67. Fettah A, Karakas Z. COVID-19 and Hemoglobinopathies. *Sağlık Bilimlerinde İleri Araştırmalar Dergisi*. 2020; 3(Suppl.1): S63-S67.

68. Ricerca BM, Di Girolamo A, Rund D. Infections in thalassemia and hemoglobinopathies: focus on therapy-related complications. *Mediterr J Hematol Infect Dis.* 2009 ;28:1(1):e2009028.

69. Haghpanah S, Hosseini-Bensenjan M, Sayadi M, Karimi M. Incidence Rate of COVID-19 Infection in Hemoglobinopathies: A Systematic Review and Meta-analysis. *Hemoglobin*. 2021;45(6):371-379.

70. World Health Organization Activities Tracking Sars-Cov-2 Variants [cited 2022 12 November]. Available from: https://www.who.int/activities/tracking-SARS-CoV-2-variants.

71. World Health Organization Activities Tracking Sars-Cov-2 Variants Previously circulating VOIs [cited 2022 12 November]. Available from: https://www.who.int/activities/tracking-SARS-CoV-2-variants/previously-circulating-vois.

72. Flores-Vega VR, Monroy-Molina JV, Jiménez-Hernández LE, Torres AG, Santos-Preciado JI, Rosales-Reyes R. SARS-CoV-2: Evolution and Emergence of New Viral Variants. *Viruses.* 2022;14:653.

73. Okyay P. Current situation and future prospects of the Covid-19 pandemic. *Sağlık Bilimlerinde İleri Araştırmalar Dergisi*. 2021; 4(Suppl.1): S97-S103.

74. Sanjuán R, Nebot MR, Chirico N, Mansky LM, Belshaw R. Viral mutation rates. J Virol. (2010) 84:9733–48.

75. Robson F, Khan KS, Le TK, Paris C, Demirbag S, Barfuss P, et al. Coronavirus RNA. proofreading: molecular basis and therapeutic targeting. *Mol Cell*. 2020;79:710–27.

76. Gribble J, Stevens LJ, Agostini ML, Anderson-Daniels J, Chappell JD, Lu X, et al. The coronavirus proofreading exoribonuclease mediates extensive viral recombination. *PLoS Pathog*. 2021; 17:e1009226.

77. Harvey WT, Carabelli AM, Jackson B, Gupta RK, Thomson EC, Harrison EM, et al. SARS-CoV-2 variants, spike mutations and immune escape. *Nat Rev Microbiol*. 2021; 19:409–24.

78. Xia X. Domains and functions of spike protein in sars-cov-2 in the context of vaccine design. *Viruses*. 2021;13:109.

79. Thakur S, Sasi S, Pillai SG, Nag A, Shukla D, Singhal R, et al. SARS-CoV-2 Mutations and Their Impact on Diagnostics, Therapeutics and Vaccines. *Front. Med*. 2022;9:815389.

80. Zhang L, Jackson CB, Mou H, Ojha A, Peng H, Quinlan BD, et al. SARSCoV-2 spike-protein D614G mutation increases virion spike density and infectivity. *Nat Commun*. 2020;11:6013.

81. Bianchi M, Benvenuto D, Giovanetti M, Angeletti S, Ciccozzi M, Pascarella SJBRI. Sars-CoV-2 envelope and membrane proteins: structural differences linked to virus characteristics? *Biomed Res Int*. 2020;30(2020):4389089.

82. Dutta NK, Mazumdar K, Gordy JT. The nucleocapsid protein of SARSCoV-2: a target for vaccine development. *J Virol*. 2020;94:00647- 20.

83. Mishra SK, Tripathi TJA. One year update on the COVID19 pandemic: Where are we now? *Actatropica*. 2020;214:105778.

84. Covariants Enabled by data from GISAID Homepage [cited 2022 15 November]. Available from: https://covariants.org/).

85. Dayan S. COVID-19 ve Aşı. *Dicle Tıp Dergisi*. 2021;48:98-113.

86. Gomez PL, Robinson JM. Vaccine Manufacturing. In: Plotkin's Vaccines, 7th, Plotkin S, Orenstein W, Offit P, Edwards K (Eds), Elsevier, 2018. p.51. 5.

87. World Health Organization. Draft landscape of COVID-19 candidate vaccines [cited 2022 15 November]. Available from: https://www.who.int/publications/m/item/draft-landscape-of-covid-19-candidate-vaccines.

88. Dinesh K. Yadav, Neelam Yadav, Satyendra Mohan Paul Khurana. Chapter 26 - Vaccines: Present Status and Applications, Editor(s): Ashish S. Verma, Anchal Singh, Animal Biotechnology, Academic Press, 2014, Pages 491-508.

89. Yu J, Tostanoski LH, Peter L, Mercado NB, McMahan K, Mahrokhian SH, et al. DNA vaccine protection against SARS-CoV-2 in rhesus macaques. *Science* 2020; 14;369(6505):806-811.

90. Case JB, Rothlauf PW, Chen RE, Kafai NM, Fox JM, Smith BK, et al. Replication Competent Vesicular Stomatitis Virus Vaccine Vector Protects against SARS-CoV-2-Mediated Pathogenesis in Mice. *Cell Host Microbe.* 2020;28:465.

91. Zhu FC, Li YH, Guan XH, Hou LH, Wang WJ, Li JX, et al. Safety, tolerability, and immunogenicity of a recombinant adenovirus type-5 vectored COVID-19 vaccine: a dose-escalation, openlabel, non-randomised, first-in-human trial. *Lancet*. 2020; 13;395(10240):1845-1854.

92. Pollet J, Chen W, Strych U. Recombinant protein vaccines, a proven approach against coronavirus pandemics. *Advanced Drug Delivery Reviews*. 2021;170:71-82.

93. Kershner I, Zimmer K. "Israel's Vaccination Results Point a Way Out of Virus Pandemic," New York Times, Apr 5, 2021.

94. Emary KR, Golubchik T, Aley PK, Ariani CV, Angus B, Bibi S, et al. Efficacy of ChAdOx1 nCoV-19 (AZD1222) vaccine against SARS-CoV-2 VOC 202012/01 (B.1.1.7). *Lancet.* 2021;Feb 4 (preprint).

95. Parsons L. Novavax's COVID-19 vaccine 'Highly' effective against UK variant. Pharma Times [cited 2021 15 March]. Available from:

https://www.pharmatimes.com/news/novavaxs_covid19_vaccine_highly_effective_against_uk_variant_1365241

96. Moderna. Moderna COVID-19 Vaccine Retains Neutralizing Activity Against Emerging Variants First Identified in the U.K. and the Republic of South Africa. Moderna [cited 2021 25 January]. Available from: https://investors.modernatx.com/news/news-details/2021/Moderna-COVID-19-Vaccine-Retains-Neutralizing-Activity-Against-Emerging-Variants-First-Identified-in-the-U.K.-and-the-Republic-of-South-Africa/default.aspx

97. WHO Coronavirus (COVID-19) Dashboard | WHO Coronavirus (COVID-19) Dashboard With Vaccination Data [cited 2022 15 November]. Available from: https://covid19.who.int/?mapFilter=vaccinations

98. T.C. Sağlık Bakanlığı Covid-19 Aşısı Bilgilendirme Platformu [cited 2022 15 November]. Available from: https://covid19asi.saglik.gov.tr/

99. Dimastromatteo J, Charles EJ, Laubach VE. Molecular imaging of pulmonary diseases. *Respir Res*. 2018;19(1):17.

100. Li X, Zeng W, Li X, Chen H, Shi L, Li X, et al. CT imaging changes of corona virus disease 2019(COVID-19): a multi-center study in Southwest *China. J Transl Med.* 2020;18(1):154.

101. Kevadiya BD, Machhi J, Herskovitz J, Oleynikov MD, Blomberg WR, Bajwa N, et al. Diagnostics for SARS-CoV-2 infections. *Nat Mater*. 2021;20(5):593-605.

102. Rai, P. Kumar BK, Deekshit VK, Karunasagar I, Karunasagar I. Detection technologies and recent developments in the diagnosis of COVID-19 infection. *Appl Microbiol Biotechnol*. 2021;105(2):441-455.

103. Gorbalenya AE, Baker SC, Baric RS, de Groot RJ, Drosten C, Gulyaeva AA, et al. Severe acute respiratory syndrome-related coronavirus: The species and its viruses – a statement of the Coronavirus Study Group. *bioRxiv*. 2020:2020.02.07.937862.

104. Bwire GM, Majigo MV, Njiro BJ, Mawazo A. Detection profile of SARS-CoV-2 using RT-PCR in different types of clinical specimens: A systematic review and meta-analysis. *J Med Virol*. 2021;93(2):719-25.

105. Bayramoglu G, Ozalp VC, Dincbal U, Arica MY. Fast and Sensitive Detection of Salmonella in Milk Samples Using Aptamer-Functionalized Magnetic Silica Solid Phase and MCM-41-Aptamer Gate System. *Acs Biomater Sci Eng*. 2018;4(4):1437-44.

106. Borsa BA, Sudagidan M, Aldag ME, Baris II, Acar EE, Acuner C, et al. Antibiotic administration in targeted nanoparticles protects the faecal microbiota of mice. RSC *Med Chem*. 2021;12(3):380-383.

107. Hernandez FJ, Hernandez LI, Pinto A, Schafer T, Ozalp VC. Targeting cancer cells with controlled release nanocapsules based on a single aptamer. *Chem Commun (Camb)*. 2013;49(13):1285-7.

108. Kavruk M, Celikbicak O, Ozalp VC, Borsa BA, Hernandez FJ, Bayramoglu G, et al. Antibiotic loaded nanocapsules functionalized with aptamer gates for targeted destruction of pathogens. *Chem Commun*. 2015;51(40):8492-5.

109. Sudagidan M, Yildiz G, Onen S, Al R, Temiz Ş N, Yurt MNZ, et al. Targeted mesoporous silica nanoparticles for improved inhibition of disinfectant resistant Listeria monocytogenes and lower environmental pollution. *J Hazard Mater*. 2021;418:126364.

110. Tasbasi BB, Guner BC, Sudagidan M, Ucak S, Kavruk M, Ozalp VC. Label-free lateral flow assay for Listeria monocytogenes by aptamer-gated release of signal molecules. *Anal Biochem*. 2019;587:113449.

111. Borsa BA, Tuna BG, Hernandez FJ, Hernandez LI, Bayramoglu G, Arica MY, et al. Staphylococcus aureus detection in blood samples by silica nanoparticle-oligonucleotides conjugates. *Biosens Bioelectron*. 2016;86:27-32.

112. Aznar E, Oroval M, Pascual L, Murguía JR, Martínez-Máñez R, Sancenón F. Gated Materials for On-Command Release of Guest Molecules. *Chem Rev*. 2016; 116(2):561-718.

113. Sancenón F, Pascual L, Oroval M, Aznar E, Martínez-Máñez R. Gated Silica Mesoporous Materials in Sensing Applications. *ChemistryOpen*. 2015;4(4):418-37.

114. Wang Y, Bai X, Wen W, Zhang X, Wang S. Ultrasensitive Electrochemical Biosensor for HIV Gene Detection Based on Graphene Stabilized Gold Nanoclusters with Exonuclease Amplification. *ACS Appl Mater Interfaces*. 2015;7(33):18872-9.

115. Ercan M, Ozalp VC, Tuna BG. Genotyping of single nucleotide polymorphism by probe-gated silica nanoparticles. *Anal Biochem*. 2017;537:78-83.

116. Ribes À, Santiago-Felipe S, Aviñó A, Candela-Noguera V, Eritja R, Sancenón F, et al. Design of oligonucleotide-capped mesoporous silica nanoparticles for the detection of miRNA-145 by duplex and triplex formation. *Sens Actuators B Chem*. 2018;277:598-603.

117. Pan H, Zhang P, Gao D, Zhang Y, Li P, Liu L, et al. Noninvasive visualization of respiratory viral infection using bioorthogonal conjugated near-infrared-emitting quantum dots. *ACS Nano*. 2014;8(6):5468-5477.

118. Chan J, Dodani SC, Chang CJ. Reaction-based small-molecule fluorescent probes for chemoselective bioimaging. *Nat Chem*. 2012;4(12):973-984.

119. Annibale P, Vanni S, Scarselli M, Rothlisberger U, Radenovic A. Identification of clustering artifacts in photoactivated localization microscopy. Nat Methods, 2011;8(7):527-528.

120. Sharma A. Khan R, Catanante G, Sherazi TA, Bhand S, Hayat A, et al. Designed Strategies for Fluorescence-Based Biosensors for the Detection of Mycotoxins. *Toxins*. 2018;10:197.

121. Clegg, R. M. Fluorescence resonance energy transfer. *Curr Opin Biotechnol*. 1995;6(1):103-110.

122. Selvin PR. The renaissance of fluorescence resonance energy transfer. *Nat Struct Biol*, 2000;7(9):730-734.

123. Moitra P, Alafeef M, Dighe K, Frieman MB, Pan D. Selective Naked-Eye Detection of SARS-CoV-2 Mediated by N Gene Targeted Antisense Oligonucleotide Capped Plasmonic Nanoparticles. *ACS Nano.* 2020;14(6):7617-7627.

124. Chamorro-Garcia, A, Merkoçi, A. Nanobiosensors in diagnostics. *Nanobiomedicine* (*Rij*). 2016;3:1849543516663574.

125. Li L, Lin H, Lei C, Nie Z, Huang Y, Yao S. Label-free fluorescence assay for thrombin based on unmodified quantum dots. *Biosens Bioelectron*. 2014;15(54):42-47.

126. Kong B, Zhu A, Ding C, Zhao X, Li B, Tian Y. Carbon dot-based inorganic-organic nanosystem for two-photon imaging and biosensing of pH variation in living cells and tissues. *Adv Mater*. 2012;14;24(43):5844-8.

127. Ding C, Zhu A, Tian Y. Functional surface engineering of C-dots for fluorescent biosensing and in vivo bioimaging. *Acc Chem Res*. 2014;21;47(1):20-30.

128. Ting DSW, Carin L, Dzau V, Wong TY. Digital technology and COVID-19. *Nat Med*. 2020;26:459–61.

129. Mollaei HR, Afshar AA, Kalantar-Neyestanaki D, Fazlalipour M, Aflatoonian B. Comparison five primer sets from different genome region of COVID-19 for detection of virus infection by conventional RT-PCR. *Iran J Microbiol*. 2020;12(3):185-193.

130. SARS-CoV-2 Emerging Plus, Manual version 06-KA, Release and Revision Date: 21.05.2021/31.05.2021. *Biospeedy* [cited 2022 15 October]. Available from: https://www.bioeksen.com.tr/Media/Documents/biospeedy--sarscov2emerging-plus-ifu47442.pdf.

131. Bio-Speedy® Direct RT-qPCR SARS-CoV-2 Instructions For Use [cited 2022 15 October]. Availbale from: https://www.fda.gov/media/141823/download

132. Castillo RR, de la Torre L, García-Ochoa F, Ladero M, Vallet-Regí M. Production of MCM-41 Nanoparticles with Control of Particle Size and Structural Properties: Optimizing Operational Conditions during Scale-Up. *Int. J. Mol. Sci*. 2020;21:7899.

133. Vandeventer PE, Lin JS, Zwang TJ, Nadim A, Johal MS, Niemz A. Multiphasic DNA adsorption to silica surfaces under varying buffer, pH, and ionic strength conditions. *J. Phys. Chem*. B 2012;17;116(19):5661-5670.

134. Choi HK, Chang JH, Ko IH, Lee JH, Jeong BY, Kim JH, et al. Electrostatic interaction effect for human DNA separation with functionalized mesoporous silicas. *J. Solid State Chem*. 2011; 184:805-810.

135. Jiang S, Zhuang JQ, Wang C, Li J, Yang WS. Highly efficient adsorption of DNA on Fe3+-iminodiacetic acid modified silica particles. *Colloids and Surfaces A: Physicochemical and Engineering Aspects*. 2012:409;143-148.

136. Li X, Zhang JX, Gu HC. Study on the adsorption mechanism of DNA with mesoporous silica nanoparticles in aqueous solution. *Langmuir*. 2012;28:2827-2834.

137. Vandeventer PE, Lin JS, Zwang TJ, Nadim A, Johal MS, Niemz A. Multiphasic DNA adsorption to silica surfaces under varying buffer, pH, and ionic strength conditions. J. Phys. Chem. B 2012;17;116(19):5661-5670.

138. Geng T, Bao N, Gall OZ, Lu C. Modulating DNA adsorption on silica beads using an electrical switch. *Chem. Commun.* 2009;21(7):800-802.

139. Sun XY, Li PZ, Ai B, Wang YB.Surface modification of MCM-41 and its application in DNA adsorption[J]. *Chin. Chem. Lett*., 2016;27(01):139-144.

140. Starr TN, Greaney AJ, Addetia A, Hannon WW, Choudhary MC, Dingens AS, et al. Prospective mapping of viral mutations that escape antibodies used to treat COVID-19. *Science*. 2021;371(6531):850-4.

141. Zhang JX, Fang JZ, Duan W, Wu LR, Zhang AW, Dalchau N, et al. Predicting DNA hybridization kinetics from sequence. *Nat Chem*. 2018;10(1):91-8.

142. Furukawa NW, Brooks JT, Sobel J. Evidence supporting transmission of severe acute respiratory syndrome coronavirus 2 while presymptomatic or asymptomatic. *Emerg Infect Dis.* 2020;26.

143. Choi JR, Hu J, Wang S, Yang H, Wan Abas WAB, Pingguan-Murphy B, et al. based point-of-care testing for diagnosis of dengue infections. *Crit Rev Biotechnol*. 2017;37:100–11.

144. Yew CHT, Azari P, Choi JR, Muhamad F, Pingguan-Murphy B. Electrospun polycaprolactone nanofibers as a reaction membrane for lateral flow assay. *Polymers*. 2018;10:1387.

145. Hu J, Choi JR, Wang S, Gong Y, Feng S, Pingguan-Murphy B, et al. Multiple test zones for improved detection performance in lateral flow assays. *Sens Actuators B Chem*. 2017;243:484–8.

146. Bernheim A, Mei X, Huang M, Yang Y, Fayad ZA, Zhang N, et al. Chest CT findings in coronavirus disease-19 (COVID-19): relationship to duration of infection. *Radiology*. 2020;200463.

147. Asif M, Ajmal M, Ashraf G, Muhammad N, Aziz A, Iftikhar T, et al. The role of biosensors in coronavirus disease-2019 outbreak. *Current Opinion in Electrochemistry*. 2020;23:174-184.

148. Kokkinos C. Electrochemical DNA Biosensors Based on Labeling with Nanoparticles. *Nanomaterials*. 2019; 9(10):1361.

149. Saylan Y, Erdem Ö, Ünal S, Denizli A. An Alternative Medical Diagnosis Method: Biosensors for Virus Detection. *Biosensors*. 2019; 9(2):65.

150. Ozer T, Geiss BJ, Henry CS. Review-Chemical and Biological Sensors for Viral Detection. *J Electrochem Soc*. 2020 Jan;167(3):037523

151. Lucia C, Federico PB, Alejandra GC. An ultrasensitive, rapid, and portable coronavirus SARS-CoV-2 sequence detection method based on CRISPR-Cas12. *bioRxiv*, 2020.

152. Huffman JA, Perring AE, Savage NJ, Clot B, Crouzy B, Tummon F, et al. Real-time sensing of bioaerosols: Review and current perspectives. *Aerosol Sci. Technol.* 2020; 54,:465–495.

153. Srivastava M, Srivastava N, Mishra PK, Malhotra BD. Prospects of nanomaterials-enabled biosensors for COVID-19 detection. *Sci Total Environ*. 2021;754:142363.

154. Lim WY, Lan BL, Ramakrishnan N. Emerging Biosensors to Detect Severe Acute Respiratory Syndrome Coronavirus 2 (SARS-CoV-2): A Review. *Biosensors*. 2021; 11(11):434.

155. Fernández Gavela A, Grajales García D, Ramirez JC, Lechuga LM. Last Advances in Silicon-Based Optical Biosensors. *Sensors* 2016;16:285.

156. Chakravarty S, Lai WC, Zou Y, Drabkin H A, Gemmill R M, Simon GR, et al. Multiplexed specific label-free detection of NCI-H358 lung cancer cell line lysates with silicon based photonic crystal microcavity biosensors. *Biosensors and Bioelectronics.* 2013;43:50-55.

157. Luan E, Shoman H, Ratner DM, Cheung KC, Chrostowski L. Silicon Photonic Biosensors Using Label-Free Detection. *Sensors.* 2018;18:3519.

158. Soler M, Huertas CS, Lechuga LM. Label-free plasmonic biosensors for point-of-care diagnostics: a review. *Expert Review of Molecular Diagnostics*. 2019;19(1):71-81.